Supplementary material for: A new model of the coupled carbon, nitrogen, and phosphorus cycles in the terrestrial biosphere (QUINCY v1.0; revision 1996)

Tea Thum[1], Silvia Caldararu[1], Jan Engel[1], Melanie Kern[1,2,3], Marleen Pallandt[1,2], Reiner Schnur[4], Lin Yu[1], and Sönke Zaehle[1,5]

[1]Max Planck Institute for Biogeochemistry, Hans-Knöll Str. 10, Jena, Germany
[2]International Max Planck Research School (IMPRS) for Global Biogeochemical Cycles, Jena, Germany
[3]Technical University Munich - School of Life Sciences, Weihenstephan, Germany
[4]Max Planck Institute for Meteorology, Hamburg, Germany
[5]Michael Stifel Center Jena for Data-driven and Simulation Science, Jena, Germany

Correspondence: Tea Thum (tthum@bgc-jena.mpg.de), Sönke Zaehle (szaehle@bgc-jena.mpg.de)

This Supplementary Material includes a detailed model description with equations as well as some supplementary figures. Section S1 summarises the general structure and vertical discretisation of vegetation and soil, and introduces general parameters (Tab S1). Section S2 describes the canopy processes, such as photosynthesis and stomatal coupling, with parameters in Tab. S2. Section S3 introduces vegetation growth, turnover and dynamics and the corresponding parameters are in Tab. S3. The soil biochemistry is described in Section S4, and its parameters are in Tab. S4. Section S5 describes the implementation of the isotope code, with parameters in Tab. S5. Section S6 describes the radiation scheme, surface energy balance and soil hydrology, with parameters described in Tab. S6. The PFT-specific parameters are listed in Tab. S7. Where no explicit reference to other studies is given, the equations have been developed in this study.

S1 General model structure, modularity, and discretisation

Each gridcell of the model is subdivided into nested tiles, each of which is occupied by one specific vegetation-type, representing a plant functional type (PFT). The number of tiles per gridcell is flexible, making it is easy to implement more/different PFTs in the future. In the model, vegetation is represented by an average individual composed of a range of structural pools (leaves, sapwood, heartwood, coarse roots, fine roots, and fruit), a fast overturning, respiring non-structural pool (labile), as well as a seasonal, non-respiring, and non-structural storage pool (reserve). Tree vegetation types are furthermore characterised by their height (m), diameter (m), and stand density (m^{-2}). Soil biogeochemistry is represented using five organic pools: metabolic (met), structural (str) and and woody (wl) litter, as well as fast (f) and slow (s) overturning soil organic matter. Each of these pools contains carbon (C), nitrogen (N) and phosphorus (P), as well as ^{13}C, ^{14}C, and ^{15}N. The unit of the pools is $mol\ X\ m^{-2}$ for vegetation and $mol\ X\ m^{-3}$ for soil biogeochemical pools, where X represents any of these elements. In addition, the model represents the following soil biogeochemical pools (NH_4, NO_3, NO_y, N_2O, N_2, and PO_4), with equivalent units.

The model operates on a half-hourly time-scale (denoted as dt). Vegetation processes, e.g. the photosynthesis and respiration responses to temperature, the responses of nutrient uptake and foliar nutrient concentrations to nutrient availability, are assumed to respond to these instantaneous conditions and associated fluxes with a process-specific lag time ($\tau_{mavg}^{process}$, see Tab. S1), representing a form of memory for instance in the calculation of allocation or vegetation dynamic responses. Where appropriate, the fluxes or pool sizes are calculated as running means with a time-averaging filter as

$$X_{mavg,new}^{process} = X_{mavg,old}^{process} \times (1 - \omega) + X_{current} \times \omega, where \tag{S1a}$$

$$\omega = \frac{dt}{\tau_{mavg}^{process}} \tag{S1b}$$

where $X_{current}$ is the instantaneous state or flux of interest, and $X_{mavg,old}^{process}$, as well as $X_{mavg,new}^{process}$ are the averaged values of the previous and current time step, respectively. The equations where these lag times are playing a role are also shown in Tab. S1.

S1.1   Vertical discretisation

The canopy is discretised into 10 layers (denoted by subscript cl), with exponentially increasing layer depth (LAI_{cl}) to allow for a better resolution of top-of-canopy processes with high light and nitrogen gradients. In accordance with observations of canopy N distribution (Niinemets et al., 1998), less N is allocated to the lower, darker canopy layers: as in Zaehle and Friend (2010), the total canopy N content (N_{leaf}) is distributed to each canopy layer cl following

$$N_{leaf,cl} = N_{leaf,cl=1} \times e^{-k_n \times LAI_c}, where \tag{S2a}$$

$$N_{leaf,cl=1} = \frac{k_n}{1 - e^{-k_n \times LAI}} N_{leaf} \tag{S2b}$$

where LAI_c is the cumulative leaf area above the centre-point of the canopy layer, and LAI the total leaf area, and $cl = 1$ is the top layer.

All soil state-variables (temperature, moisture, texture, soil biogeochemical pools) and fluxes are discretised into 15 soil layers (denoted by subscript (sl). Layer thickness increases exponentially with increasing layer depth up to a total depth of 9.5 m, and with a minimum layer thickness for the top layer of 0.065 m. Following observations presented by Jackson et al. (1996), fine roots and coarse roots are assumed to be distributed in exponentially decreasing density along the soil profile according to

$$X_{root,sl} = X_{root,sl=1} \times e^{-k_{root\_dist} \times depth_{sl}}, where \tag{S3a}$$

$$X_{root,sl=1} = \frac{k_{rd}}{1 - e^{-k_{root\_dist} \times depth_r}} X_{root} \tag{S3b}$$

where k_{rd} is a PFT-specific parameter (see Tab. S7), $depth_{sl}$ the depth of the soil layer's mid point, $depth_r$ the rooting depth, derived from site characteristics and X_{root} the respective fine or coarse root mass.

For clarity in the following, the subscript for canopy and soil layer is ignored if processes are treated similarly across layers.

S1.2 Modularity

The code structure of QUINCY has been designed in a modular way, with two intentions.

Modularity regarding the scope of the model: The model can be run configured as a canopy flux scheme (simplified representation of LAI dynamics given the phenology subroutines, full consideration of soil hydrology, surface energy, canopy radiation and photosynthesis), a stand-alone vegetation model (all of the canopy flux schemes, but with LAI dependent on vegetation growth and dynamics, however without biogeochemical soil feedbacks), a stand-alone soil biogeochemical model (driven by pre-calculated soil moisture and temperature as well as atmospheric and plant litter inputs), a configuration of any of the former without considering soil moisture constraints, and the fully coupled canopy, vegetation and soil model as applied here. This approach allows for testing the implications of particular processes at reduced model complexity.

Modularity regarding alternative process representations: The subroutine structure of the model facilitates the testing of alternative process hypotheses: These include alternative assumptions about temperature acclimation, the vertical structure of the soil (bulk or one-dimensional with flexible numbers of layers), as well as sub-modules to be tested in future studies.

S2 Canopy processes

S2.1 Canopy nitrogen allocation

The leaf area index (LAI) and canopy nitrogen content (N_{leaf}) are dynamic properties of the model, as described in Section S3, and are discretised to canopy layers given by Eq. S2. $N_{leaf,cl}$ is partitioned into photosynthetic and non-photosynthetic, or structural, N. The fraction of structural N ($fN_{struc,cl}$) is calculated as a function of the total leaf N in the respective canopy layer (Zaehle and Friend, 2010):

$$fN_{struc,cl} = k_0^{struc} - k_1^{struc} N_{leaf,cl} \tag{S4}$$

where k_0^{struc} is a PFT-specific parameter and k_1^{struc} is an empirical constant.

The photosynthetic N is further separated into the fraction that is associated with Rubisco (fN_{rub}), electron transport (fN_{et}), chlorophyll (fN_{chl}) and in the case of C4 plants, a fourth fraction for PEP carboxylase fN_{pepc}.

As in (Zaehle and Friend, 2010), the fraction of N in chlorophyll for each layer is calculated as decreasing with canopy depth:

$$fN_{chl} = \frac{k_0^{chl} - k_1^{chl} e^{-k_{fn}^{chl} LAI_c}}{a_{chl}^n}, \tag{S5}$$

where k_0^{chl}, k_1^{chl} and k^{chl} are empirical parameters and a_{chl}^n is the molecular N content of chlorophyll.

The values of fN_{rub} and fN_{et} are calculated assuming a fixed ratio of the V_{cmax} and J_{max} photosynthetic parameters at 25°C, r_{J2V}, given the calculated values of the structural and photosynthetic fractions. The PEP carboxylase fraction, fN_{pep}, is considered to be a constant.

S2.2 Leaf-level net photosynthesis

Photosynthesis and stomatal conductance are calculated for the mid-points of each canopy layer and light-quality class (sunlit and shaded; as defined in Sect. S6.1). For clarity, the subscript $_{cl}$ is omitted in this section. The calculation of leaf-level photosynthesis is based on Kull and Kruijt (1998), extended for C4 photosynthesis according to Friend et al. (2009). The Kull-photosynthesis scheme explicitly and dynamically separates each leaf (layer) into a fraction that is light-saturated, under which photosynthesis is controlled by Farquhar-type co-limitation model (Farquhar et al., 1982), and the remainder, which is light-harvesting limited, and therefore strongly depends in the leaf chlorophyll content (see Kull and Kruijt, 1998, for details).

The temperature response curves as described in Bernacchi et al. (2001). Unless stated otherwise, temperature sensitivities follow the form:

$$f_x(T_{air}) = e^{E_0^x - E_1^x/(R \times T_{air})} \tag{S6}$$

where T_{air} is the air temperature (K), R is the universal gas constant (Jmol^{-1}K^{-1}), and the process-wise E_0^x and E_1^x are given in Table S2. Note that the current version of QUINCY does not include a representation of canopy temperature and we are therefore using air temperature for all aboveground processes.

In light-saturated conditions, gross photosynthesis (A_g) in C3 plants is calculated as the minimum of two potential rates, The electron-transport capacity limited carboxylation (A_j) and the Rubisco-limited rate of photosynthesis (A_v). A_j is given by

$$A_j = m_1 \times J_{max}, where \tag{S7a}$$
$$m_1 = \frac{c_i}{c_i + 2 \times \Gamma*}, \tag{S7b}$$
$$J_{max} = n_1 \times N_{leaf}, \tag{S7c}$$
$$n_1 = g_{jmax}(T_{air}) \times \beta_{soil}^{ps} \times \beta_{sinklim}^{ps} \times \beta_{soa}^{ps} \times j_{max}^n \times fN_{et} \tag{S7d}$$

where c_i is the intercellular partial pressure of CO_2 (Pa, Eq. S17), and $\Gamma*$ is the CO_2 compensation point in the absence of dark respiration. $\beta_{sinklim}^{ps}$ is a signal to reduce photosynthesis in the case of C sink limitation (Eq. S43) and β_{soa}^{ps} is accounting for the effect of low-temperature acclimation in the evergreen species (Eq. S46). Excessive soil moisture stress constraints (as discussed in Rogers et al. (2017)) are assumed to reduce light-saturated photosynthetic activity by:

$$\beta_{soil}^{ps} = 1 - \frac{\Psi_{soil}}{\Psi_{leaf}^{min}}, \tag{S8}$$

where Ψ_{soil} is the soil water potential in the root zone (Eq. S121) and Ψ_{leaf}^{min} is the PFT-specific minimum leaf water potential. The temperature sensitivity of electron transport is assumed to follow the bell-shaped form described by June et al. (2004), where T_{jmax}^{opt} is the optimum temperature for J_{max} according to Friend (2010), as follows:

$$g_{jmax}(T_{air}) = e^{-\left(\frac{T_{air} - \bar{T}_{jmax}^{opt}}{T_\Omega}\right)^2}, \tag{S9a}$$

$$T_{jmax}^{opt} = k0_{jmax}^{topt} + k1_{jmax}^{topt} \times T_{air}; T_{jmax,min}^{opt} < T_{jmax}^{opt} \leq T_{jmax,max}^{opt}, \tag{S9b}$$

where T_Ω is a PFT-specific parameter, $k0_{jmax}^{topt}$ and $k1_{jmax}^{topt}$ are parameters, T_{air} is the air temperature, and $\bar{T}_{jmax}^{opt}$ in Eq. S9 is the mean of the daytime T_{jmax}^{opt} over the past few days (τ_{mavg}^{jmax}), thereby accounting for temperature acclimation of photosynthesis as in Friend (2010).

A_v, the Rubisco-limited rate of photosynthesis, is given by

$$A_v = m_2 \times V_{cmax}, where \tag{S10a}$$

$$m_2 = \frac{c_i}{c_i + k_c(1 + O_i/k_o)}, \tag{S10b}$$

$$V_{cmax} = n_2 \times N_{leaf} \tag{S10c}$$

$$n_2 = f_{vcmax}(T_{air}) \times \beta_{soil}^{ps} \times \beta_{sinklim}^{ps} \times \beta_{soa}^{ps} \times v_{cmax}^n \times fN_{rub} \tag{S10d}$$

where O_i is the intercellular partial pressure of O_2, and k_c and k_o are the Michaelis-Menten constants for CO_2 and O_2 respectively, derived E_0^{kc}, E_1^{kc}, or E_0^{ko}, E_0^{ko} using Eq. S6.

The N-specific light-saturated rate of C3 photosynthesis can then be calculated as:

$$m_{sat} = min(n_1 \times m_1, n_2 \times m_2) \tag{S11}$$

Friend et al. (2009) adjusted the scheme by Kull and Kruijt (1998) using the Collatz formulation of C4 photosynthesis Collatz et al. (1992). The simplified assumption is that A_j and A_v can be calculated as above, but at saturating c_i ($c_{i,max}$). Bundle-sheath transport limitation (A_p) is then further limiting C4 photosynthesis, given by

$$A_p = V_{pmax} \times m_3, where \tag{S12a}$$

$$V_{pmax} = n_3 \times N_{leaf} \tag{S12b}$$

$$n_3 = g_{pepc}(T_{air}) \times v_{pepc}^n \times fN_{pepc}, \tag{S12c}$$

$$m_3 = \frac{c_i}{p}, \tag{S12d}$$

where the temperature response is

$$g_{pepc}(T_{air}) = 2^{(T_{air} - T_{ref}^{pepc})/T_{base}^{pepc}} \tag{S13}$$

The N-specific light-saturated rate of C4 photosynthesis can be calculated as

$$m_{sat} = min(n_1 \times m_1, n_2 \times m_2, n_3 \times m_3) \tag{S14}$$

The light-harvesting limited rate of photosynthesis (A_h) can be written as

$$A_h = m_1 \times \alpha_i \times PPFD_a, \tag{S15a}$$

$$PPFD_a = PPFD_0(1 - e^{-k_a \times C_{chl}}), where \tag{S15b}$$

$$C_{chl} = a_{chl}^n \times fN_{chl} \times N_{leaf} \tag{S15c}$$

where α_i is the intrinsic quantum efficiency for CO_2 uptake, $PPFD_0$ is the photosynthetic photon flux density (PPFD) penetrating sunlit or shaded foliage, converted from the adsorbed radiation of the canopy layer (Eq. S102), and k_a as well as a_{chl}^n are parameters specified in Table S2.

As Kull and Kruijt (1998) show, this system of equations (Eq. S7-S15) can be solved to yield gross photosynthesis (A_g) for one canopy layer and light-class as:

$$A_g = (1 - \frac{\Gamma^*}{c_i})[m_{sat}N_{sat} + \alpha_i PPFD_a(e^{-k_a \times a_{chl}^n \times fN_{chl} \times N_{sat}} - e^{-k_a \times a_{chl}^n \times fN_{chl} \times N_{leaf}}), where \tag{S16a}$$

$$for N_{sat} = 0 : \ N_{lim} < 0 \tag{S16b}$$

$$for N_{sat} = N_{lim} : \ N_{lim} < N_{leaf} \tag{S16c}$$

$$for N_{sat} = N_{leaf} : \ N_{lim} \geq N_{leaf}, and \tag{S16d}$$

$$N_{lim} = -\frac{ln(m_{sat}/[\alpha_i \times PPFD \times k_a \times a_{chl}^n \times fN_{chl} \times m_1])}{k_a \times a_{chl}^n \times fN_{chl}} \tag{S16e}$$

$$\tag{S16f}$$

S2.3 Stomatal coupling

The combination of leaf-level net photosynthesis ($A_{n,cl}$), stomatal conductance ($g_{s,cl}$), and leaf internal CO_2 concentration ($c_{i,cl}$) satisfying Eq. S17 is sought iteratively for each canopy layer (following broadly Ball et al., 1987):

$$A_n = (A_{g,sunlit} \times f_{sunlit} + A_{g,shaded} \times (1 - f_{sunlit})) - R_l \tag{S17a}$$

$$g_s = [g_0 + g_1 \frac{A_n \beta_{air} \beta_{soil}^{gs}}{c_a}] \times R \times T_{air}/p \tag{S17b}$$

$$c_i = c_1 \times c_a - c_2 \times A_n \times (\frac{D_{air}^{wv2co2}}{g_s} + \frac{D_{turb}^{wv2co2}}{g_a}) \times R \times T_{air} \tag{S17c}$$

where f_{sunlit} is the fraction of sunlit leaves in a canopy layer (see Eq. S101), R_l is the maintenance respiration of leaves (see Sect. S3.2), g_0 and g_1 are PFT-specific parameters, R is the molar gas constant, T_{air} is air temperature (K), p air pressure (Pa), c_1 converts CO_2 concentration from ppm to Pa, c_2 converts $\mu mol m^{-2} s^{-1}$ to $mol m^{-2} s^{-1}$, g_a is the aerodynamic conductance (calculated following Eq. S110), and the D's are the diffusion coefficient corrections for CO_2 and water (Bonan, 2015).

β_{air} is taken as relative humidity (Ball et al., 1987; Knauer et al., 2015) and β_{soil}^{gs} is the stomatal response to soil moisture, described by:

$$\beta_{soil}^{gs} = 1 - \frac{\Psi_{soil}}{\Psi_{leaf}^{min}} \tag{S18}$$

where Ψ_{soil} is the soil water potential in the root zone (Eq. S121) and Ψ_{leaf}^{min} is the PFT-specific minimum leaf water potential.

S2.4   Canopy integration

Canopy-level fluxes are derived by summing the product of layer-level fluxes or state-variables and the depth of the layer

$$F = \sum_{cl=1}^{ncanopy} F_{cl} \times LAI_{cl}, \tag{S19}$$

where F is the canopy-level equivalent of a leaf-level variable F_{cl} (per unit leaf-area), such as gross photosynthesis (A_g), net photosynthesis (A_n), and leaf-level stomatal conductance (g_s), (see Sect. S2.2 and S2.3) and LAI_{cl} is the leaf area index of the canopy layer. The resulting canopy net assimilation A_g is used as input to the vegetation model (Eq. S20), the canopy conductance (G_s) is used for the calculation of ecosystem transpiration (Eq. S118).

S3   Vegetation growth, turnover and dynamics

S3.1   Labile pool dynamics

The general equation for labile pool dynamics resembles Zaehle and Friend (2010), and similar approaches: growth of a plant is modelled dependent on the partitioning of its labile resource to new tissue growth, storage production, as well as – in the case of C – respiration for maintenance and resource uptake:

$$\frac{dC_{labile}}{dt} = A_g + \Delta S_C - R_m - R_r - (1 + f_{resp,growth}) \times G_C \tag{S20a}$$

$$\frac{dN_{labile}}{dt} = U_{root,N} + \Delta S_N - G_N \tag{S20b}$$

$$\frac{dP_{labile}}{dt} = U_{root,P} + \Delta S_P - G_P \tag{S20c}$$

where R_m is maintenance respiration, R_r is resource uptake respiration (for both see Sect. S3.2), ΔS_X is the net exchange between the labile and reserve pool (Sect. S3.6), $f_{resp,growth}$ is the constant fraction of respiration associated with growth, G_X are the growth rates to build new tissues, $U_{root,X}$ are nutrient rates of root uptake.

7

S3.2 Maintenance respiration

Following (Sprugel et al. (1995), as in (Zaehle and Friend, 2010)), maintenance respiration ($R_{m,i}$) for every vegetation pool (i) is estimated from its N content (N_i) as

$$R_{m,i} = f_{temp} \times f^i_{resp,maint} \times N_i \tag{S21}$$

where $f^i_{resp,maint}$ is the maintenance respiration per unit N, which differs between woody and non-woody pools, and f_{temp} is the instantaneous temperature response of respiration (Lloyd and Taylor (1994))

$$f_{temp} = e^{t_{k1}\left(\frac{1}{t_{k2}} - \frac{1}{T-t_{k3}}\right)} \tag{S22}$$

where t_{k1}, t_{k2} and t_{k3} are temperature sensitivity parameters and T is the instantaneous air or soil temperature for above- and belowground tissues, respectively. Following Atkin et al. (2014), the basal respiration rate acclimates to temperature

$$f_{maint\_rate} = f_{maint\_rate\_ref} 10^{f_{resp\_acclim}(T_{acclim} - T_{acclim,ref})} \tag{S23}$$

where $f_{maint\_rate,ref}$ is the N-specific maintenance respiration rate at the temperature $T_{acclim,ref}$, f_{resp_acclim} is the slope of the temperature acclimation and T_{acclim} is the running average of air or soil temperature (τ^{resp}_{mavg}), respectively.

Resource uptake respiration for nutrients is given by specific costs ($cost_i$, Zerihun et al. (1998)) to transform nutrients from mineral sources (i) into organic material and the actual plants uptake $U_{plant,i}$ (S4.5) as

$$R_{r,i} = cost_i \times U_{plant,i} \tag{S24}$$

where i is either NH_4 or NO_3.

S3.3 Growth

The equations in this section have been developed for the QUINCY model. The potential, source-limited growth rate (G^*_X) is given by the product of the maximum turnover rate of the labile pool ($1/\tau_{labile}$) and the actual labile pool size (X_{labile}). Three sink limitation processes operate, which control the down-regulation of this potential growth rate to the actual growth rates (G_X):

- the temperature and moisture sensitivity of the meristem (Eq. S25);

- the requirement for maintenance respiration (Eq. S21), which takes priority over new growth; and

- the co-limitation of growth by the nutrients required to grow specific pools (Eq. S28).

The temperature and moisture control on the meristem, and therefore the growth rate, is represented by a reduction of the maximum turnover rate of the labile pool at low temperatures and low soil moisture conditions.

$$k^*_{labile} = \frac{1}{\tau_{labile}} \times e^{-(\lambda^{labile}_{temp} \times T_{air})^{k^{labile}_{temp}}} \times e^{-(\lambda^{labile}_{\Theta} \times \Theta)^{k^{labile}_{\Theta}}} \tag{S25}$$

where T_{air} is air temperature in degrees Celsius, Θ is the fractional soil moisture content (Eq. S120), and the λ and k are parameters. k^*_{labile} is set to zero outside the growing season (see Sect. S3.8).

Respiration is assumed to have priority over growth. However, under severe C deficit, the meristem activity also down-regulates maintenance and resource uptake respiration.

5   To ensure that carbon growth (G_C) does not exceed the size of the labile carbon pool, the turnover rate of the labile pool to growth is corrected by the current respiration rate, and constrained to positive solutions:

$$G^*_C = k^*_{labile} \times C_{labile} \times dt - R_m - R_r; G^*_C \geq 0 \tag{S26}$$

Given G^*_C, and the stoichiometric requirements for biomass growth (req^{growth}_{NC}, and req^{growth}_{PN}, respectively):

$$req^{growth}_{XY} = \sum_i^{pools} f^i_{alloc} \times \frac{X_i}{Y_i} \tag{S27}$$

10   where f^i_{alloc} are the allocation fractions (Sect. S3.4) to each pool i, and $\frac{X_i}{Y_i}$ are the target stoichiometries of C:N:P (Sect. S3.5) of the leaf, fine root, coarse root, sapwood, and fruits pools. The actual growth rates can be calculated as

$$G_P = req^{growth}_{N:P} \times G_N = req^{growth}_{P:N} \times req^{growth}_{N:C} \times G_C \tag{S28a}$$

$$G_C \leq G^*_C \tag{S28b}$$

$$G_N \leq \frac{k^{nut}_{labile}}{\tau_{labile}} \times N_{labile} \times dt \tag{S28c}$$

15    $$G_P \leq \frac{(k^{nut}_{labile})^2}{\tau_{labile}} \times P_{labile} \times dt, \tag{S28d}$$

Note that only the minimum of the three rates in eq. S28a can actually be realised. The other two growth rates are adjusted, implying a relative accumulation of these elements in the labile pool. The use of k^{nut}_{labile}, and $(k^{nut}_{labile})^2$ for phosphorus, implies a stronger mobilisation capacity for nitrogen (amino-acids) and phosphorus (a inorganic anion) than for reserve carbon (starch), which requires transformation to be used for growth. The assumption behind this is that the temperature and moisture control of the meristem is already accounted for by G_C, and that the plant is able to mobilise the required nutrients from the labile

20   pool to support this growth.

Outside the growing season, all growth fluxes are set to zero (see Sect. S3.8).

S3.4   Growth partitioning

The labile pool partitioned to growth is first split into reproductive (fruit pool) and structural (leaves, fine and coarse roots and

25   sap wood) growth.

The fraction of carbon growth allocated to fruit depends on the ability of the plant to build reserves (ΔS_C, see Sect. S3.6), implying that fruit growth is suppressed during phases of rapid leaf growth (beginning of the growing season), as well as periods of C starvation (e.g. severe drought).

$$f_{alloc,C}^{fruit} = k1_{alloc}^{fruit} + (k2_{alloc}^{fruit} - k1_{alloc}^{fruit}) \times exp^{-(\lambda_{alloc}^{fruit} \times (\Delta S_C + k3_{alloc}^{fruit}))^{k4_{alloc}^{fruit}}} \tag{S29}$$

5   where the maximum fraction of allocation to fruits ($k2_{alloc}^{fruit}$) is a PFT-specific parameter (this study).

The allocation of the remaining growth ($(1 - f_{alloc,C}^{fruit}) \times G_C$) to the structural pools leaves, fine root, coarse roots, and sapwood follows a set of following allometric relationships (Zaehle and Friend, 2010).

In grasses, halms are assumed to be a proportion of leaf mass, and no height restrictions apply.

$$C_{leaf} = k_{htol} \times C_{sap\_wood} \tag{S30}$$

10   In trees and shrubs, leaf and woody biomass are linked through the pipe-model hypothesis (requiring a constant ratio of leaf area, LA, to sapwood area, SA)

$$C_{leaf} = \frac{k_{latosa} \times C_{sap\_wood}}{sla \times \rho_{wood} \times H} <=> LA = k_{latosa} \times SA, \tag{S31}$$

where sla, k_{latosa}, and ρ_{wood} are the PFT-specific specific leaf area, leaf to sapwood area ratio, and wood density, respectively. H is the mean forest canopy height calculated as:

15    $H = k1_{allom} \times D^{k2_{allom}}, \tag{S32}$

where the diameter at breast height (D) is determined from woody biomass, assuming that the entire trunk is a cylinder. As an extension to the pipe-model theory below-ground, coarse root biomass is assumed to be proportional to sap wood mass:

$$C_{coarse\_root} = k_{ctos} \times C_{sap\_wood} \tag{S33}$$

where k_{ctos} is a PFT-specific parameters.

20   For both trees and grasses, fine root and leaves are assumed to be in homeostatic balance between transpiring leaf surface and root mass

$$C_{leaf} = f^{ltor} \times k_{rtos} \times \frac{k_{latosa}}{sla \times \rho_{wood}} \times C_{fine\_root} \tag{S34}$$

where k_{rtos}, sla, k_{latosa}, and ρ_{wood} are PFT-specific parameters. f^{ltor} is the long-term average (τ_{mavg}^{alloc}) of the nutrient and water limitation scalar, which represents the widely observed phenomenon of increased root allocation with water or nutrient
25   shortage and is calculated here as the minimum of three functions describing N, P and water limitation respectively, calculated as:

$$f^{ltor} = min(\frac{N_{labile}/C_{labile}}{req_{NC}^{growth}}, \frac{P_{labile}/N_{labile}}{req_{PN}^{growth}}, \frac{W_{soil,root}}{W_{soil,crit}^{alloc}}) \tag{S35}$$

X_{labile} refers to the content of the respective element in the labile pool and req_{NC}^{growth} and req_{PN}^{growth} are the N:C and P:N ratios required for growth, respectively (see eqn. S27). For the water limited allocation, $W_{soil,crit}^{alloc}$ is the critical level of soil moisture below which root allocation increases and $W_{soil,root}$ is calculated as the ratio between the current water content in the root zone and the water content in the root zone at field capacity.

S3.5 Tissue stoichiometry

Following Meyerholt and Zaehle (2015), C:N:P stoichiometry for slow-overturning structural tissues (sap wood, coarse roots) as well as fruits, is assumed to be time-invariant and modelled as dependent on the PFT-specific mean foliar stoichiometry ($\chi_{leaf}^{C:N}$, and $\chi_{leaf}^{N:P}$) and set ratios (see Table S3). Heartwood stoichiometry differs from sapwood stoichiometry because a fraction of the nutrients are retranslocated (k_{resorb}^{wood}) to the labile pool upon heartwood formation.

Following Zaehle and Friend (2010), the C:N and N:P ratios of leaves are varied in response to the nutrient demand and supply so that:

$$\chi_{leaf|t+1}^{X:Y} = \chi_{leaf}^{X:Y} \times (1 + \delta_{leaf}^{\chi} \times \Gamma_{XY}) \tag{S36}$$

where $\chi_{leaf}^{X:Y}$ denotes either the C:N or N:P ratio of the leaves, δ_{leaf}^{χ} is a parameter denoting the maximum amount that leaf nutrients can change per timestep and $\Gamma_{X:Y}$ heuristically accounts for limits to the plasticity of foliar stoichiometry as:

$$\Gamma_{X:Y} = \begin{cases} e^{-(\lambda_{leaf}^{\chi} \frac{\chi_{leaf}^{X:Y}}{\chi_{leaf,min}^{X:Y} + \chi_{leaf,max}^{X:Y}})^{k_{leaf}^{\chi}}} & \text{if } \chi_{labile}^{Y:X} \leq req_{Y:X}^{growth} \\ -(1 - e^{-(\lambda_{leaf}^{\chi} \frac{\chi_{leaf}^{X:Y}}{\chi_{leaf,min}^{X:Y} + \chi_{leaf,max}^{X:Y}})^{k_{leaf}^{\chi}}}) & \text{if } \chi_{labile}^{Y:X} > req_{Y:X}^{growth} \end{cases} \tag{S37}$$

In the above, $\chi_{leaf,min}^{X:Y}$ and $\chi_{leaf,max}^{X:Y}$ are PFT-specific parameters. The λ_{leaf}^{χ} and k_{leaf}^{χ} are parameters (Tab. S3) The condition refers to the relationship between the nutrients available for growth in the labile pool and the nutrients required for growth (Eq. S27), averaged at the time-scale of τ_{mavg}^{χ}. The stoichiometric ratios of the fine roots vary proportionally to those of the leaves, whereas the stoichiometry of wood is assumed time-invariant (Meyerholt and Zaehle, 2015). The stoichiometry of the labile and reserve pools are prognostic properties, as described in Sect. S3.6.

S3.6 Long-term reserve dynamics

While labile-reserve dynamics have been part of the OCN model (Zaehle and Friend, 2010), the underlying equations have been reworked to increase robustness and traceability. The target leaf carbon pool (C_{leaf}^{target}) is determined by the current allometry, and corresponds to the leaf area index implied by current sapwood area.

The target labile carbon pool size buffers short term fluctuations in GPP, and is assumed to correspond to the maximum of the cumulated GPP or R_m over the turnover time of the labile pool, while the target of the labile nitrogen and phosphorus

11

pool corresponds to the average stoichiometric growth requirement over the turnover time of the labile pool:

$$C_{labile}^{target} = max(\int_{t=-\tau_{labile}^0}^{t=0} GPP \times dt, \int_{t=-\tau_{labile}^0}^{t=0} R_m \times dt) \tag{S38a}$$

$$N_{labile}^{target} = req_{NC}^{growth} \times C_{labile}^{target} \tag{S38b}$$

$$P_{labile}^{target} = req_{PN}^{growth} \times N_{labile}^{target} \tag{S38c}$$

5   The target size of the reserve pool depends on the C required to replace the annual growth of leaves and fine roots. It is scaled by a PFT-specific constant as a measure of risk avoidance ($k_{reserve}^{target}$), with larger values indicating a preference for storage over growth.

$$C_{reserve}^{target} = min(k_{reserve} \times (1 + f_{resp,growth}) \times \frac{LAI^{target}}{sla}, \sum_{i=l,f,s} f_{reserve,max,i} \times C_i), where \tag{S39a}$$

$$k_{reserve} = k_{reserve}^{target} \times (min(1, \frac{1}{\tau_{leaf}}) + \frac{1}{\tau_{fine\_root} \times R_{leaf:fine\_root}}) \tag{S39b}$$

10   where LAI^{target} is the target leaf area index, which is constrained to values below LAI_{max}^{target} (see Sect. S3.4) and sla the PFT-specific specific leaf area, τ_{leaf} and τ_{fine_root} are the PFT-specific turnover times of foliage and fine roots, and $R_{leaf:fine\_root}$ is the leaf to root ratio (Eq. S35) averaged over the lifetime of the fine roots (τ_{mavg}^{root}). The N and P target pools are defined in an equivalent manner, respecting the current target stoichiometry of leaves and fine roots (Sect. S3.5).

    The net exchange between the labile and reserve pool is calculated as

15
$$\Delta S_X = \frac{1}{\tau_{labile}} \times (\Phi_{maint}^X \times X_{reserve} - \Phi_{store}^X \times X_{labile}) \times dt; with \tag{S40a}$$

$$\Phi_{maint}^X = e^{-(\lambda_{maint}^\Phi \times \frac{X_{labile}}{X_{labile}^{target}})^{k_{maint}^\Phi}}, and \tag{S40b}$$

$$\Phi_{store}^X = 1 - e^{-(\lambda_{store}^\Phi \times \frac{X_{reserve}}{X_{reserve}^{target}})^{k_{store}^\Phi}} \tag{S40c}$$

where λ_{maint}^Φ, k_{maint}^Φ, λ_{store}^Φ, and k_{store}^Φ are parameters of a Weibull-type function. Under conditions of severe resource stress (i.e. low labile pool size corresponding to its target size), the build up of reserves, is reduced according to

20
$$\Phi_{store}^X = \frac{1 - \Phi_{maint}^X}{1 - k_{\Phi,inter}} \Phi_{store}^X, \; if \; \Phi_{maint}^X > k_{\Phi,inter} \tag{S41}$$

where $k_{\Phi,inter}$ is a parameter. To support leaf and fine-root growth at the beginning of the growing season, ΔS_X is further modified by the phenological pull (Φ_{phen}^X) during the growing season as follows:

$$\Delta S_X = \Delta S_X + k^*_{labile} \times \Phi^X_{phen} \times X_{reserve} \times dt, with \tag{S42a}$$

$$\Phi^X_{phen} = e^{-(\lambda^\Phi_{phen} \times \frac{X_{leaf}}{X^{target}_{leaf}})^{k^\Phi_{phen}}} \tag{S42b}$$

where λ^Φ_{phen}, and k^Φ_{phen} are parameters of a Weibull-type function.

S3.7 Photosynthetic sink limitation

The observation that growth and photosynthesis may differ in their response to environmental stressors (Hartmann et al., 2018) is considered in QUINCY such that in case the labile carbon pool exceeds its target size substantially because growth is limited by temperature, moisture, or because sufficient nutrients are lacking to allow growth (Eq. S28a), sink-limitation down-regulates photosynthetic activity so that:

$$\beta^{ps}_{sinklim} = \beta^{ps}_{sinklim,min} + (1 - \beta^{ps}_{sinklim,min}) \times e^{-(\lambda^{ps}_{sinklim} \times X)^{k^{ps}_{sinklim}}}, where \tag{S43a}$$

$$X = \frac{C_{labile} - C^{target}_{labile}}{C^{target}_{labile}} \tag{S43b}$$

Here, $\beta_{sinklim,min}$, $\lambda^{ps}_{sinklim}$ and $k^{ps}_{sinklim}$ are parameters (see Table S3) and C^{target}_{labile} is the target value for the labile pool (Eq. S38).

In addition, if the C:N or N:P ratios of the labile pool exceed those of the target labile pool, indicating strong nutrient stress, the sink limitation factor is further modified as a function of the stoichiometric ratio of the labile pool and that of the labile target as:

$$\beta^{ps}_{sinklim} = \beta^{ps}_{sinklim} \times min(1, \frac{\chi^{N:C}_{labile}}{k^{CNP}_{sinklim} \times \chi^{N:C}_{labile,target}}, \frac{\chi^{P:N}_{labile}}{k^{CNP}_{sinklim} \times \chi^{P:N}_{labile,target}}) \tag{S44}$$

where $k^{CNP}_{sinklim}$ is a parameter.

S3.8 Phenology

The phenology of vegetation, describing the seasonal development of foliage biomass, is simulated prognostically given the ability of the plant to grow new tissues, which depends on the size and turnover of the meristems (Eq. S28), as well as the fractional allocation of growth to plant organs (see Sect. S3.3). The start and end of the the growing season are determined by meteorological triggers and soil moisture, with plant growth set to zero outside the growing season (Eq. S28). The meteorological variables determining these phenological triggers are averaged over τ^{phen}_{mavg}, to smooth out the effect of day-to-day climate variability. While the beginning and ending mark the start and end of tissue production, only the turnover of the leaves is directly affected by phenological triggers. The turnover of all other tissues is assumed to be constant (see Sect. S3.9).

13

The model differentiates evergreen, cold deciduous, rain deciduous tree and shrub phenological strategies, as well as herbaceous perennial phenological strategies.

The growing season start for cold deciduous and herbaceous PFTs is described as a function of the accumulated growing degree days (GDD_{acc}) as:

$$GDD_{acc} > GDD_{req}^{max} \times exp^{-k_{dormance}^{GDD} \times NDD}, where \tag{S45a}$$

$$\frac{GDD_{acc}}{dt} = GDD_{acc} + MAX(t_{air} - t_{tair}^{GDD}, 0.0) \tag{S45b}$$

where GDD_{acc} denotes the current growing degree days above the temperature threshold (t_{air}^{GDD}) since the last beginning of dormancy, NDD is the number of dormancy days, taken as days since the last growing season, and $k_{dormance}^{GDD}$ is a PFT-specific parameter relating dormancy to the PFT-specific maximum growing degree days requirement (GDD_{req}^{max}) to account for the chilling requirements of the buds (Krinner et al., 2005), and dt denotes time-step in days.

For rain deciduous phenology, the start of the growing season is triggered when the soil moisture stress factor (β_{soil}^{gs}, see Eq. S18) is larger than a PFT-specific threshold (β_{soil}^{flush}). This criterion is also applied for herbaceous PFTs in addition to the GDD-criterion.

The end of the growing season for cold deciduous and herbaceous PFTs is triggered by decreasing average air temperatures below a PFT-specific temperature threshold (t_{air}^{sen}). For raingreen and herbaceous PFTs the end of the growing season is triggered when the soil moisture stress factor (β_{soil}^{gs}) becomes lower than a PFT-specific threshold (β_{soil}^{sen}). In addition, herbaceous PFTs end their growing season, once the weekly carbon balance ($GPP - R_m$) becomes negative. Senescence is generally only introduced once the leaf age has become larger than a PFT-specific threshold (age_{min}^{leaf}).

For the evergreen phenology, recovery of photosynthesis in spring is delayed according to the state of acclimation (S) to air temperature, which reduces photosynthesis in spring until acclimation is reached (Mäkelä et al., 2004). S is calculated as

$$\frac{dS}{dt} = \frac{1}{\tau_{soa}}(T_{air} - S) \tag{S46}$$

,

where τ_{soa} is a time constant. The reduction factor for Rubisco- and electron transport limited photosynthesis (β_{soa}) is calculated as

$$\beta_{soa} = \frac{(S - T_{min}^{soa})}{(T_{max}^{soa} - T_{min}^{soa})} \tag{S47}$$

where T_{min}^{soa} and T_{max}^{soa} are parameters and β_{soa} is constrained to the range 0.1 and 1. S is updated according to this equation starting from a set initial value.

S3.9 Turnover

As in OCN (Zaehle and Friend, 2010), the breakdown of leaf and fine-root nutrients occurs at the time-scale of $\tau_{nut\_recycle}$. The freed nutrients enter the labile pool and are replaced by new nutrients of the labile pool according to the current target C:N:P of the respective pool.

$$5 \quad \frac{X_{pool}}{dt} = (Y_{pool} \frac{X_{pool}^{target}}{Y_{pool}^{target}} - X_{pool}) \times 1/\tau_{nut\_recycle}, \tag{S48}$$

where X is either N or P, and Y C or N, respectively. The flux from the labile pool is limited by the turnover rate and size of the labile pool to ascertain that the latter cannot be exhausted.

The turnover time of most tissue types (fine and coarse roots, sapwood, and fruits) is assumed constant for each PFT (τ_{fine_root}, τ_{coarse_root}, τ_{sap_wood}, and τ_{fruit}, respectively). The fruit pool is turning into seed bed pool, which is either used
10 for re-establishment of new seedlings or turned over to form litter. While roots turn directly into litter, only a small fraction of sapwood ($f_{sap\_wood}^{branch}$) is turned to litter, assuming it is lost as branches ($\tau_{branches}$), whereas the predominant fraction of sapwood turns into non-respiring hardwood at the timescale of τ_{sap_wood}. In evergreen trees, foliar turnover to litter is assumed to be constant (τ_{leaves}). For deciduous and herbaceous PFTs only minor turnover happens at τ_{leaves} during the growing season. At the end of the growing season (see Sect. S3.8), foliar turnover is set to a constant rate

$$15 \quad f_{turn}^{leaf} = min(f_{shed,max} \times \frac{LAI^{target}}{LAI}, 1) \tag{S49}$$

Resorption of nutrients to the labile pool during litterfall is assumed to only occur during foliage turnover (leaf scenescence) and the conversion from life sap-wood to dead heartwood (see for instance data in White et al., 2000) at a constant fraction (k_{resorb}^{X}), whereas fine root turnover is assumed to be dominated by predation and therefore no nutrient resorption is assumed to occur. so that:

$$20 \quad flux_{pool \to litter}^{X} = (1 - k_{resorb}^{X}) \times \frac{X_{pool}}{\tau_{pool}} \times dt, and \tag{S50a}$$

$$flux_{pool \to labile}^{X} = k_{resorb}^{X} \times \frac{X_{pool}}{\tau_{pool}} \times dt, \tag{S50b}$$

where $flux_{pool \to litter}^{X}$ is the litterfall from any one pool, and $flux_{pool \to labile}^{X}$ the retranslocated flux into the labile pool.

S3.10 Vegetation dynamics

Vegetation dynamics follow largely Sitch et al. (2003). To assess stand density, we define for tree functional types the crown
25 area as:

$$CA = k_{CA} \times D^{k_{rp}} \tag{S51}$$

where k_{CA} and k_{rp} are parameters, D is the tree diameter at breast hight and CA is constrained to be less then a maximum crown area (CA_{max}). Using stand-scale LAI, individuum density ($dens_{ind}$, see Eq. S58) and crown area, the LAI of an individual tree is defined (LAI_{ind}), which is used to calculate the foliage projective cover (FPC) as:

$$FPC = CA \times dens_{ind}(1 - e^{-k_{fpc} \times LAI_{ind}}) \tag{S52}$$

5   where k_{fpc} is a parameter. To avoid strong seasonal cycles in foliage projective cover for the calculation of vegetation dynamics (Krinner et al., 2005; Zaehle and Friend, 2010), LAI_{ind} is diagnosed from the sapwood area implied by the pipe-model (Eq. S31), implying that FPC is essentially representing last year's maximum LAI. For grasses, the calculation of FPC is not required and it is set to zero.

     Differently to Sitch et al. (2003) and Zaehle and Friend (2010), the establishment flux for a PFT is dependent on the size of the 10 seed-bed pool, which itself is dependent on the turnover of the fruit pool, and an average, PFT-specific seed-bed turnover time ($\tau_{seed,est}$). The motivation for this change is that this allows to close the carbon and nutrient budgets during re-establishment and avoids the addition of extra mass during re-establishment of a population.

$$flux_{est,X} = f_{dens} \times f_{temp} \times f_{moist} \times \frac{X_{seed\_bed}}{\tau_{seed,est}} \tag{S53}$$

     where f_{temp} and f_{moist} represent limitations for establishment at low temperature and low moisture availability in the 15 form of Weibull-functions with parameters λ_{est}^{env} and k_{est}^{env}, where env refers to either weekly air temperature (T_{air}) or weekly top-soil moisture (Θ_1). Density dependency of establishment (f_{dens}) is modelled as in Sitch et al. (2003):

$$f_{dens} = MAX(FPC_{max} - FPC, 0) \tag{S54}$$

     Three types of mortality are considered as additive processes, growth-efficiency related mortality ($mort_{greff}$), density dependent mortality ($mort_{dens}$), and a PFT-specific background mortality, representing currently unaccounted for processes 20 such as disturbance or grazing.

$$f_{mort} = MIN(mort_{greff} + mort_{dens} + mort_{bg,PFT}, 1) \tag{S55}$$

     Growth-efficiency mortality, represents any kind of mortality associated with trees lacking the ability to defend themselves against stress (e.g. pathogens) and is calculated as:

$$mort_{greff} = \frac{k1_{mort\_greff}}{1 + k2_{mort\_greff} \times eff_{growth}}, where \tag{S56a}$$

25 $$eff_{growth} = \frac{NPP - \sum Turnover_i}{LAI} \tag{S56b}$$

where, as in Sitch et al. (2003), $k1_{mort\_greff}$ and $k2_{mort\_greff}$ are parameters and growth efficiency depends on net primary production minus tissue turnover (of all tissues i) per unit leaf area, calculated as running means over $\tau_{mavg}^{dynamics}$.

Space constraints in tree populations (as for grasses FPC is zero) are considered by constraining the foliage projected cover to a prescribed maximum (FPC_{max}):

$$mort_{dens} = MAX(FPC - FPC_{max}, 0) \tag{S57}$$

Litterfall from vegetation dynamics is then the product of the current pool size and f_{mort}, scaled to the timestep of the model.

For trees, the appropriate number of individuals is also removed following mortality. This does not affect the size of trees, as woody biomass and stand density are modified proportionally. On the other hand, during establishment the total pool size increases, as mass is added to the labile pools, but the average size of individuals decreases due to the added number of (small) individuals. In total, the change in vegetation individual density following establishment and mortality is written as:

$$\frac{dens_{ind}}{dt} = f_{mort} \times dens_{ind} + \frac{flux_{est,C}}{k_{seed}} \tag{S58}$$

where $flux_{est,C}$ is the carbon flux defined by Eq. S53, and k_{seed} is the PFT-specific seed size.

S4   Soil biogeochemistry

The dynamics of the soil organic pools (X_i; i = met (metabolic litter), str (structural litter), wl (woody litter), fast, slow; see Section S4.3) are structurally simplified from Parton et al. (1993), but applied here for a vertically explicit soil including a vertical transport term and are described in general as:

$$\frac{\partial}{\partial t}X_{met} = \sum(f_{vp \to met}F_{L_{vp}}) + f_{wl \to met}\eta_{wl \to met}\frac{X_{wl}}{\tau_{wl}} - \frac{X_{met}}{\tau_{met}} \tag{S59a}$$

$$\frac{\partial}{\partial t}X_{str} = \sum(f_{vp \to str}F_{L_{vp}}) + f_{wl \to str}\eta_{wl \to str}\frac{X_{wl}}{\tau_{wl}} - \frac{X_{str}}{\tau_{str}} \tag{S59b}$$

$$\frac{\partial}{\partial t}X_{wl} = \sum(f_{vp \to wl}F_{L_{vp}}) - \frac{X_{wl}}{\tau_{wl}} \tag{S59c}$$

$$\frac{\partial}{\partial t}X_{fast} = \eta_{l \to fast}(\frac{X_{met}}{\tau_{met}} + \frac{X_{str}}{\tau_{str}}) + \eta_{slow \to fast}\frac{X_{slow}}{\tau_{slow}} - \frac{X_{fast}}{\tau_{fast}} + \Phi_{l \to fast} + \Phi_{slow \to fast} + \frac{\partial}{\partial z}(D_b\frac{\partial X_{fast}}{\partial z}) \tag{S59d}$$

$$\frac{\partial}{\partial t}X_{slow} = \eta_{fast \to slow}\frac{X_{fast}}{\tau_{fast}} - \frac{X_{slow}}{\tau_{slow}} + \Phi_{fast \to slow} + \frac{\partial}{\partial z}(D_b\frac{\partial X_{slow}}{\partial z}) \tag{S59e}$$

where $F_{L_{vp}}$ is the litterfall of the various plant tissue types, $f_{vp \to i}$ are the coefficients determining the partitioning of this litterfall to the litter pools (see Section S4.1), τ_i are temperature and moisture adjusted, nitrogen-limited turnover times of the respective pools (X; i = met (metabolic litter), str (structural litter), wl (woody litter), fast, slow; see Section S4.3). In the following sections we refer to the fast pool as the microbial pool, as while microbes are not explicitly modelled in the current

model version, the fast pool is meant to largely represent the microbial pool. $\eta_{i \to j}$ are the mass transfer from pool i to j (see Section S4.3), the Φ_x are the net mineralisation terms for N and P, respectively, required to balance the carbon inflow to the fast and slow SOM pools and their respective C:N:P stoichiometry (see Sect. S4.3). The transfer of soil organic matter through bioturbation is represented with a prescribed diffusion constant (see Sect. S4.4).

The dynamics of the inorganic nitrogen pools generally follow Zaehle and Friend (2010, but with updated process formulations and explicit vertical transport) and are given by:

$$\frac{\partial}{\partial t}NH_4 = F_{dep,NH_4} - U_{plant,NH_4} - \sum(\Phi_{i,NH_4}) - U_{nit} - \frac{\partial v_{NH_4}NH_4}{\partial z} \tag{S60a}$$

$$\frac{\partial}{\partial t}NO_3 = F_{dep,NO_3} + F_{nit,NO3} - U_{plant,NO_3} - \sum(\Phi_{i,NO_3}) - U_{denit} - \frac{\partial v_{NO_3}NO_3}{\partial z} \tag{S60b}$$

$$\frac{\partial}{\partial t}NO_y = F_{nit,NO_y} + F_{denit,NO_y} - E_{NO_y} \tag{S60c}$$

$$\frac{\partial}{\partial t}N_2O = F_{nit,N_2O} + F_{denit,N_2O} - E_{N_2O} \tag{S60d}$$

$$\frac{\partial}{\partial t}N_2 = F_{nit,N_2} + F_{denit,N_2} - E_{N_2} \tag{S60e}$$

where U are the uptake rates of plants, or (de-)nitrifying bacteria, respectively (see Section S4.5 and S4.7, respectively); the F_{dep} are the atmospheric deposition fluxes; the $F_{nit,i}$, and $F_{denit,i}$ are the production of NO_y, N_2O and N_2 by nitrification and denitrification, respectively; and $\frac{\partial v_x X}{\partial z}$ the vertical transport loss term given by the product of ion concentration and water mass flow between soil layers (see Sect. S6.3). Sorption of NH_4 is not explicitly modelled, and is accounted for by a reduced mobility in water (f_{leach,NH_4}).

The dynamics of the inorganic phosphorus pools generally follows Wang et al. (2010) are described as:

$$\frac{\partial}{\partial t}PO_4 = F_{dep,PO_4} + F_{weath,PO_4} + F_{biomin,PO_4} - U_{plant,PO_4} - F_{adsorp,PO_4} - \sum(\Phi_{i,PO_4}) - \frac{\partial v_{PO_4}PO_4}{\partial z} \tag{S61a}$$

$$\frac{\partial}{\partial t}P_{lab} = F_{adsorp,PO_4} - F_{desorp,PO_4} + \frac{\partial}{\partial z}(D_b\frac{\partial P_{lab}}{\partial z}) \tag{S61b}$$

$$\frac{\partial}{\partial t}P_{sorb} = F_{desorp,PO_4} - F_{occlusion,PO_4} + \frac{\partial}{\partial z}(D_b\frac{\partial P_{sorb}}{\partial z}) \tag{S61c}$$

$$\frac{\partial}{\partial t}P_{ocl} = k_{ocl}P_{sorb} + \frac{\partial}{\partial z}(D_b\frac{\partial P_{ocl}}{\partial z}) \tag{S61d}$$

$$\frac{\partial}{\partial t}P_{primary} = -F_{weath,PO_4} \tag{S61e}$$

where P_{lab}, P_{sorb}, P_{ocl}, and $P_{primary}$ are labile, absorbed, occluded, and primary P, respectively; the F_{dep,PO_4}, F_{weath,PO_4}, F_{biomin,PO_4}, F_{adsorp,PO_4}, and F_{adsorp,PO_4} are the atmospheric deposition, weathering, fast adsorption, and phosphorus fluxes, respectively (see Section S4.8). All pools except the primary phosphorus pool are assumed to be affected by bioturbation (see Sect. S4.4).

S4.1 Partitioning of litterfall to litter pools

Non-woody litterfall is partitioned to the metabolic and structural litter according to the CENTURY approach (Parton et al., 1993). Litter from labile and reserve pools is assumed to enter the metabolic pools, litter from sap- and heartwood enters the

woody pool. The metabolic fraction of litterfall from each vegetation pool ($_{vp}$, i.e. leaves, fine and coarse roots, fruits and seed-bed) is determined as:

$$f_{vp \to met, C} = f_{met, max, C} - k_{met, C} \times LC_{vp} \frac{C_{vp}}{N_{vp}} \tag{S62}$$

where $f_{vp \to met, C}$ is constrained to positive solutions, $f_{met, max, C}$ is the maximum fraction allocated to the metabolic pool, $k_{met, C}$ a factor relating the metabolic litter fraction to the lignin to nitrogen ratio, LC_{vp} the tissue-specific fraction of the lignin content of that tissue type, and $\frac{C_{vp}}{N_{vp}}$ the C:N ratio of litterfall from that tissue. The lignin content is assumed constant for all but the leaf tissues. For the latter, an empirical dependency between lignin content and specific leaf-area (sla) is used (White et al., 2000).

$$LC_{leaf} = LC_{leaf, max} + k_{leaf2sla} \times sla \tag{S63}$$

The remainder of litterfall is allocated to the structural pool. For N and P, the partitioning assumes that the relative proportions of C:N and N:P are preserved in the partitioning according to:

$$f_{vp \to met, X} = \frac{1}{1 + \frac{1 - f_{vp \to met, C}}{k_{met, vp, X} \times f_{vp \to met, C}}} \tag{S64}$$

Contrary to versions of the CENTURY model, woody decomposition is assumed to be a two-stage process to account for the large fraction of CO_2 loss during woody decomposition. The first step implies physical destabilisation and a first level of biochemical processing, which releases a constant fraction of carbon ($1 - \eta_{C, wl \to met, str}$) to heterotrophic respiration. During this step, a fraction of the nutrients ($1 - \eta_N | \eta_P$) is leached to the mineral phase to account for inefficiencies of the microbiota in mineral processing decomposing wood. The remaining destabilised woody material ($\eta_{C, wl \to met, str}$) is assumed to enter the metabolic and structural litter (Eq. S62 and S64) and is then decomposed as such.

S4.2 SOM and litter turnover rates

The turnover times (τ_i^{base}) of the litter and SOM pools respond to soil temperature (T_{soil}) following a peaked Arrhenius function (with parameters for the activation ($E_{a, decomp}$) and de-activation ($E_{d, decomp}$) of soil organic matter decomposition, see Tab. S4), and the soil matrix potential (Ψ_{soil}) as follows:

$$\tau_i^* = \tau_i^{base} \times f(T_{soil}) \times g(\Psi_{soil}), \; where \tag{S65a}$$

$$f(T_{soil}) = \frac{E_{d, decomp} \times e^{E_{a, decomp} \times T}}{E_{d, decomp} - E_{a, decomp} \times (1 - e^{E_{d, decomp} \times T})}, \; with \tag{S65b}$$

$$T = \frac{T_{soil} - T_{opt, decomp}}{T_{soil} \times T_{opt, decomp} \times R}, \; and \tag{S65c}$$

$$g(\Psi_{soil}) = 1 - \Psi_{soil} / \Psi_{dec, min} \tag{S65d}$$

S4.3 SOM formation

Matter entering the fast and slow SOM pool (Eq. S59) is required to fulfill the prescribed stoichiometry of the SOM pools (χ_{SOM}). These are assumed constant with the exception of the fast SOM C:N ratio, which varies with available NH_4 following

CENTURY (Parton et al., 1993):

$$\chi_{SOM^{C:N}_{fast}} = MAX(\chi_{SOM^{C:N}_{fast,max}} - f_\chi \times NH_4, \chi_{SOM^{C:N}_{fast,min}}) \tag{S66}$$

where $\chi_{SOM^{C:N}_{fast,min}}$, $\chi_{SOM^{C:N}_{fast,max}}$ and f_χ are parameters.

The difference in stoichiometry of the matter entering the pool and the required stoichiometry of the pool leads to the estimate of the potential immobilisation flux:

$$\Phi^*_{l\to fast,NH_4} = \frac{\eta_{C,litter\to fast}}{\chi_{SOM^{C:N}_{fast}}}(\frac{C_{met}}{\tau^*_{met}} + \frac{C_{str}}{\tau^*_{str}}) - \eta_N(\frac{N_{met}}{\tau^*_{met}} + \frac{N_{str}}{\tau^*_{str}}) \tag{S67}$$

where τ^*_i are the temperature and moisture constrained turnover times (Eq. S65).

The actual immobilisation rate ($\Phi_{l\to fast,NH_4}$) is limited to the amount of ammonium (NH_4 available, subject to co-occurring potential N uptake from plants ($U^*_{NH_4,plant}$, Eq. S73), and nitrifiers (U^*_{nit}; Eq. S76). Note that, similar as for the plant uptake, the uptake of ammonium is limited by Michaelis-Menten kinetics to account for reduced accessibility of N at very low values.

$$\Phi_{l\to fast,NH_4} = \frac{NH_4}{max(NH_4, U^*_{NH_4,plant} + U^*_{nit} + \Phi^*_{l\to fast,NH_4})} \times \Phi^*_{l\to fast,NH_4} \tag{S68}$$

In the case that the amount of available nitrogen ($\Phi_{l\to fast,NH_4}$) is insufficient to ensure that the newly formed fast SOM has a C:N ratio of $\chi_{SOM^{C:N}_{fast}}$, the turnover times of the metabolic and structural litter pool are increased, leading to a reduced decomposition rate of litter and therefore a reduced immobilisation requirement for litter decomposition (Parton et al. (1993)):

$$\tau_{met|str} = \tau^*_{met|str} \frac{\frac{\eta_{l\to fast,C}}{\chi_{SOM^{C:N}_{fast}}}(\frac{C_{met}}{\tau^*_{met}} + \frac{C_{str}}{\tau^*_{str}}) - \eta_N(\frac{N_{met}}{\tau^*_{met}} + \frac{N_{str}}{\tau^*_{str}})}{\Phi_{l\to fast,NH_4}} \tag{S69}$$

Should the available NH_4 be insufficient to maintain the uptake rates of plants (Eq. S73) and nitrifiers (Eq. S76), these fluxes are downregulated in proportion.

The potential immobilisation flux of phosphorus ($\Phi^*_{P,l\to fast}$) is defined in a similar manner as potential NH_4 immobilisation, but now considering the actual turnover time of the litter pools:

$$\Phi^*_{P,l\to fast} = \frac{\eta_{C,litter\to fast}}{\chi_{SOM^{C:N}_{fast}}\chi_{SOM^{N:P}_{fast}}}(\frac{C_{met}}{\tau_{met}} + \frac{C_{str}}{\tau_{str}}) - \eta_P(\frac{P_{met}}{\tau_{met}} + \frac{P_{str}}{\tau_{str}}) \tag{S70a}$$

$$\Phi_{P,l\to fast} = \frac{PO_4}{max(PO_4, U^*_{PO_4,plant} + \Phi^*_{P,l\to fast})} \times \Phi^*_{P,l\to fast} \tag{S70b}$$

Because the C:N:P stoichiometry and uptake use-efficiencies are organised such that decomposition of these pools is always leading to net mineralisation of nutrients, the $\Phi_{slow\to fast}$ values are negative and do not require special treatment to affect the carbon-use efficiency or turnover rates (i.e. $\tau_{fast} = \tau^*_{fast}$, and $\tau_{slow} = \tau^*_{slow}$). The processing of fast and slow SOM is assumed to also include higher-order trophic levels of heterotrophic respiration Parton et al. (1993), therefore only a fraction of the respired material ($\eta_{C,fast\to slow}$ and $\eta_{C,slow\to fast}$) is assumed to enter the subsequent pool:

$$\Phi_{fast \to slow, NH_4} = \frac{\frac{\eta_{C,fast \to slow}}{\chi_{SOM_{slow}^{C:N}}} C_{fast} - N_{fast}}{\tau_{fast}} \tag{S71a}$$

$$\Phi_{slow \to fast, NH_4} = \frac{\frac{\eta_{C,slow \to fast}}{\chi_{SOM_{fast}^{C:N}}} C_{slow} - N_{slow}}{\tau_{slow}} \tag{S71b}$$

$$\Phi_{fast \to slow, PO_4} = \frac{\frac{\eta_{C,fast \to slow}}{\chi_{SOM_{slow}^{C:N}} \chi_{SOM_{slow}^{N:P}}} C_{fast} - P_{fast}}{\tau_{fast}} \tag{S71c}$$

$$\Phi_{slow \to fast, PO_4} = \frac{\frac{\eta_{C,slow \to fast}}{\chi_{SOM_{fast}^{C:N}} \chi_{SOM_{fast}^{N:P}}} C_{slow} - P_{slow}}{\tau_{slow}} - F_{biomin, PO_4} \tag{S71d}$$

S4.4 Bioturbation

Bioturbation is treated as simple diffusive flux with a rate constant D_b, as in Koven et al. (2013), but declining with soil depth in proportion to the fraction of roots in the layer to account for reduced biological activity with increasing soil depth:

$$D_b = \frac{root_{frac}}{dz} \times \frac{k_{org}^{diff}}{\rho_{soil}^{cor}}, \; and \tag{S72a}$$

$$\rho_{soil}^{cor} = MAX(\rho_{org}^{bulk}, \rho_{OM} + \rho_{soil} - \rho_{OM} \frac{\rho_{soil}}{\rho_{org}^{bulk}}) \tag{S72b}$$

where $root_{frac}$ and dz are the root fraction and depth of the soil layer, ρ_{soil}^{cor} is the soil bulk density corrected with soil organic matter, ρ_{org}^{bulk} is the bulk density of organic material, ρ_{OM} is the organic matter density of the soil layer which depends on the organic matter content in the soil layer, ρ_{soil} is the bulk density of fine mineral soil, and k_{org}^{diff} is the diffusion coefficient for organic material due to bioturbation.

S4.5 Plant uptake rates

The potential uptake rates of plants for X= NH_4, NO_3, and PO_4 follow an extended Michaelis-Menten kinetics:

$$U_X^* = v_{max,X}(T_{soil}, \Psi) \times X \times (K_{m1,X}(T_{soil}, \Theta) + \frac{1}{K_{m2,X}(T_{soil}, \Theta) + X}) \times f_{demand}^X \times C_{fine\_root}, \; where \tag{S73a}$$

$$v_{max,X}(T_{soil}, \Psi) = v_{max,X} \frac{E_{d,uptake} \times e^{E_{a,uptake} \times T}}{E_{d,uptake} - E_{a,uptake} \times (1 - e^{E_{d,uptake} \times T})} \times \frac{\Psi_{fine\_root}}{\Psi_{leaf,min}}, \; with \tag{S73b}$$

$$T = \frac{T_{soil} - T_{opt,uptake}}{T_{soil} \times T_{opt,uptake} \times R}, \; and \tag{S73c}$$

$$K_{m1,X}(T_{soil}, \Theta) = K_{m1,X} / (e^{-\frac{E_{a,hsc}}{R} \times (\frac{1}{T_{soil}} - \frac{1}{T_{ref}^r})} \times (\frac{\Theta}{\Theta_{fc}})^{k_{hsc}}), \; and \tag{S73d}$$

$$K_{m2,X}(T_{soil}, \Theta) = K_{m2,X} \times e^{-\frac{E_{a,hsc}}{R} \times (\frac{1}{T_{soil}} - \frac{1}{T_{ref}^r})} \times (\frac{\Theta}{\Theta_{fc}})^{k_{hsc}}, \; and \tag{S73e}$$

$$f_{demand}^X = 1 - e^{-(\frac{\chi_{max}^{X:Y} - \chi_{labile}^{X:Y}}{\chi_{max}^{X:Y} \times (1 - K_{demand}^{half,X})})^{k_{demand}}} \tag{S73f}$$

where $v_{max,X}$ is the PFT-specific temperature-sensitive maximum uptake rate per unit biomass, adjusted by the current root zone moisture potential (Ψ_{fine_root}) to account for limited transport of nutrients towards the roots in dry soils, C_{fine_root} is the biomass density of fine roots (mol C m^{-3}, see Eq. S3), T_{soil} is the soil temperature and the K_m parameters are nutrient sensitivities of the low and high affinity transporters. These affinities are assumed to be temperature sensitive and are adjusted to soil moisture to account for the difference between mass-based and soil solution concentrations (Ahrens et al., 2015). The potential uptake of nutrients can be down-regulated by plants given their internal demand f_{demand}^X, where X refers to either N or P and $X:Y$ refers to either the short-term average (τ_{mavg}^{uptake}) of the labile N:C or P:N ratios. $\chi_{max}^{X:Y}$ corresponds to the X:Y ratio of growing a unit of leaves and fine roots at the current leaf-to-root ratio (see S3.4, $K_{demand}^{half,X}$ is a parameter denoting the fraction of $\chi_{max}^{X:Y}$ at which uptake is reduced to 50% and k_{demand} is shape parameter.

S4.6 Asymbiotic biological nitrogen fixation

The asymbiotic biological nitrogen fixation (BNF) is represented as:

$$F_{BNF}^{NH_4} = v_{max,BNF} \times f(T_{soil}) \tag{S74}$$

where $v_{max,BNF}$ is a parameter representing the base rate of fixation and the temperature response is calculated as above (Eq. S65). BNF is suppressed if the sum of NH$_4$ and NO$_3$ in any soil layer exceeds a critical threshold N_{limit}^{BNF} (Zaehle et al., 2010). The distribution of $F_{BNF}^{NH_4}$ across soil layers follows the distribution of fine roots, as indicator for C inputs into the soil. All N fixed through this mechanism is added to the mineral NH$_4$ soil pool.

S4.7 Nitrification and denitrification

Calculation of nitrification and denitrification follows Xu-Ri and Prentice (2008); Zaehle et al. (2011), which relies on the separation of the soil into aerobic and anaerobic volume fractions ($anvf$):

$$anvf = e^{-(\lambda_{anvf} \times (1-afps))^{k_{anvf}}}, where \tag{S75a}$$

$$afps = \frac{W_{fc} - W_{soil}}{W_{fc}} \tag{S75b}$$

where λ_{anvf} and k_{anvf} are parameters, $afps$ is the air filled pore space, and the W_x are the soil moisture contents as defined in Sect. S6.3.

The potential rate of nitrification (U_{nit}^*) in the aerobic fraction of the soil is modified by temperature and soil moisture according to:

$$U_{nit}^* = v_{max,nit} \times f(T_{soil}) \times g(\Theta) \times NH_4, where \tag{S76a}$$

$$f(T_{soil}) = E_{d,nit} \frac{e^{\frac{E_{a,nit} \times kt}{R_{gas}}}}{E_{d,nit} - E_{a,nit} \times (1 - e^{\frac{E_{d,nit} \times kt}{R_{gas}}})} \tag{S76b}$$

$$kt = \frac{T_{soil} - T_{opt,nit}}{T_{soil} \times T_{opt,nit}} \tag{S76c}$$

$$g(\Theta) = 1 - afps \tag{S76d}$$

The actual rate of nitrification (U_{nit}), given the potential rate and competing demands from plant and microbial uptake (Sect. S4.3, is partitioned into its products (NO_3, NO_y, and N_2O) according to

$$F_{nit,NO_3} = (1 - f_{nit}^{NO_y} - f_{nit}^{N_2O}) \times U_{nit} \tag{S77a}$$

$$F_{nit,NO_y} = f_{nit}^{NO_y} \times U_{nit} \tag{S77b}$$

$$F_{nit,N_2O} = f_{nit}^{N_2O} \times U_{nit} \tag{S77c}$$

where the $F_{nit,X}$ are the nitrification fluxes for NO_3, NO_y, and N_2O, respectively (Eq. S60).

The potential rate of denitrification (U_{denit}^*) in the anaerobic fraction of the soil is modified by temperature:

$$U_{denit}^* = anvf \times v_{max,denit}(T_{soil}) \times \frac{C_{fast}}{K_{m,denit}^{fast} + C_{fast}} \frac{NO_3}{K_{m,denit}^{NO_3} + NO_3}, where \tag{S78a}$$

$$v_{max,denit}(T_{soil}) = v_{max,denit} \times e^{-\frac{E_{a,denit}}{R} \times (\frac{1}{T_{soil}} - \frac{1}{T_{ref}'})} \tag{S78b}$$

The actual rate of denitrification (U_{denit}), given the potential rate and competing demands from plant uptake (Sect. S4.3), is partitioned into its products (NO_y, N_2O, and N_2) according to

$$F_{denit,NO_y} = f_{denit}^{NO_y} \times U_{denit} \tag{S79a}$$

$$F_{denit,N_2O} = f_{denit}^{N_2O} \times U_{denit} \tag{S79b}$$

$$F_{denit,N_2} = (1 - f_{denit}^{NO_y} - f_{denit}^{NO_y}) \times U_{denit} \tag{S79c}$$

where the $F_{denit,X}$ are the denitrification fluxes for NO_y, N_2O, and N_2, respectively (Eq. S60). The model currently ignores the effect of ammonia volatilisation, which is of low relevance for natural, unfertilised ecosystems.

S4.8 Phosphorus weathering and biomineralisation

Weathering is modelled following Wang et al. (2010) as:

$$F_{weath,PO_4} = f(T_{soil}) \times g(\Theta) \times f(C_{fine\_root}) \times k_{weath} \times \rho_{soil}^{cor}, \ where \tag{S80a}$$

$$f(T_{soil}) = e^{-\frac{Ea,hsc}{R} \times (\frac{1}{T_{soil}} - \frac{1}{T_{ref}^r})}, \tag{S80b}$$

$$g(\Theta) = (\frac{\Theta}{\Theta_{fc}})^3, and \tag{S80c}$$

$$f(C_{fine\_root}) = \frac{C_{fine\_root}}{K_{m,weath}^{root} + C_{fine\_root}} \tag{S80d}$$

5 where k_{weath} is the rate constant for weathering, and ρ_{soil}^{cor} is the soil bulk density corrected by SOM content. The weathering rate decreases with soil depth as the fine root C decreases, given the half-saturation root density $K_{m,weath}^{root}$, and is modified by soil temperature and moisture.

The potential biomineralisation rate of PO$_4$ (McGill and Cole, 1981) is determined as an additional turnover of the P contained in the slow SOM pool, modified by temperature and moisture modifiers, and affected by the concentration of PO_4

10 and the root biomass:

$$F_{biomin,PO_4}^* = \frac{C_{slow}}{\chi_{SOM_{slow}^{C:N}} \times \chi_{SOM_{slow}^{N:P}} \times \tau_{biomin}} \times f(C_{fine\_root}) \times f(PO_4) \times f(T_{soil}) \times g(\Theta), \ where \tag{S81a}$$

$$f(C_{fine\_root}) = \frac{C_{fine\_root}}{K_{m,biomin}^{root} + C_{fine\_root}}, \ and \tag{S81b}$$

$$f(PO_4) = \frac{K_{m,biomin}^{PO_4}}{K_{m,biomin}^{PO_4} + PO_4} \tag{S81c}$$

where $K_{m,biomin}^{root}$ and $K_{m,biomin}^{PO_4}$ are constants constraining the biomineralisation rate under low root biomass and high PO_4

15 concentration, respectively; the temperature and moisture responses are calculated as those in Eq. S65. The biomineralisation rate is further constrained so that it does not alter the stoichiometry of the fast pool.

$$F_{biomin,PO_4} = MIN(F_{biomin,PO_4}^*, \frac{\frac{\eta_{C,slow \to fast}}{\chi_{SOM_{slow}^{C:N}} \chi_{SOM_{slow}^{N:P}}} C_{slow} - P_{slow}}{\tau_{slow}}) \tag{S82}$$

S4.9 Phosphorus adsorption and (ab)sorption

PO$_4$ desorption follows Yang et al. (2014):

20 $$F_{desorp,PO_4} = f(T_{soil}, E_{a,abs}) \times k_{abs} \times P_{lab} - f(T_{soil}, E_{a,des}) \times k_{des} \times P_{sorb}, \ where \tag{S83a}$$

$$f(T_{soil,E_a}) = e^{-\frac{E_a}{R} \times (\frac{1}{T_{soil}} - \frac{1}{T_{ref}^r})} \tag{S83b}$$

where k_{abs} and k_{des} are the rate constants of (ab)sorption and desorption, and $E_{a,abs}$ and $E_{a,des}$ the respective activation energies.

The adsorption (F_{adsorp,PO_4}) flux from soil solution to the soil adsorption sites is calculated assuming constant Langmuir equilibrium (Barrow, 1978) between soluble and adsorbed P:

$$PO_4 = \frac{S_{max} \times PO_4}{K_S + PO_4}, \, thus \tag{S84a}$$

$$\frac{\partial P_{lab}}{\partial t} = \frac{S_{max} \times PO_4}{(K_S + PO_4)^2} \frac{\partial PO_4}{\partial t}, \tag{S84b}$$

by rearranging Eq. S84b

$$\frac{\partial P_{lab}}{\partial t} = k_p \frac{\partial(P_{lab} + PO_4)}{\partial t} \tag{S84c}$$

$$\frac{\partial PO_4}{\partial t} = (1 - k_p)\frac{\partial(P_{lab} + PO_4)}{\partial t}, \, where \tag{S84d}$$

$$k_p = \frac{S_{max} \times PO_4}{(K_S + PO_4)^2 + S_{max}PO_4}, \tag{S84e}$$

where S_{max} and K_S are the maximum sorption capacity, and the half-saturation concentration coefficient of the soil, and are modified by soil moisture and SOM content as follows:

$$S_{max} = \Theta_{soil} \times (S_{om}^{max}V_{om}^{frac}\rho_{org}^{bulk} + S_{mineral}^{max}V_{mineral}^{frac}\rho_{soil}), \, and \tag{S85a}$$

$$K_S = K_{m,om}^{sorb}V_{om}^{frac}\rho_{org}^{bulk} + K_{m,mineral}^{sorb}V_{mineral}^{frac}\rho_{soil} \tag{S85b}$$

where V_{om}^{frac} and $V_{mineral}^{frac}$ are volumetric fractions of organic matter and fine soil minerals, respectively. S_{om}^{max} and $S_{mineral}^{max}$ are the maximum PO_4 sorption capacity of pure organic matter and pure fine soil, respectively. $K_{m,om}^{sorb}$ and $K_{m,mineral}^{sorb}$ are the half-saturation concentration coefficient of pure organic matter and pure fine soil, respectively.

Based on Eq.S60f and Eq.S61a, the equilibrium in Eq.S84 could be solved .

$$\frac{\partial(P_{lab} + PO_4)}{\partial t} = F_{dep,PO_4} + F_{weath,PO_4} + F_{biomin,PO_4} - U_{plant,PO_4} - F_{desorp,PO_4}$$
$$- \sum(\Phi_{i,PO_4}) - \frac{\partial v_{PO_4}PO_4}{\partial z} + \frac{\partial}{\partial z}(D_b \frac{\partial P_{lab}}{\partial z}) \tag{S86}$$

S4.10   Soil in- and outfluxes

Currently, gas diffusion is not modelled explicitly. Instead, CO_2 is assumed to be directly released to the atmosphere. The carbon efflux per soil layer is described as:

$$F_{CO_2}^{\uparrow} = ((1-\eta_{C,litter \to fast})(\frac{C_{met}}{\tau_{met}} + \frac{C_{str}}{\tau_{str}}) + (1-\eta_{C,wl \to met|str})\frac{C_{wl}}{\tau_{wl}} + (1-\eta_{C,fast \to slow})\frac{C_{fast}}{\tau_{fast}} + (1-\eta_{C,slow \to fast})\frac{C_{slow}}{\tau_{slow}})\Delta t, \tag{S87}$$

and similar for ^{13}C and ^{14}C fluxes.

Slightly differently from that, the emission of gaseous N species is assumed to follow Xu-Ri and Prentice (2008), which considers the effect of temperature and moisture on gas loss. However, transfer between soil layers is equally not treated explicitly.

$$F_X^\uparrow = f(T_{soil}) \times afps \times X, where \tag{S88a}$$

$$f(T_{soil}) = e^{-\frac{E_{a,diff}}{R} \times (\frac{1}{T_{soil}} - \frac{1}{T_{ref}^r})} \tag{S88b}$$

and $afps$ is the air-filled pore fraction of the soil (see Eq. S75.)

S5 Isotopic composition and fractionation

The carbon (C) and nitrogen (N) flows and pool tracked in the model are comprising all major isotopes (i.e. C = ^{12}C + ^{13}C + ^{14}C, and N = ^{14}N + ^{15}N). The model explicitly tracks the mass flow of ^{13}C, ^{14}C and ^{15}N as separate entities for all biogeochemical pools and fluxes. The molar mixing ratio (R_X) of the isotope (e.g. ^{13}C) to the main element (e.g. ^{12}C) of each biogeochemical pool can be calculated as

$$R_{13C} = \frac{^{13}C}{^{12}C} = \frac{^{13}C}{C - ^{13}C} \tag{S89}$$

and by convention

$$\delta_{13C} = (\frac{R_{13C}}{R_{ref,13C}} - 1) \times 1000 \tag{S90}$$

where $R_{ref,13C}$ is the reference isotopic molar mixing ratio and δ_{13C} is in ‰. Similar calculations are done for the ratio of ^{15}N to ^{14}N and the reference value $R_{ref,15N}$. By convention, the delta notation of ^{14}C is dependent on the ^{13}C content, see (Levin et al., 2010), and the molar mass of ^{14}C is ignored in the calculations of ^{13}C because of the extremely low concentrations.

Biogeochemical processes discriminate against the heavier isotope, and this fractionation process is treated by calculating the mixing ratio of the isotope of the resulting flux as

$$R_{sink} = \frac{R_{source}}{\frac{\epsilon_{process}}{1000} + 1} \tag{S91}$$

where R_{source} is the molar mixing ratio of the source pool of the reaction, R_{sink} is the molar mixing ratio of the resulting matter flux, and $\epsilon_{process}$ is a process and isotope specific discrimination rate.

Isotopic discrimination of ^{13}C and ^{14}C by photosynthesis is modelled according to the general equation derived by Farquhar et al. (1982); Drake (2014), so that

$$D_x = a_x + (c_x + \phi_{C4} \times b_x - a_x)\frac{c_i}{c_a} \tag{S92}$$

where a_x, and b_x are isotope-specific constants (^{13}C and ^{14}C, respectively, see Table S5). c_x and ϕ_{C4} account for the additional bundle-sheath processes in C4 plants. For C3 plants, these processes do not play a role and these parameters are 0 and 1, respectively. In the model, currently only photosynthesis is assumed to result in C-isotope discrimination, ignoring the effect of the smaller and uncertain discrimination by tissue construction, storage formation and respiration (Brüggemann et al., 2011).

Isotopic discrimination for various nitrogen cycle processes (biological nitrogen fixation, ammonification, plant and microbial N uptake, and processes associated with nitrification and denitrification) are taken from (Robinson, 2001). According to (Robinson, 2001), in case of near-complete consumption of the source pool, the discrimination is reduced as

$$\epsilon_{process}^{corr} = \epsilon_{process}(f_{source} - 1)log(\frac{1 - f_{source}}{f_{source}}) \tag{S93}$$

where f_{source} is the ratio of the source consumption to the source pool size.

S6 Radiation, surface energy balance and soil hydrology

S6.1 Net surface shortwave radiation budget

Canopy radiation interception is calculated with a multi-layer scheme following Spitters (1986), with radiation levels calculated at the mid-point of each canopy layer. The scheme uses up to 20 (default 10) canopy layers, with exponentially increasing layer thickness as the canopy depth increases. The original scheme, as used in OCN (Zaehle and Friend, 2010), has been extended to diagnose canopy albedo, to account for clumping (see eq. S96), and to approximate the attenuation of the shortwave radiation back-scatter from the soil to allow for a smooth transition of surface albedo from soil to vegetation values with increasing leaf coverage. The scheme is applied separately to the visible (vis) and near-infrared (nir) radiation band, where the parameterisation of the visible radiation is based on the assumption that the radiation interception and reflection are similar to that of the photosynthetically active range (i.e. 400-700 nm). In the following, the subscripts for visible and near-infrared are omitted for readability.

Light levels decrease exponentially in the canopy, such that the attenuation of direct (dr) and diffuse (df) top-of-the-canopy irradiance ($I_{dr\downarrow,0}$ and $I_{df\downarrow,0}$, respectively) at any cumulative leaf area index (LAI_c; from the top) is given by:

$$I_{df\downarrow} = (1 - \rho_{rad}) \times I_{df\downarrow,0} \times e^{-k_{df} \times LAI_c} \tag{S94a}$$

$$I_{dr\downarrow} = (1 - \rho_{rad}) \times I_{dr\downarrow,0} \times e^{-\sqrt{1-\sigma} \times k_{bl} \times LAI_c} \tag{S94b}$$

$$I_{dr,dr\downarrow} = I_{dr\downarrow,0} \times e^{-k_{bl} \times LAI_c} \tag{S94c}$$

$$I_{dr,df\downarrow} = I_{dr\downarrow} - I_{dr,dr\downarrow} \tag{S94d}$$

where $I_{dr,df\downarrow}$ is the diffuse part of the direct beam resulting from scattering of the direct beam and $I_{dr,dr\downarrow}$ is the direct beam remaining direct at the canopy depth LAI_c, and ρ_{rad} is the reflection coefficient of the green canopy, as defined in Eq. S97. For a spherical leaf angle distribution with leaves distributed randomly within the canopy volume, the extinction coefficients of the diffuse flux (k_{df}) and that of the direct component of the direct flux (k_{bl}) are approximated, respectively, by:

$$k_{df} = k_{df,0}\sqrt{1-\sigma} \times \Omega \tag{S95a}$$

$$k_{bl} = \frac{k_{bl,0} \times \Omega}{cos(\gamma^*)} \tag{S95b}$$

where Ω is the clumping index according to Campbell and Norman (1998), which is calculated as:

$$\Omega = \Omega_0/(\Omega_0 + (1 - \Omega_0) \times e^{-k_{csf} \times acos(\gamma^*)^{\phi_{crown}}}), \tag{S96}$$

where Ω_0 and ϕ_{crown} are the PFT-specific clumping factor at nadir and crown shape factor, respectively, and k_{csf} is a correction factor.

The reflection coefficient (ρ_{rad}) of the green canopy is given by:

$$\rho_{rad} = \frac{1 - \sqrt{1-\sigma}}{1 + \sqrt{1-\sigma}} \times \frac{2}{1 + \rho^{sbeta} \times cos(\gamma^*)}, \tag{S97}$$

where the first term on the right hand side is the reflection of a horizontally oriented canopy, and the second term empirically adjusts the reflection to a spherical distribution. σ is the PFT-specific single leaf scattering coefficient and ρ^{sbeta} is a conversion constant. Because all equations for leaf reflection and absorption coefficients are only valid for high solar elevation, the true zenith angle (γ) is constrained to values larger than $10°$ (γ^*). Note that Spitters (1986) use the sine of the solar elevation angle.

Below the canopy (bc), i.e. at the soil surface, the downwelling energy flux ($I_{bc\downarrow}$) is divided into a part that is absorbed by the soil ($I_{a,soil}$) and a part that is backscattered as diffuse radiation ($I_{bc\uparrow}$), depending on the soil's albedo (alb_{soil}):

$$I_{bc\downarrow} = (1 - \rho_{rad}) \times (I_{df\downarrow,0} \times e^{-k_{df} \times LAI} + I_{dr\downarrow,0} \times e^{-\sqrt{1-\sigma} \times k_{bl} \times LAI}) \tag{S98a}$$

$$I_{a,soil} = (1 - alb_{soil}) \times I_{bc\downarrow} \tag{S98b}$$

$$I_{bc\uparrow} = alb_{soil} \times I_{bc\downarrow} \tag{S98c}$$

To first-order, the diffuse light profile of the canopy accounting for the backscatter of diffuse radiation from the soil can be approximated as

$$I_{df\downarrow\uparrow} = (1 - \rho_{rad}) \times (I_{df\downarrow,0} \times e^{-k_{df} \times LAI_c} + \times I_{bc\uparrow} \times e^{-k_{df} \times (LAI - LAI_c)}) \tag{S99}$$

Absorption (A^{rad}) is taken to be complementary to transmission, therefore the absorbed diffuse and direct energy flux at a cumulative leaf area LAI_c can be written as:

$$A_{df}^{rad} = k_{df} \times I_{df\downarrow\uparrow} \tag{S100a}$$

$$A_{dr}^{rad} = (1-\sigma) \times k_{bl} \times I_{dr} \tag{S100b}$$

$$A_{dr,dr}^{rad} = (1-\sigma) \times k_{bl} \times I_{dr\downarrow,0} \times e^{-k_{bl}\times LAI_c} \tag{S100c}$$

$$A_{dr,df}^{rad} = A_{dr}^{rad} - A_{dr,dr}^{rad} \tag{S100d}$$

The canopy is then split into a sunlit and a shaded part, with the sunlit fraction defined as:

$$f_{sunlit} = e^{-k_{bl}\times LAI_c} \tag{S101}$$

following eq. S94c. The sunlit part receives both diffuse and direct radiation, whereas the shaded part only received diffuse radiation. Thus,

$$A_{shaded}^{rad} = A_{df}^{rad} + A_{dr,df}^{rad} \tag{S102a}$$

$$A_{sunlit}^{rad} = A_{shaded}^{rad} + (1-\sigma) \times k_{bl} \times I_{dr\downarrow,0} \tag{S102b}$$

The canopy albedo is diagnosed (rather than simply taken as ρ_{rad}) as:

$$alb_{can} = 1 - \frac{I_{bc\downarrow} + (1-f_{sunlit}) \times A_{shaded}^{rad} + f_{sunlit} \times A_{sunlit}^{rad}}{I_{df\downarrow,0} + I_{dr\downarrow,0}} \tag{S103}$$

The total shortwave upward flux is diffuse and calculated as the backscattered flux of the canopy plus the backscattered flux from the soil, which is transmitted diffusely through the canopy:

$$I_{df\uparrow} = alb_{can} \times (I_{df\downarrow,0} + I_{dr\downarrow,0} - I_{bc\downarrow}) + (1-\rho_{rad}) \times I_{bc\uparrow} \times e^{-k_{df}\times LAI} \tag{S104}$$

Based on this, the total surface albedo alb_{surf} (i.e. the albedo derived from vegetation and soil radiation transfer, absorption, and reflection) and net shortwave flux I_{net} can be calculated as:

$$alb_{surf} = \frac{I_{df\uparrow}}{I_{df\downarrow,0} + I_{dr\downarrow,0}} \tag{S105a}$$

$$I_{net} = (1 - alb_{surf}) \times (I_{df\downarrow,0} + I_{dr\downarrow,0}) \tag{S105b}$$

S6.2 Surface energy balance

The representation of the surface energy balance including the turbulent momentum and heat exchanges, surface, and soil temperature calculations follows largely the scheme of JSBACH 3, as described by Roeckner et al. (2003). The net radiation

(R_{net}) at the surface consists of the following components:

$$R_{net} = (1 - \alpha_s)R_{sd} + R_{ld} - \epsilon\sigma_{SB}T_s{}^4 \tag{S106}$$

where the term $\alpha_s \times R_{sd}$ is the net surface shortwave balance, denoted as I_{net} in Eq. S105, R_{ld} the downwelling longwave radiation, ϵ the surface emissivity, σ_{SB} the Stefan-Boltzmann constant, and T_s is the surface temperature.

5　The surface energy balance can then be written as

$$C_{s,l}\frac{\partial T_s}{\partial t} = R_{net} + LE + H + G \tag{S107}$$

where $C_{s,l}$ is the heat capacity of the surface layer, H is the sensible heat flux, LE the latent heat flux, composed of interception loss E_i, soil evaporation E_s and transpiration E_v, as described in Section S6.3. G is the ground heat flux, which is obtained from the solution of the thermal diffusion equation, which is used to diagnose the temperature profile within the soil

10　$$C_s\frac{\partial T}{\partial t} = -\frac{\partial G}{\partial z} = -\frac{\partial}{\partial z}\left(-\lambda_s\frac{\partial T}{\partial z}\right) \tag{S108}$$

where C_s is the volumetric heat capacity of the soil, G is the thermal heat flux (positive downward), $\lambda_s = C_s\kappa_s$ is the thermal conductivity, κ_s the thermal diffusivity, both derived from soil texture, and z the depth. This equation is solved down to a prescribed depth assuming zero flux conditions at the bottom and surface temperature T_s at the top as obtained from Eq. S107.

15　The sensible heat flux H is obtained from the temperature gradient according to

$$H = \rho_{air}C_p\frac{T_{air} - T_s}{r_a} \tag{S109}$$

where ρ_{air} and C_p are density and heat capacity of the surface atmospheric layer, and T_{air} and T_s are air and surface temperature. r_a is the aerodynamic resistance:

$$r_a = (C_h\,|v_h|)^{-1} \tag{S110}$$

20　and depends on the transfer coefficient for heat C_h Roeckner et al. (2003). and the absolute value of horizontal wind velocity v_h.

S6.3　Surface and soil hydrology

Surface hydrology is represented in very simple terms in QUINCY, because it is meant to be replaced by the JSBACH 4 hydrology in a future version. The model largely follows JSBACH 3 Roeckner et al. (2003), with some modifications. The
25　model represents surface hydrology for a number of soil layers (see Section S1) and including a canopy skin layer (hereafter referred to as skin). It represents interception (F_{inter}) by and interception loss (E_i) from the canopy, infiltration (F_{inf}), bare

soil evaporation (E_a), and surface runoff generation (F_{runoff}) at the soil surface, water movement in the soil (F_{diff}, F_{pref}), as well as deep drainage, and transpiration by vegetation (E_v) distributed across the rooting zone. The water budget can be described as follows

$$\frac{W_{skin}}{dt} = F_{inter} - E_i \tag{S111a}$$

$$\frac{W_{soil,sl=1}}{dt} = F_{inf} - E_a - f_{frans,sl=1}E_v - F_{diff,sl=1\rightarrow sl=2} \tag{S111b}$$

$$\frac{W_{soil,sl=2,n}}{dt} = (1 - \frac{k_{pref}}{dz_{sl}})F_{pref,sl-1} - f_{frans,sl}F_{trans} + F_{diff,sl-1\rightarrow sl} - F_{diff,sl\rightarrow sl+1} \tag{S111c}$$

$$\tag{S111d}$$

Precipitation ($Precip$) becomes intercepted by the canopy (F_{inter}), within the limits of the maximum size of the canopy skin reservoir(W_{skin}), with the remaining throughfall ($F_{through}$) reaching the first soil layer.

$$F_{inter} = MIN(k_{eff,inter} \times Precip, \frac{w_{skin,max} \times LAI - W_{skin}}{dt}) \tag{S112a}$$

$$F_{through} = Precip - F_{inter} \tag{S112b}$$

where $w_{skin,max}$ is a parameter.

$F_{through}$ is infiltrating into the first soil layer (F_{inf}) within the limits of its water content at field capacity ($W_{fc,sl=1}$), but –different to Roeckner et al. (2003) – reduced by a constant fraction (k_{pref}), which is assumed to be leaked preferentially to the next lower layer. The difference between $F_{through}$ and F_{inf}, i.e. the excess water unable to remain in the surface layer, is partitioned into surface runoff (F_{runoff}) and preferential flow to the second layer ($F_{pref,sl=1}$).

$$F_{inf} = (1 - \frac{k_{pref}}{dz_{sl}}) \times MIN(F_{through}, \frac{W_{fc,sl=1} - W_{act,sl=1}}{dt}) \tag{S113a}$$

$$F_{runoff} = (1 - k_{pref,runoff})(F_{through} - F_{inf}), and \tag{S113b}$$

$$F_{pref,sl=1} = \frac{k_{pref}}{dz_{sl}}F_{inf} + k_{pref,runoff}(F_{through} - F_{inf}) \tag{S113c}$$

Preferential flow to the lower layers is assumed to occur for any water leakage following infiltration according to

$$F_{inf,sl} = (1 - \frac{k_{pref}}{dz_{sl}}) \times F_{pref,sl-1} \tag{S114a}$$

$$F_{pref,sl} = \frac{k_{pref}}{dz_{sl}}F_{inf,sl} \times F_{pref,sl-1} \tag{S114b}$$

Different from Roeckner et al. (2003), the diffusive flux between two layers of depth dz is given by the Richards-equation:

$$F_{diff,sl-1\rightarrow sl} = \frac{\bar{K}_{diff,sl-1\rightarrow sl}}{0.5 \times (dz_{sl-1} + dz_{sl})}(\Psi_{soil,sl} - \Psi_{soil,sl-1}), where \tag{S115a}$$

$$\bar{K}_{diff,sl-1\rightarrow sl} = \frac{dz_{sl-1}K_{diff,sat,sl-1}(\frac{\Theta_{act,sl-1}}{\Theta_{sat,sl-1}})^{k_{C,sl}^{diff}} + dz_{sl}K_{diff,sat,sl}(\frac{\Theta_{act,sl}}{\Theta_{sat,sl}})^{k_{C,sl}^{diff}}}{dz_{sl-1} + dz_{sl}} \tag{S115b}$$

where $K_{diff,sat,sl}$ and $k_{C,sl}^{diff}$ are derived from soil texture according to Saxton and Rawls (2006), Θ_{sl} is the volumentric water content given by Eq. S120, and $\Psi_{soil,sl}$ is the soil water matrix potential given by Eq. S121. Saturation of a soil layer leads to increased percolation to the next lower layer. The lower boundary layer in the soil is modelled as a zero gradient boundary, i.e. only percolation flow leads to drainage from the soil column.

5   Interception loss (E_i) is calculated from the filled fraction of canopy skin reservoir (W_{skin}), i.e. the ratio of the actual to the maximum size of the canopy water storage

$$E_i = \rho_{air} \frac{q_a - q_s(T_s, p_s)}{r_a} \frac{W_{skin}}{w_{skin,max} \times LAI}, \tag{S116}$$

where ρ_{air} is air density, q_a specific humidity in lowest atmospheric level, q_s saturation specific humidity at surface temperature T_s and pressure p_s, r_a is the aerodynamic resistance, and LAI is the current leaf area index of the vegetation.

10   Evaporation from the soil surface (E_s) is calculated as:

$$E_s = \rho_{air} \frac{q_a - q_s(T_s, p_s)}{r_a^*} \Theta_{soil,1} (1 - exp(k_{fpc} \times LAI)) \tag{S117}$$

where $\Theta_{soil,1}$ the fractional soil water content of the first soil layer. The term $(1 - exp(k_{fpc} \times LAI))$ has been added to the model of Roeckner et al. (2003) to account for the reduced energy available for evaporation underneath a closed canopy.

Transpiration from the dry vegetation surfaces (E_v) is

15    $$E_v = \rho_{air} \frac{q_a - q_s(T_s, p_s)}{r_a + r} \tag{S118}$$

where stomatal resistance r of the canopy is the inverse of the stomatal conductance of the canopy (see Eq. S17).

The partitioning of the transpiration flux across soil layers $f_{trans,sl}$ is calculated based on the layered soil water potential ($\Psi_{soil,sl}$), the fractional root distribution ($f_{root,sl}$), as well as a PFT-specific minimum soil water potential,

$$f_{trans,sl} = \frac{f_{root,sl} \times \beta_{gs,soil,sl}}{\sum\limits_{i=1}^{n} f_{root,i} \times \beta_{gs,soil,i}}, where \tag{S119a}$$

20    $$\beta_{gs,soil,sl} = \Psi_{soil,sl} / \Psi_{soil,min} \tag{S119b}$$

The soil model keeps track of water in terms of amount of water ($W_{skin|soil}$; m), which in the soil can be converted to the layers fractional water content (Θ) as:

$$\Theta_{soil,sl} = \frac{W_{soil,sl}}{dz_{sl}} \tag{S120}$$

with a soil water matrix potential ($\Psi_{soil,sl}$) derived from a pedotransfer function Saxton and Rawls (2006) as follows:

25    $$\Psi_{soil,sl} = k_A^{\Psi} \Theta_{soil,sl}^{k_B^{\Psi}} \tag{S121}$$

where k_A^{Ψ}, and k_B^{Ψ} are soil texture dependent parameters Saxton and Rawls (2006).

The net water transport between layers is used as input to the vertical flow of soluable biogeochemical pools.

Table S1. Memory time scale for processes

Symbol	Description	Value	Unit	Eq.
τ_{mavg}^{jmax}	Acclimation of temperature optimum for photosynthesis	7	days	S9
τ_{mavg}^{resp}	Acclimation of temperature response of maintenance respiration	30	days	S23
τ_{mavg}^{soa}	Frost response of photosynthesis (state-of-acclimation)	2	days	S46
τ_{mavg}^{labile}	Labile pool dynamics	7	days	S20
τ_{mavg}^{uptake}	Demand for nutrient uptake	3	days	S73
τ_{mavg}^{χ}	Response of foliar stoichiometry	20	days	S37
τ_{mavg}^{pheno}	Phenological processes	7	days	S45
τ_{mavg}^{alloc}	Allometric responses	30	years	S34
$\tau_{mavg}^{dynamics}$	Vegetation dynamics processes	365	days	S56

Table S2. Photosynthesis parameters

Symbol	Description	Value	Unit	Equation	Citation
j_{max}^{n}	electron-transport limited carboxylation rate per unit N	4.4	$\frac{\mu mol\,CO_2}{mmol\,N}$	S7	Niinemets and Tenhunen (1997)
v_{cmax}^{n}	Rubisco limited carboxylation rate per unit N	1.8	$\frac{\mu mol\,CO_2}{mmol\,N}$	S10	Niinemets and Tenhunen (1997)
v_{pepc}^{n}	PePC limited carboxylation rate per unit N	98777.97	$\frac{\mu mol\,CO_2}{mmol\,N}$	S12	Tazoe et al. (2006)
fN_{pep}	Fraction of N in PEP and PPKD (C4 plants only)	0.045	-	Sect. S2.1	Makino et al. (2003)
r_{J2V}	Jmax25/Vcmax25 (C3/C4) plants	1.97 / 1.4	-	Sect. S2.1	Wullschleger (1993)
a_{chl}^{n}	Chlorophyll N content	25.12	$\frac{mol}{mmol}$	S15	Evans (1989)
α_i	Intrinsic quantum efficiency	0.0561	$\frac{\mu mol\,CO_2}{mol\,quanta}$	S15	Kull and Kruijt (1998)
k_a	Extinction coefficient for PAR on chlorophyll	0.005	mol^{-1}	S15	Kull and Kruijt (1998)
k_n	Extinction coefficient to describe decline of N within the canopy	0.11	-	S2	Zaehle and Friend (2010)
k_1^{struc}	Slope of structural leaf N with total N	7.14×10^3	$g^{-1}N$	S4	Friend et al. (1997)
k_0^{chl}	Chlorophyll distribution with canopy depth for C3/C4 plants	6.0 / 15.0	-	S5	Zaehle and Friend (2010)
k_1^{chl}	Chlorophyll distribution with canopy depth for C3/C4 plants	3.6 / 4.4	-	S5	Zaehle and Friend (2010)
k_{fn}^{chl}	Chlorophyll distribution with canopy depth	0.7	-	S5	Friend (2001)

Table S2. Photosynthesis parameters (ctnd.)

Symbol	Description	Value	Unit	Equation	Citation
E_0^{kc}	Scaling constant of k_c	38.05	-	S6	Bernacchi et al. (2001)
E_1^{kc}	Activation energy of k_c	79.43	$\frac{\text{kJ}}{\text{mol}}$	S6	Bernacchi et al. (2001)
E_0^{ko}	Scaling constant of k_o	20.3	-	S6	Bernacchi et al. (2001)
E_1^{ko}	Activation energy of k_o	36.38	$\frac{\text{kJ}}{\text{mol}}$	S6	Bernacchi et al. (2001)
$E_0^{\Gamma^*}$	Scaling constant of photosynthetic compensation point	19.02	-	S6	Bernacchi et al. (2001)
$E_1^{\Gamma^*}$	Activation energy of photosynthetic compensation point	37.83	$\frac{\text{kJ}}{\text{mol}}$	S6	Bernacchi et al. (2001)
E_0^{vcmax}	Scaling constant of of Rubisco	26.35	-	S6	Bernacchi et al. (2001)
E_1^{vcmax}	Temperature sensitivity of Rubisco	65.33	$\frac{\text{kJ}}{\text{mol}}$	S6	Bernacchi et al. (2001)
$k0_{jmax}^{topt}$	Offset of the T_{jmax}^{opt} to T_{air} relationship	17.0	$°C$	S9	Friend (2010)
$k1_{jmax}^{topt}$	Slope of the T_{jmax}^{opt} to T_{air} relationship	0.35	-	S9	Friend (2010)
$T_{jmax,min}^{opt}$	Minimum of T_{jmax}^{opt}	17.0	$°C$	S9	Friend (2010)
$T_{jmax,max}^{opt}$	Maximum of T_{jmax}^{opt}	38.0	$°C$	S9	Friend (2010)
T_{ref}^{pepc}	Reference temperature of PePC C4 photosynthesis	25.0	$°C$	S13	Friend et al. (2009)
T_{base}^{pepc}	Base temperature of PePC C4 photosynthesis	10.0	$°C$	S13	Friend et al. (2009)
D_{air}^{wv2co2}	Ratio of diffusion coefficient for H_2O and CO_2 in air	1.6	-	S17	Monteith and Unsworth (2013)
D_{turb}^{wv2co2}	Ratio of diffusion coefficient for H_2O and CO_2 in turbulent air	1.37	-	S17	Monteith and Unsworth (2013)
O_i	Partial Pressure of O_2	20.9	kPa	S10	-
$c_{i,max}$	Saturating Ci in C4 plants	7800.0	Pa		Friend et al. (2009)

Table S3. Vegetation growth and dynamics parameters

Symbol	Description	Value	Unit	Equation	Citation
Respiration					
$f_{resp,growth}$	Growth respiration fraction per unit new biomass	0.25	$\frac{molC}{molC}$	S20	Sprugel et al. (1995)
$f_{resp,maint}^{non-woody}$	Maintenance respiration rate for fine roots and leaves	1.0	$\frac{\mu molCO_2}{mmolN\,s}$	S21	Sprugel et al. (1995)
$f_{resp,maint}^{woody}$	Maintenance respiration rate for wood	0.25	$\frac{\mu molCO_2}{mmolN\,s}$	S21	Sprugel et al. (1995)
t_{k1}	Coefficient for temperature sensitivity of respiration	308.56	K	S22	Lloyd and Taylor (1994)
t_{k2}	Coefficient for temperature sensitivity of respiration	56.02	K	S22	Lloyd and Taylor (1994)
t_{k3}	Coefficient for temperature sensitivity of respiration	227.13	K	S22	Lloyd and Taylor (1994)
$T_{acclim,ref}$	Base temperature for respiration acclimation	283.15	K	S23	Atkin et al. (2014)
f_{resp_acclim}	Respiration temperature acclimation factor	-0.008	K^{-1}	S23	Atkin et al. (2014)
$cost_{NH4}$	Transformation and uptake cost for plant uptake of NH_4	1.7	$gCg^{-1}N$	S24	Zerihun et al. (1998)
$cost_{NO3}$	Transformation and uptake cost for plant uptake of NO_3	2.3	$gCg^{-1}N$	S24	Zerihun et al. (1998)
Labile Pool					
τ_{labile}	Turnover time of the labile pool	5	days	S25	This study
λ_{temp}^{labile}	Temperature response function of labile pool	0.5	K^{-1}	S25	This study
k_{temp}^{labile}	Shape parameter of the labile pool's temperature response	2.0	-	S25	This study
$\lambda_{\theta}^{labile}$	Moisture response function of labile pool	10.0	-	S25	This study
k_{θ}^{labile}	Moisture response function of labile pool	2.0	-	S25	This study
k_{labile}^{nut}	Rate at which N/P can be quicker retrieved than C	1.2	-	S28	This study
Allometry and allocation					
$k1_{alloc}^{fruit}$	Minimum fraction of allocation going to fruit	0.01	-	S29	This study
$k3_{alloc}^{fruit}$	Reserve usage rate below which fruit growth starts	0.1	$\frac{\mu molC}{m^2\,s}$	S29	This study
λ_{alloc}^{fruit}	Shape parameter in the fruit allocation response to reserve changes	10.0	-	S29	This study
$k4_{alloc}^{fruit}$	Shape parameter in the fruit allocation response to reserve changes	2.0	-	S29	This study
$W_{soil,crit}^{alloc}$	Fraction of root zone water at field capacity below which root allocation starts responding	0.8	-	S35	This study
k_{htol}	Stem mass to leaf mass ratio of grasses	0.05	-	S30	Zaehle and Friend (2010)

Table S3. Vegetation growth and dynamics parameters (ctnd.)

Symbol	Description	Value	Unit	Equation	Citation
Stoichiometry					
C_m	Carbon mass per unit dry weight of leaves	0.48	$\frac{\text{gC}}{\text{gDW}}$	-	Kattge et al. (2011)
$\chi_{root}^{C:N}$	Relative C:N of fine roots compared to leaves	0.85	-	Sect. S3.5	Zaehle and Friend (2010)
$\chi_{wood}^{C:N}$	Relative C:N of woody biomass compared to leaves	0.145	-	Sect. S3.5	Zaehle and Friend (2010)
$\chi_{root}^{N:P}$	Relative N:P of fine roots compared to leaves	1.0	-	Sect. S3.5	This study
$\chi_{wood}^{N:P}$	Relative N:P of woody biomass compared to leaves	1.0	-	Sect. S3.5	This study
δ_{leaf}^{χ}	Maximum rate of foliar stoichiometry change	0.0048	day^{-1}	S36	(Zaehle and Friend, 2010)
λ_{leaf}^{χ}	Shape parameter in leaf stoichiometry nutrient response	2.0	-	S37	(Zaehle and Friend, 2010)
k_{leaf}^{χ}	Shape parameter in leaf stoichiometry nutrient response	8.0	-	S37	(Zaehle and Friend, 2010)
Reserve dynamics					
LAI_{max}^{target}	Maximum LAI target for reserve use calculations	5.0	$\frac{\text{m}^2}{\text{m}^2}$	S39	This study
$\lambda_{maint,C}^{\Phi}$	Shape parameter for pull from reserve C to labile C pools	4.0	-	S40	This study
$k_{maint,C}^{\Phi}$	Shape parameter for pull from reserve C to labile C pools	1.2	-	S40	This study
$k_{maint,NP}^{\Phi}$	Shape parameter for pull from reserve N|P to labile N|P pools	1.6	-	S40	This study
$\lambda_{maint,NP}^{\Phi}$	Shape parameter for pull from reserve N|P to labile N|P pools	3.0	-	S40	This study
λ_{store}^{Φ}	Shape parameter for pull from labile to reserve pool	2.0	-	S40	This study
k_{store}^{Φ}	Shape parameter for pull from labile to reserve pool	3.0	-	S40	This study
λ_{phen}^{Φ}	Shape parameter in storage response function to phenology	1.3	-	S42	This study
k_{phen}^{Φ}	Shape parameter in storage response function to phenology	8.0	-	S42	This study
$\lambda_{sinklim}^{ps}$	Photosynthetic sink limitation with labile C accumulation	0.1	-	S43	This study
$k_{sinklim}^{ps}$	Photosynthetic sink limitation with labile C accumulation	2.0	-	S43	This study
$k_{sinklim}^{CNP}$	Photosynthetic sink limitation with nutrient limitation	4.0	-	S44	This study
$\beta_{sinklim,min}^{ps}$	Lower bound of photosynthetic sink limitation	0.25	-	S43	This study
$f_{store,max}^{leaf}$	Maximum reserve storage in leaves relative to leaf mass	0.02	-	Sect. S3.6	This study
$f_{store,max}^{root}$	Maximum reserve storage in fine roots relative to fine root mass	0.2	-	Sect. S3.6	This study
$f_{store,max}^{wood}$	Maximum reserve storage in sap wood relative to sap wood mass	0.15	-	Sect. S3.6	This study
k_{Φ}^{inter}	Threshold value of Φ_{maint}^{X} beyond which Φ_{store}^{X} is reduced	0.75	-	S41	This study

Table S3. Vegetation growth and dynamics parameters (ctnd.)

Symbol	Description	Value	Unit	Equation	Citation
Phenology					
t_{air}^{GDD}	Temperature threshold for the accumulation of growing degree days	°C	5	-	by convention
τ_{soa}	Time constant in calculation state of acclimation	114	hours	S46	This study
T_{min}^{soa}	Min temp. in β_{soa} calculation	-3	°C	S47	This study
T_{max}^{soa}	Max temp. in β_{soa} calculation	17	°C	S47	This study
Turnover					
$\tau_{nut\_recycle}$	Time scale of foliar and fine root nutrient turnover	10.0	days	S48	Zaehle and Friend (2010)
$f_{shed,max}$	Maximum rate of leaf shedding	0.05	days	S49	This study
k_{resorb}^{leaf}	Fraction of nutrient resorption before leaf shedding	0.5	-	S50	This study
k_{resorb}^{wood}	Fraction of nutrient resorption before wood death	0.2	-	S50	This study
Vegetation dynamics					
k_{CA}	Scaling parameter in crown area to diameter relationship	100.0	-	S51	Sitch et al. (2003)
k_{rp}	Scaling exponent in crown area to diameter relationship	1.6	-	S51	Sitch et al. (2003)
CA_{max}	Maximum crown area	15.0	m^2	S51	Sitch et al. (2003)
k_{fpc}	Light-extinction coefficient	0.5	-	S52	Sitch et al. (2003)
λ_{est}^{T}	Shape parameter for temperature effect on establishment	0.075	-	Sect. S3.10	This study
k_{est}^{T}	Shape parameter for temperature effect on establishment	4.0	-	Sect. S3.10	This study
$\lambda_{est}^{\Theta_1}$	Shape parameter for moisture effect on establishment	10.0	-	Sect. S3.10	This study
$k_{est}^{\Theta_1}$	Shape parameter for moisture effect on establishment	2.0	-	Sect. S3.10	This study
FPC_{max}	Maximum foliage projective cover	0.95	-	S54, S57	Sitch et al. (2003)
$k1_{mort\_greff}$	Asymptotic growth efficiency mortality rate	0.05	year^{-1}	S56	Sitch et al. (2003)
$k2_{mort\_greff}$	Scaling coefficient for growth efficiency mortality rate	0.3	$\frac{m^2\ yr}{molC}$	S56	Sitch et al. (2003)

Table S4. Soil biogeochemistry parameters

Symbol	Description	Value	Unit	Equation	Citation
Litter partitioning					
$f_{met,max,C}$	Maximum fraction of metabolic litter formation	0.85	-	S62	Parton et al. (1993)
$k_{met,C}$	Slope of metabolic fraction with lignin to N ratio	0.018	-	S62	Parton et al. (1993)
LC_{fine_root}	Lignin content of fine root	0.2565592	mol^{-1}	S62	White et al. (2000)
LC_{coarse_root}	Lignin content of coarse roots	0.8163248	mol^{-1}	S62	assuming woody values
LC_{woody_litter}	Lignin content of woody litter	0.8163248	mol^{-1}	S62	White et al. (2000)
LC_{fruit}	Lignin content of seed bed	0.2565592	mol^{-1}	S62	set to fine-roots
LC_{seed_bed}	Lignin content of fine root	0.2565592	mol^{-1}	S62	set to fine-roots
$LC_{leaf,max}$	Maximum lignin content of leaves	0.3440226	mol^{-1}	S63	White et al. (2000)
$k_{leaf2sla}$	Slope of lignin to sla relationship	-0.4328854	m^{-2}	S63	White et al. (2000)
$k_{met,vp,N}$	Proportionality factor controlling C:N of metabolic vs. structural pool	5.0	-	S64	Parton et al. (1993)
$k_{met,vp,P}$	Proportionality factor controlling C:P of metabolic vs. structural pool	5.0	-	S64	Parton et al. (1993)
$\eta_{C,wl\rightarrow met,str}$	Fraction of woody litter C transformed into metabolic or structural litter	0.3	-	Sect. S4.1	following Parton et al. (1993)
Turnover times and their rate modifiers					
τ_{met}^{base}	Turnover time of metabolic litter	0.033	years	S65	Parton et al. (1993)
τ_{str}^{base}	Turnover time of structural litter	0.124	years	S65	Parton et al. (1993)
τ_{wl}^{base}	Turnover time of woody litter	2.5	years	S65	This study
τ_{fast}^{base}	Turnover time of fast SOM pool	2.0	years	S65	This study
τ_{slow}^{base}	Turnover time of slow SOM pool	100.0	years	S65	This study
$T_{opt,decomp}$	Temperature of peak decomposition rate	313.15	K	S65	This study
$E_{a,decomp}$	Activation energy for decomposition	53000.0	$Jmol^{-1}$	S65	Ahrens et al. (2015)
$E_{d,decomp}$	De-activation energy for decomposition	100000.0	$Jmol^{-1}$	S65	Ahrens et al. (2015)
$\Psi_{dec,min}$	Minimum water potential for decomposition	-2.0	MPa	S65	This study

Table S4. Soil biogeochemistry parameters (ctnd.)

Symbol	Description	Value	Unit	Equation	Citation
SOM dynamics					
$\chi_{SOM^{C:N}_{fast,max}}$	Maximum C:N ratio of fast SOM	15.27693	$\frac{mol}{mol}$	S66	Manzoni et al. (2008)
$\chi_{SOM^{C:N}_{fast,min}}$	Minimum C:N ratio of fast SOM	5.830891	$\frac{mol}{mol}$	S66	Manzoni et al. (2008)
f_χ	Slope of fast SOM C:N to mineral soil N	51000.0	$\frac{kg}{mol}$	S66	Parton et al. (1993)
$\chi_{SOM^{C:N}_{slow}}$	C:N ratio of slow SOM pool	10.4956	$\frac{mol}{mol}$	S71	Parton et al. (1993)
$\chi_{SOM^{N:P}_{slow}}$	N:P ratio of slow SOM pool	30.98107	$\frac{mol}{mol}$	S71	This study
$\chi_{SOM^{N:P}_{fast}}$	N:P ratio of fast SOM pool	30.98107	$\frac{mol}{mol}$	S70	This study
η_N	Microbial nitrogen-use efficiency	0.8	$\frac{mol}{mol}$	S67	Manzoni et al. (2008)
η_P	Microbial phosphorus-use efficiency	0.8	$\frac{mol}{mol}$	S70	Manzoni et al. (2008)
$\eta_{C,litter \to fast}$	Fraction of litter transformed into fast SOM	0.45	-	S70	Parton et al. (1993)
$\eta_{C,fast \to slow}$	Fraction of fast SOM transformed into slow SOM	0.15	-	S71	Parton et al. (1993)
$\eta_{C,slow \to fast}$	Fraction of slow SOM transformed into fast SOM	0.3	-	S71	Parton et al. (1993)
k_{org}^{diff}	Diffusion velocity due to bioturbation	0.15	$\frac{m^2 \, kg}{m^3 \, yr}$	S72	Koven et al. (2013)
ρ_{org}^{bulk}	Bulk density of organic material	150.3935	$\frac{kg}{m^3}$	S72	Ahrens et al. (2015)
Nutrient uptake kinetics					
$T_{opt,uptake}$	Temperature of peak uptake rate	313.15	K	S73	This study
$E_{a,uptake}$	Activation energy for uptake	53000.0	$Jmol^{-1}$	S73	Ahrens et al. (2015)
$E_{d,uptake}$	De-activation energy for uptake	100000.0	$Jmol^{-1}$	S73	Ahrens et al. (2015)
K_{m1,NH_4}	Low-affinity NH_4 uptake	0.0416	$\frac{m^3}{mol}$	S73	Kronzucker et al. (1996)
K_{m1,NO_3}	Low-affinity parameter for plant uptake	0.0416	$\frac{m^3}{mol}$	S73	Kronzucker et al. (1995)
K_{m1,PO_4}	Low-affinity parameter for plant uptake	229.6667	$\frac{L}{mol}$	S73	Kavka and Polle (2016)
K_{m2,NH_4}	High-affinity parameter for plant uptake	1.0	$\frac{mol}{m^3}$	S73	Kronzucker et al. (1996)
K_{m2,NO_3}	High-affinity parameter for plant uptake	1.0	$\frac{mol}{m^3}$	S73	Kronzucker et al. (1995)
K_{m2,PO_4}	High-affinity parameter for plant uptake	0.000022	$\frac{mol}{L}$	S73	Kavka and Polle (2016)
$E_{a,hsc}$	Activation energy of half-saturation point	30000.0	$\frac{J}{mol}$	S73	Ahrens p. com. 2016
k_{hsc}	Scaling factor for the sensitivity of half-saturation constant to moisture limitation	0.001	-	S73	Davidson et al. (2012)
$K_{demand}^{half,N}$	Fraction of target labile N at which uptake is reduced to 50%	0.75	-	S73	This study
$K_{demand}^{half,P}$	Fraction of target labile P at which uptake is reduced to 50%	0.9	-	S73	This study
k_{demand}	Nutrient uptake response function to labile nutrient concentration	2.0	-	S73	This study
N_{limit}^{BNF}	Maximum sum of NH_4 and NO_3 at which BNF occurs	0.05	$\frac{molN}{m^2}$	Sect. S4.6	Zaehle and Friend (2010)
$v_{max,BNF}$	Maximum rate of BNF	0.005	$\frac{molN}{m^2 \, s}$	S74	Zaehle and Friend (2010)

Table S4. Soil biogeochemistry parameters (ctnd.)

Symbol	Description	Value	Unit	Equation	Citation
Nitrification, denitrification, and BNF parameters					
λ_{anvf}	Weibull function to relate anaerobic volume fraction to soil moisture	1.3	-	S75	Zaehle and Friend (2010)
k_{anvf}	Weibull function to relate anaerobic volume fraction to soil moisture	3.0	-	S75	Zaehle and Friend (2010)
$v_{max,nit}$	Maximum nitrification rate	0.4	day^{-1}	S76	Xu-Ri and Prentice (2008)
$E_{a,nit}$	Activation energy of nitrification	80000	$\frac{J}{mol}$	S76	Xu-Ri and Prentice (2008)
$E_{d,nit}$	De-activation energy of nitrification	200000	$\frac{J}{mol}$	S76	Xu-Ri and Prentice (2008)
$T_{opt,nit}$	Optimum temperature for nitrification	311.15	K	S76	Xu-Ri and Prentice (2008)
$f_{nit}^{NO_y}$	Fraction of nitrification lost to NO_y	0.02	-	S77	Xu-Ri and Prentice (2008)
$f_{nit}^{N_2O}$	Fraction of nitrification lost to N_2O	0.002	-	S77	Xu-Ri and Prentice (2008)
$E_{a,denit}$	Activation energy of denitrification	47000	$\frac{J}{mol}$	S78	Xu-Ri and Prentice (2008)
$v_{max,denit}$	Maximum denitrification rate	0.1	day^{-1}	S78	Xu-Ri and Prentice (2008)
$K_{m,denit}^{fast}$	Half-saturation constant C of denitrification	20.0	$\frac{mol}{m^3}$	S78	Xu-Ri and Prentice (2008)
$K_{m,denit}^{NO_3}$	Half-saturation constant NO_3 of denitrification	1162.598	$\frac{mol}{m^3}$	S78	Xu-Ri and Prentice (2008)
$f_{denit}^{NO_y}$	Fraction of denitrification lost to NO_y	0.002	-	S79	Xu-Ri and Prentice (2008)
$f_{denit}^{N_2O}$	Fraction of denitrification lost to N_2O	0.02	-	S79	Xu-Ri and Prentice (2008)
$E_{a,diff}$	Activation energy of gas diffusion	47000	$\frac{J}{mol}$	S88	Xu-Ri and Prentice (2008)

Table S4. Soil biogeochemistry parameters (ctnd.)

Symbol	Description	Value	Unit	Equation	Citation
Soil P fluxes					
k_{ocl}	Occlusion coefficient of sorbed PO_4	3.86	$10^{-13} \mathrm{s}^{-1}$	S61	Yang et al. (2014)
k_{weath}	Weathering rate constant of mineral soil	8.16208	$10^{-14} \frac{\mathrm{molP}}{\mathrm{m}^3 \, \mathrm{s}}$	S80	Wang et al. (2010)
$K_{m,weath}^{root}$	Half-saturation root biomass for PO_4 weathering	10.0	$\frac{\mathrm{molC}}{\mathrm{m}^3}$	S80	calibrated
$K_{m,biomin}^{PO_4}$	Half-saturation solute P concentration for PO_4 bio-chemical mineralization	0.001	$\frac{\mathrm{molP}}{\mathrm{m}^3}$	S81	estimated
$K_{m,biomin}^{root}$	Half-saturation root C biomass for PO_4 biochemical mineralization	20.0	$\frac{\mathrm{molC}}{\mathrm{m}^3}$	S81	calibrated
k_{abs}	PO_4 (ab)sorption rate from P_{lab} to P_{sorb}	651.8519	$\frac{\mathrm{\mu mol}}{\mathrm{kg\,soil\,s}}$	S83	Yang et al. (2014)
$E_{a,abs}$	Activation energy for sorption to mineral surfaces	5000.0	$\frac{\mathrm{J}}{\mathrm{mol}}$	S83	Ahrens p. com. 2016
k_{des}	PO_4 desorption rate from P_{sorb} to P_{lab}	0.000733	$\frac{\mathrm{mol}}{\mathrm{kg\,soil\,s}}$	S83	Yang et al. (2014)
$E_{a,des}$	Activation energy for desorption from mineral surfaces	20000.0	$\frac{\mathrm{J}}{\mathrm{mol}}$	S83	Ahrens p. com. 2016
S_{om}^{max}	PO_4 sorption capacity of organic matter	0.4	$\frac{\mathrm{mmolP}}{\mathrm{kg\,OM}}$	S85	This study[1]
$S_{mineral}^{max}$	PO_4 sorption capacity of mineral soil	0.0387	$\frac{\mathrm{molP}}{\mathrm{kg\,soil}}$	S85	This study[1]
$K_{m,om}^{sorb}$	Half-saturation concentration for PO_4 adsorption to OM	0.045	$\frac{\mathrm{mmolP}}{\mathrm{kg\,OM}}$	S85	This study[1]
$K_{m,mineral}^{sorb}$	Half-saturation concentration for PO_4 adsorption to soil mineral	0.00225	$\frac{\mathrm{mmolP}}{\mathrm{kg\,soil}}$	S85	This study[1]

[1]: Based on a literature review including Abekoe and Sahrawat (2001); Ahmed et al. (2008); Chakraborty et al. (2012); Debicka et al. (2015); Dossa et al. (2008); Fan et al. (2014); Guedes et al. (2016); Harrell and Wang (2006); Hartono et al. (2005); Herlihy and McCarthy (2006); Holford et al. (1974); Horta et al. (2013); Huang et al. (2005); Janardhanan and Daroub (2010); Kolahchi and Jalali (2013); Olander and Vitousek (2005); Pal (2011); Sakadevan and Bavor (1998); Sanyal et al. (1993); Sato and Comerford (2005); Shirvani et al. (2010); Singh et al. (2005); Singh et al. (2006); Villapando and Graetz (2001); Wisawapipat et al. (2009); Xu et al. (2006); Zafar et al. (2016); Zhou and Li (2001); Zou et al. (2011)

Table S5. Parameters for the calculation of isotopic fractionation and mixing ratios calculation

Symbol	Description	Value	Unit	Equation	Citation
a_{13C}	Discrimination of ^{13}C due to stomatal diffusion	4.4	‰	S92	Drake (2014)
b_{13C}	Discrimination of ^{13}C due to Rubisco	27.0	‰	S92	Drake (2014)
c_{13C}	Discrimination of ^{13}C due to PEP C	5.7	‰	S92	Drake (2014)
a_{14C}	Discrimination of ^{14}C due to stomatal diffusion	8.668	‰	S92	Drake (2014)
b_{14C}	Discrimination of ^{14}C due to Rubisco	51.03	‰	S92	Drake (2014)
c_{14C}	Discrimination of ^{14}C due to PEP C	10.773	‰	S92	Drake (2014)
ϕ_{C4}	Leakage rate of bundle sheath cells	0.16	-	S92	Drake (2014)
$R_{ref,C13}$	Reference isotopic mixing ratio of ^{13}C/^{12}C; PDB standard	0.0112372	$\frac{mol}{mol}$	S90	-
$R_{ref,C13}$	Reference isotopic mixing ratio of ^{15}N/^{14}N	0.0036765	$\frac{mol}{mol}$	S90	Robinson (2001)
$\epsilon_{uptake,NH_4}^{mic}$	Discrimination due to microbial NH_4 uptake	17.0	‰	S91	Robinson (2001)
$\epsilon_{uptake,NH_4}^{plant}$	Discrimination due to plant NH_4 uptake	13.5	‰	S91	Robinson (2001)
$\epsilon_{uptake,NO_3}^{plant}$	Discrimination due to plant NO_3 uptake	9.5	‰	S91	Robinson (2001)
ϵ_{nit}	Discrimination due to nitrification	47.5	‰	S91	Robinson (2001)
$\epsilon_{nitrate,production}$	Discrimination due to NO_3 production	25.0	‰	S91	Robinson (2001)
ϵ_{denit}	Discrimination due to denitrification	31.0	‰	S91	Robinson (2001)
$\epsilon_{ammonification}$	Discrimination due to NH_4 production	2.5	‰	S91	Robinson (2001)

Table S6. Parameters for the albedo, fAPAR and surface energy and water calculation

Albedo and fAPAR					
Symbol	Description	Value	Unit	Equation	Citation
ρ^{sbeta}	Scaling factor of solar angle in reflection calculation	1.6	-	S97	Spitters (1986)
$k_{bl,0}^{vis}$	Extinction coefficient over black leaves (VIS range)	0.5	-	S95	Spitters (1986)
$k_{df,0}^{vis}$	Extinction coefficient for diffuse radiation (VIS range)	0.8	-	S95	Spitters (1986)
$k_{bl,0}^{nir}$	Extinction coefficient over black leaves (NIR range)	0.5	-	S95	Spitters (1986)
$k_{df,0}^{nir}$	Extinction coefficient for diffuse radiation (NIR range)	0.8	-	S95	Spitters (1986)
k_{csf}	Crown shape correction parameter	2.2	-	S96	(Campbell and Norman, 1998)
alb_{soil}^{vis}	Soil albedo (VIS range)	0.15	-	S98	Bonan (2015)
alb_{soil}^{nir}	Soil albedo (NIR range)	0.30	-	S98	Bonan (2015)
Surface energy and water balance					
$k_{eff,inter}$	Efficiency of interception of precipitation as rain	0.25	-	S112	Raddatz et al. (2007)
$w_{skin,max}$	Maximum water storage per unit LAI	0.0002	m	S112	Raddatz et al. (2007)
k_{pref}	Preferential flow fraction of infiltrating water	0.01	m^{-1}	S113	This study
$k_{pref,runoff}$	Infiltrating fraction of surface runoff	0.95	-	S113	Krinner et al. (2005)

Table S7. PFT-specific parameters

Symbol	Description	Unit	Equation	Citation
σ_{vis}	Single leaf scattering albedo (VIS range)	-	S97	Otto et al. (2014); Spitters (1986)
σ_{nir}	Single leaf scattering albedo (NIR range)	-	S97	Otto et al. (2014); Spitters (1986)
Ω_0	Canopy clumping factor	-	S96	Campbell and Norman (1998)
ϕ_{crown}	Crown shape factor	-	S96	Campbell and Norman (1998)
sla	Specific leaf area	$\frac{\text{m}^2}{\text{molC}}$	-	Kattge et al. (2011)
$\chi_{leaf}^{C:N}$	Default foliar C:N	$\frac{\text{gC}}{\text{gN}}$	Sect. S3.5	Kattge et al. (2011)
$\chi_{leaf,min}^{C:N}$	Minimum foliar C:N	$\frac{\text{gC}}{\text{gN}}$	S37	Kattge et al. (2011)
$\chi_{leaf,max}^{C:N}$	Maximum foliar C:N	$\frac{\text{gC}}{\text{gN}}$	S37	Kattge et al. (2011)
$\chi_{leaf}^{N:P}$	Default foliar N:P	$\frac{\text{gN}}{\text{gP}}$	Sect. S3.5	Kattge et al. (2011)
$\chi_{leaf,min}^{N:P}$	Minimum foliar N:P	$\frac{\text{gN}}{\text{gP}}$	S37	Kattge et al. (2011)
$\chi_{leaf,min}^{N:P}$	Maximum foliar N:P	$\frac{\text{gN}}{\text{gP}}$	S37	Kattge et al. (2011)
k_0^{struc}	Maximum fraction of structural foliar N	-	S4	Friend et al. (1997); Kattge et al. (2011)
$fN_{struc,cl}^{min}$	Minimum fraction of structural foliar N	-	S4	This study
T_Ω	Shape parameter of J_{max} temperature response	K	S9	Friend (2010)
g_0	Intercept of the A_n g_s relationship	-	S17	Lin et al. (2015)
g_1	Slope of the A_n g_s relationship	-	S17	Lin et al. (2015)
g_{min}	Minimum stomatal conductance	$\frac{\text{m}}{\text{s}}$	S17	This study
τ_{leaf}	Turnover time of leaves	years	Sect. S3.9	Kattge et al. (2011)
τ_{fine_root}	Turnover time of fine roots	years	Sect. S3.9	Ahrens et al. (2014)
τ_{coarse_root}	Turnover time of coarse roots	years	Sect. S3.9	Ahrens et al. (2014)
τ_{branch}	Turnover time of branches	years	Sect. S3.9	This study
τ_{sap_wood}	Turnover time of the sapwood	years	Sect. S3.9	Sitch et al. (2003)
τ_{fruit}	Turnover time of the fruit	years	Sect. S3.9	This study
τ_{seed_litter}	Turnover time of the seed bed to litter	years	S3.9	This study
$\tau_{seed,est}$	Turnover time of the seed bed to establishment	years	S53	This study
$v_{max,NH_4|NO_3}$	Maximum plant N uptake rate	$\frac{\mu\text{mol N}}{\text{mol C s}}$	S73	Zaehle et al. (2010)
v_{max,PO_4}	Maximum plant P uptake rate	$\frac{\mu\text{mol P}}{\text{mol C s}}$	S73	Kavka and Polle (2016)

Table S7. PFT-specific parameters (ctnd.)

Symbol	Description	Unit	Equation	Citation
GDD_{req}^{max}	Maximum GDD requirement in the absence of chilling	°C days	S45	This study
$k_{dormance}^{GDD}$	Response of GDD to number of dormant days	days^{-1}	S45	This study
β_{soil}^{flush}	Soil water level inducing leaf flushing	-	Sect. S3.8	This study
β_{soil}^{sen}	Soil water stress inducing leaf senescence	-	Sect. S3.8	This study
t_{air}^{sen}	Air temperature threshold inducing leaf senescence	°C	Sect. S3.8	This study
age_{min}^{leaf}	Minimum leaf age before senescence	days	Sect. S3.8	This study
$f_{sap\_wood}^{branch}$	Fraction of sapwood in branches	-	Sect. S4.2	This study
ρ_{wood}	Wood density	$\frac{\text{g C}}{\text{cm}^3}$	S31	Chave et al. (2009); Zanne et al. (2009)
k_{latosa}	Leaf area to sapwood area ratio	-	S31	Zaehle et al. (2010)
k_{ctos}	Coarse root to sapwood mass ratio	-	S33	This study
k_{rtos}	Trade-off parameter for hydraulic investment into sapwood or fine roots	-	S34	This study
$k2_{alloc}^{fruit}$	Maximum fraction of growth allocated to fruit	-	S29	This study
$k1_{allom}$	Parameter in height diameter relationship	-	S32	Zaehle et al. (2010)
$k2_{allom}$	Parameter in height diameter relationship	-	S32	Zaehle et al. (2010)
Ψ_{leaf}^{min}	Minimum leaf water potential	MPa	S18	Hickler et al. (2006)
$k_{reserve}^{target}$	Target size of the long-term reserve pool	-	S39	This study
k_{root_dist}	Exponent describing the vertical root profile	-	S3	Jackson et al. (1996)
k_{seed}	Seed size	molC	S58	This study
$mort_{bg,PFT}$	Background mortality rate	year^{-1}	S56	Sitch et al. (2003)

Table S8. PFT-specific parameter values

Parameter	TrBE	TeBE	TrBR	TeBS	BNE	BNS	TeH	TrH
PS pathway	C3	C3	C3	C3	C3	C3	C3	C4
σ_{vis}	0.17	0.17	0.17	0.17	0.15	0.15	0.2	0.2
σ_{nir}	0.76	0.76	0.76	0.76	0.73	0.73	0.8	0.8
Ω_0	0.9	0.9	0.9	0.9	0.5	0.7	1.0	1.0
ϕ_{crown}	3.34	3.34	3.34	3.34	2.19	2.88	3.34	3.34
sla	0.24	0.22	0.39	0.39	0.13	0.25	0.50	0.48
$\chi_{leaf}^{C:N}$	28.4	35.0	22.5	22.5	39.7	24.8	26.9	33.9
$\chi_{leaf,min}^{C:N}$	14.0	14.0	14.0	14.0	24.0	16.0	13.7	17.1
$\chi_{leaf,max}^{C:N}$	38.7	38.7	38.7	38.7	64.9	31.0	40.0	48.0
$\chi_{leaf}^{N:P}$	16.8	14.0	12.7	12.7	8.4	9.1	10.7	8.9
$\chi_{leaf,min}^{N:P}$	8.4	7.0	6.3	6.3	4.2	4.5	5.3	4.4
$\chi_{leaf,min}^{N:P}$	25.3	21.0	19.0	19.0	12.6	13.6	16.0	13.3
k_0^{struc}	0.75	0.70	0.63	0.63	0.83	0.79	0.3	0.3
$fN_{struc,cl}^{min}$	0.57	0.52	0.45	0.45	0.65	0.61	0.12	0.12
T_Ω	18.0	18.0	18.0	18.0	18.0	18.0	18.0	18.0
g_0	0.01	0.01	0.01	0.01	0.01	0.01	0.03	0.03
g_1	9.3	8.3	7.0	10.9	5.5	7.0	9.3	2.0
g_{min}	0.00006	0.00006	0.00006	0.00006	0.00003	0.00003	0.00006	0.00006
τ_{leaf}	1.4	1.32	0.48	0.48	3.31	0.51	0.32	0.32
τ_{fine_root}	0.7	0.7	0.7	0.7	0.7	0.7	0.7	0.7
τ_{coarse_root}	8.0	8.0	8.0	8.0	8.0	8.0	8.0	8.0
τ_{branch}	10.0	10.0	10.0	10.0	10.0	10.0	10.0	10.0
τ_{sap_wood}	40.0	40.0	40.0	40.0	40.0	40.0	40.0	40.0
τ_{fruit}	1.0	1.0	1.0	1.0	1.0	1.0	1.0	1.0
τ_{seed_litter}	2.0	2.0	2.0	2.0	2.0	2.0	2.0	2.0
τ_{seed_est}	20.0	20.0	20.0	20.0	20.0	20.0	20.0	20.0
$v_{max,N}$	0.42	0.42	0.42	0.42	0.42	0.42	0.42	0.42
$v_{max,P}$	0.0044	0.0044	0.0044	0.0044	0.0044	0.0044	0.0044	0.0044

Table S8. Lctlib Parameter Values per PFT (ctnd.)

Parameter	TrBE	TeBE	TrBR	TeBS	BNE	BNS	TeH	TrH
Phenotype	evergreen	evergreen	raingreen	summergreen	evergreen	summergreen	perennial	perennial
GDD_{req}^{max}	0.0	0.0	0.0	800.0	0.0	800.0	10.0	10.0
$k_{dormance}^{GDD}$	0.0	0.0	0.0	0.007	0.0	0.0098	0.1	0.1
β_{soil}^{flush}	0.0	0.0	0.98	0.0	0.0	0.0	0.9	0.9
β_{soil}^{sen}	0.0	0.0	0.5	0.0	0.0	0.0	0.01	0.01
t_{air}^{sen}	0.0	0.0	0.0	8.5	0.0	5.0	0.0	0.0
age_{min}^{leaf}	10	10	10	50	10	10	10	10
Growthform	tree	tree	tree	tree	tree	tree	herb.	herb.
$f_{sap\_wood}^{branch}$	0.05	0.05	0.05	0.05	0.05	0.05	n.a.	n.a.
ρ_{wood}	0.3	0.3	0.3	0.3	0.3	0.3	n.a.	n.a.
k_{latosa}	4000.0	4000.0	4000.0	4000.0	4000.0	4000.0	n.a.	n.a.
k_{crtos}	0.1	0.1	0.1	0.1	0.1	0.1	n.a.	n.a.
k_{rtos}	4.21	4.21	4.21	4.21	4.21	4.21	10.0	10.0
$k2_{alloc}^{fruit}$	0.1	0.1	0.1	0.1	0.1	0.1	0.2	0.2
$k1_{allom}$	55.0	55.0	55.0	55.0	55.0	55.0	n.a.	n.a.
$k2_{allom}$	0.65	0.65	0.65	0.65	0.65	0.65	n.a.	n.a.
Ψ_{leaf}^{min}	-2.0	-2.0	-2.0	-2.0	-2.0	-2.0	-1.5	-1.5
$k_{reserve}^{target}$	1.0	1.2	1.0	1.0	0.5	1.0	1.0	1.0
k_{root_dist}	3.5	2.8	2.5	3.5	3.5	3.5	5.5	5.5
k_{seed}	0.5	0.5	0.5	0.5	0.5	0.5	0.1	0.1
$mort_{bg,PFT}$	0.1	0.1	0.1	0.1	0.1	0.1	0.05	0.05

Table S9. The ten most important parameters (P) determining model sensitivity, measured as ranked partial correlation coefficient (RPCC), for each of the eight variables shown in Fig. 8 at the example of FR-Hes and reference to the respective parameter description table in the Supplementary Materials (T). The variables are GPP, net N/P mineralisation, vegetation and ecosystem C, as well as leaf C:N:P. The parameter names are color-coded, the red color is referring to photosynthesis related parameter, blue to soil biogeochemistry, cyan to vegetation growth and dynamics and black to water balance.

Rank	GPP P	RPCC	T	Φ_{NH_4} P	RPCC	T	Φ_{PO_4} P	RPCC	T	Leaf C:N P	RPCC	T
1	$T_{opt,decomp}$	-0.97	S2	$T_{opt,decomp}$	-0.93	S2	$T_{opt,decomp}$	-0.89	S2	$T_{opt,decomp}$	0.96	S2
2	k_0^{struc}	-0.85	S7	$\eta_{C,litter\to fast}$	-0.58	S2	$K_{demand}^{half,N}$	0.67	S4	k_{rp}	0.80	S3
3	$\eta_{C,fast\to slow}$	-0.72	S2	k_{rp}	0.53	S3	$\eta_{C,litter\to fast}$	-0.65	S4	k_0^{struc}	-0.80	S7
4	$\eta_{C,litter\to fast}$	-0.71	S2	$\eta_{C,fast\to slow}$	-0.52	S2	$\chi_{leaf}^{N:P}$	-0.63	S7	sla	-0.70	S3
5	τ_{slow}^{base}	-0.63	S2	τ_{slow}^{base}	-0.50	S2	$\eta_{C,fast\to slow}$	-0.61	S4	$\eta_{C,litter\to fast}$	0.68	S4
6	sla	-0.58	S7	k_{resorb}^{leaf}	-0.41	S3	$\chi_{SOM_{slow}}^{C:N}$	0.36	S4	$\eta_{C,fast\to slow}$	0.65	S4
7	$T_{opt,nit}$	0.55	S2	$K_{demand}^{half,N}$	0.18	S4	k_{rp}	0.40	S3	τ_{slow}^{base}	0.59	S4
8	v_{cmax}^n	0.53	S2	sla	-0.36	S7	τ_{slow}^{base}	-0.37	S4	v_{cmax}^n	0.52	S2
9	τ_{fine_root}	0.49	S7	$\chi_{leaf}^{C:N}$	-0.35	S3	$\chi_{SOM_{slow}}^{N:P}$	0.36	S4	k_{latosa}	0.51	S7
10	$v_{max,NH_4|NO_3}$	0.22	S7	$\chi_{root}^{C:N}$	0.33	S3	k_{resorb}^{leaf}	-0.33	S3	$T_{opt,nit}$	-0.50	S2

Table S9. The ten most important parameters (P), continued.

Rank	Leaf N:P P	RPCC	T	Veg. C P	RPCC	T	Total C P	RPCC	T
1	$\chi_{root}^{N:P}$	0.94	S3	k_0^{struc}	-0.86	S2	$T_{opt,decomp}$	-0.90	S2
2	$K_{demand}^{half,N}$	-0.93	S4	k_{rp}	-0.78	S3	k_{rp}	-0.89	S3
3	$\chi_{leaf}^{N:P}$	0.84	S3	$f_{resp,maint}^{non-woody}$	-0.59	S2	k_0^{struc}	-0.71	S7
4	$\chi_{wood}^{N:P}$	0.65	S3	v_{cmax}^n	0.56	S2	k_{latosa}	-0.64	S7
5	k_{rp}	-0.50	S3	$\chi_{wood}^{N:P}$	-0.54	S3	$\eta_{C,fast\to slow}$	-0.51	S2
6	$T_{opt,decomp}$	0.45	S2	$\chi_{root}^{C:N}$	-0.52	S7	$\eta_{C,litter\to fast}$	-0.47	S2
7	v_{max,PO_4}	-0.33	S7	k_0^{chl}	-0.47	S7	τ_{slow}^{base}	-0.43	S2
8	sla	0.24	S3	k_{latosa}	-0.45	S3	$f_{resp,maint}^{non-woody}$	-0.42	S2
9	k_{latosa}	-0.19	S3	τ_{fine_root}	0.41	S7	τ_{fine_root}	0.42	S2
10	$k_{pref,runoff}$	0.17	S6	$T_{opt,decomp}$	-0.40	S4	$\chi_{wood}^{C:N}$	-0.41	S3
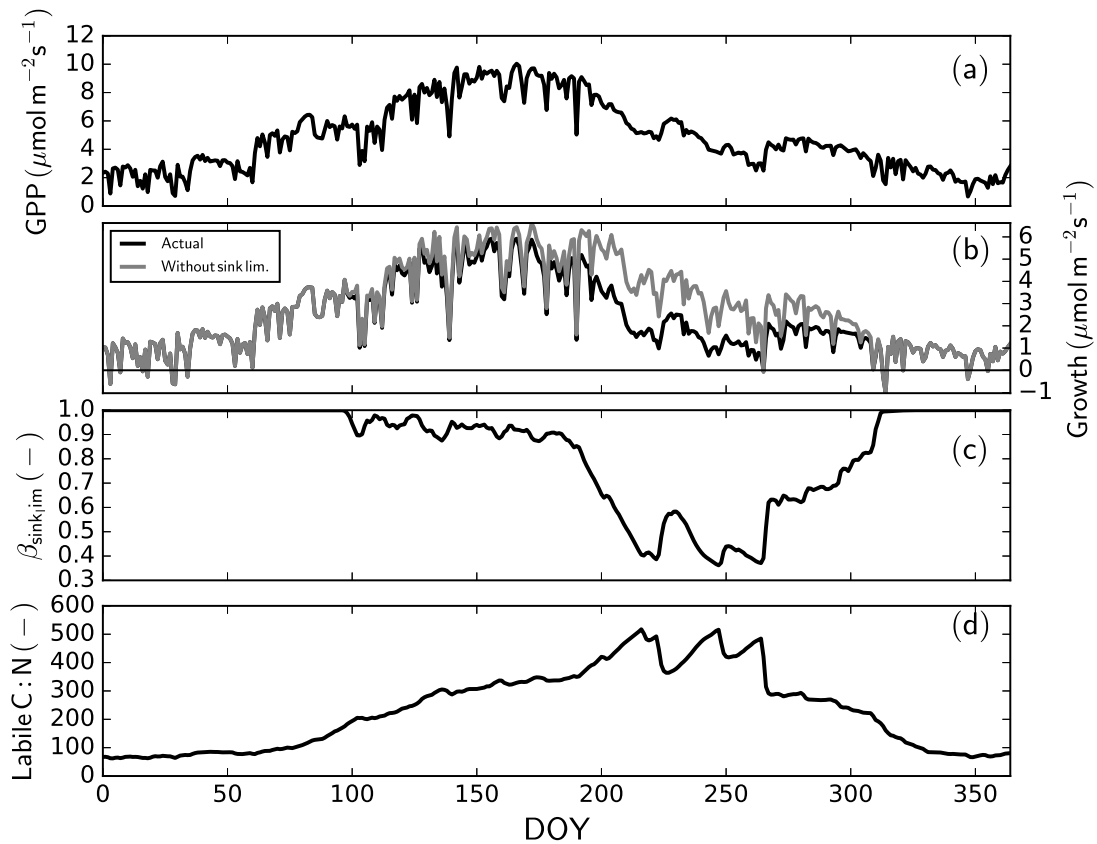
Figure S1. Effect of sink limitation on simulated photosynthesis at the evergreen broadleaf forest site IT-Cpz. Daily GPP (a), growth (b), the sink limitation scalar ($\beta^{ps}_{sinklim}$) (c) and C:N of labile pool (d) are shown for one year. The sink limitation is caused by high labile pool C:N ratio reducing the realised growth rate, which then provides a negative feedback to the photosynthesis.
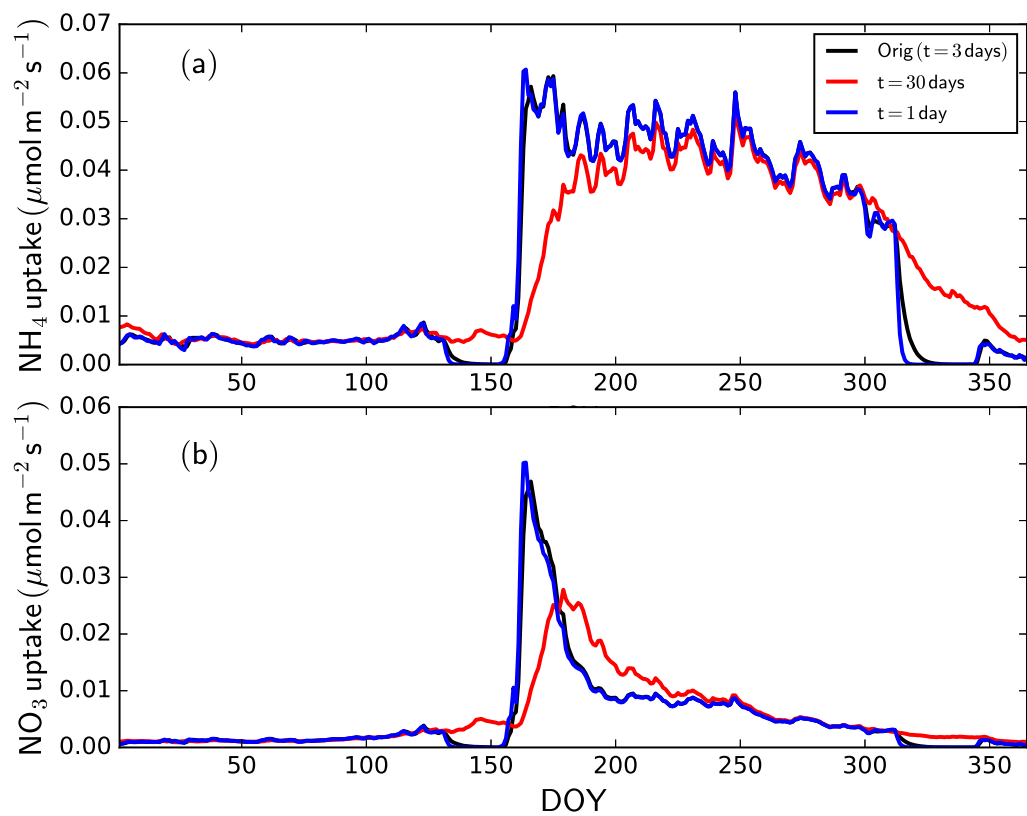
Figure S2. Effect of using a lagged response to calculate fluxes, at the example of the effect of plant nutrient demand on plant nutrient uptake in the temperate broadleaved deciduous forest of DK-Sor. Shown is the effect of altering the lag time of the demand for nutrient uptake (τ_{mavg}^{uptake}) on the nitrogen uptake fluxes for one year. The different colors respond to different lag times as explained in the legend.
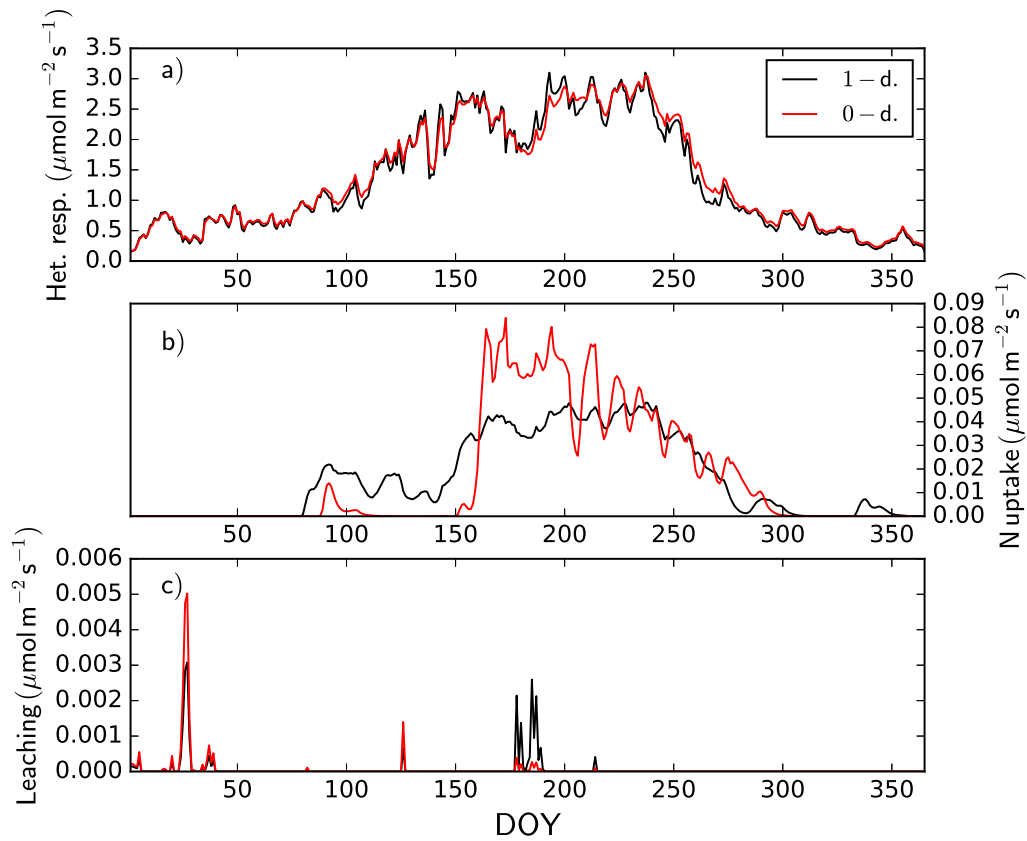
Figure S3. Effect of explicitly representing the vertical profile of the soils (1D), compared to a lumped, zero-dimensional (OD) approach. Displayed are the daily heterotrophic respiration (a) plant nitrogen uptake (b), and nitrogen leaching below the rooting zone (c) for one year at the needle-leaved evergreen forest site of FI-Hyy.
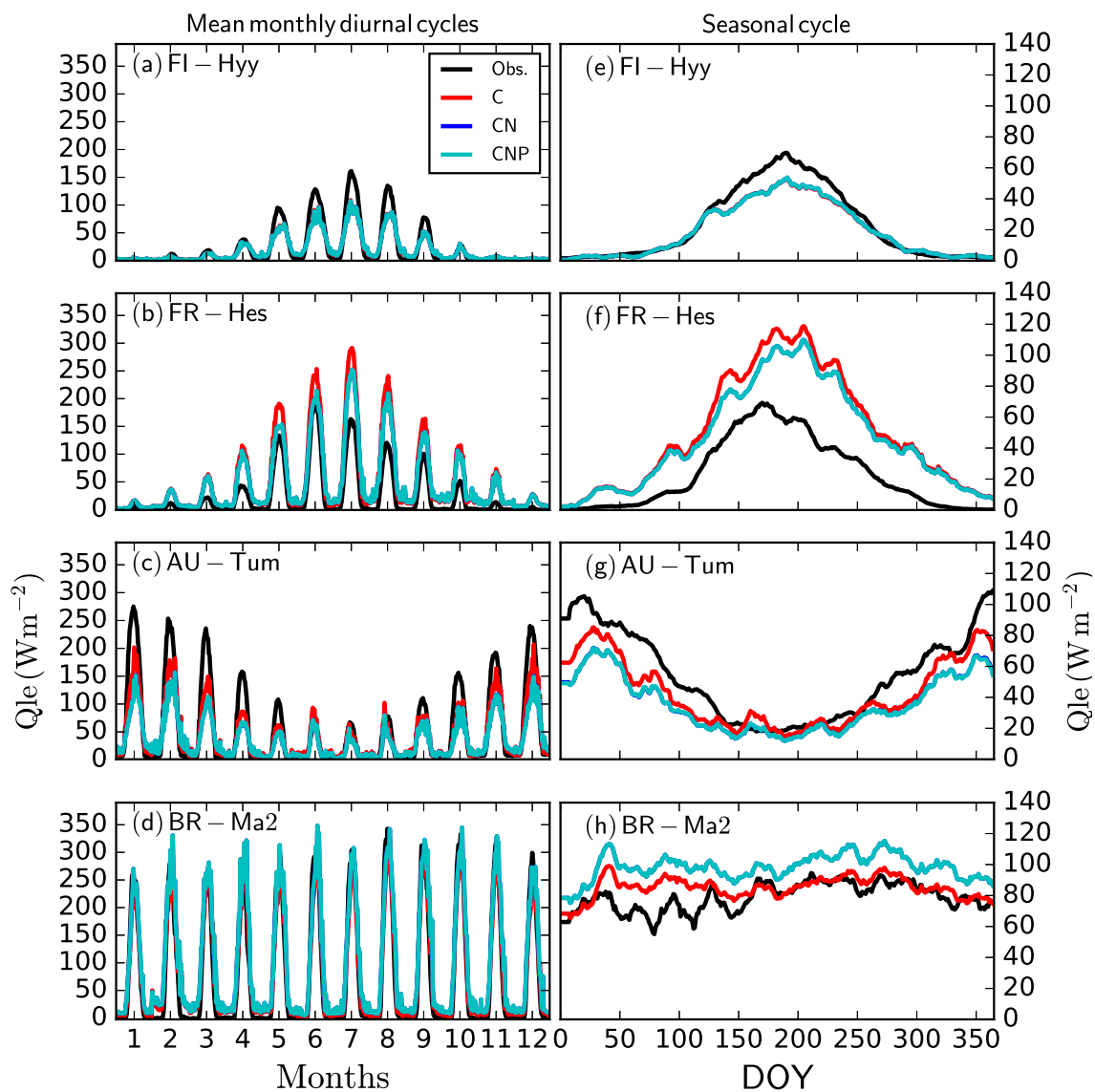
Figure S4. Simulated and observed mean monthly diurnal (a, b, c, d) and seasonal (e, f, g, h) cycles of latent heat flux (Q_{le}) at four FLUXNET sites (FI-Hyy, FR-Hes, AU-Tum, BR-Ma2). 'Obs' correspond to micrometeorological observations. 'C', 'CN' and 'CNP' refer to the model simulations with C, C&N and C&N&P options enabled. Seasonal cycles have been smoothed by a 16-day running mean.
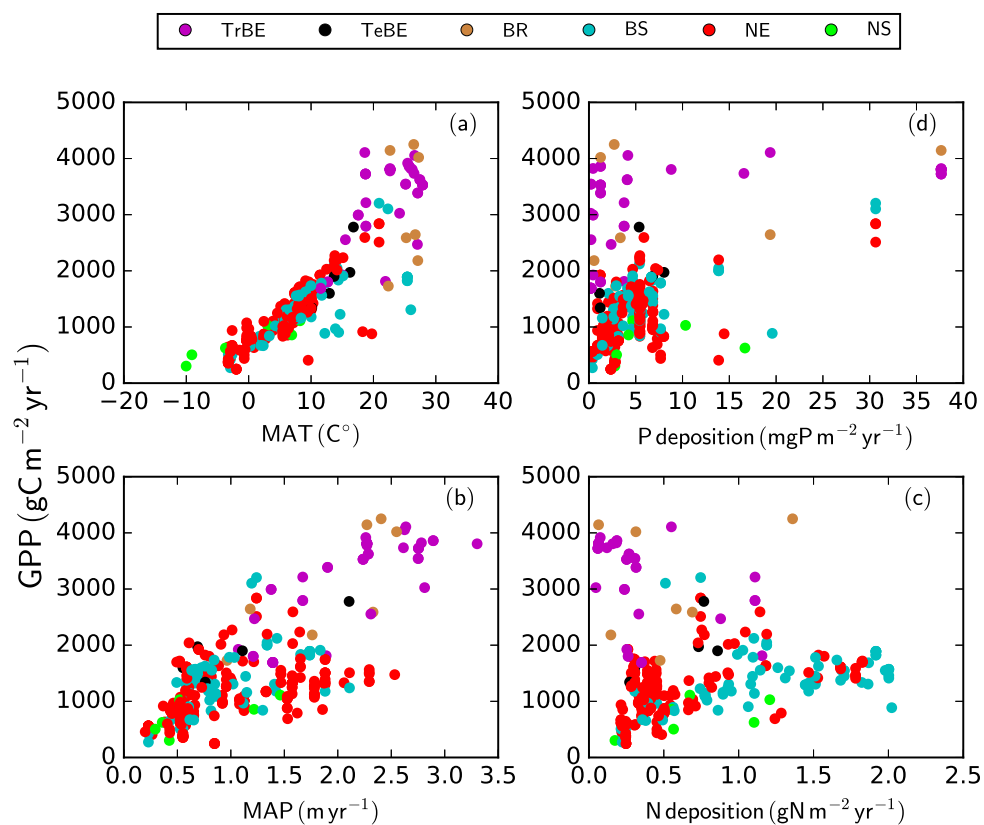
Figure S5. The GPP at the GFDB sites as a function of mean annual temperature (a), mean annual precipitation (b), nitrogen deposition (c) and phosphorus deposition (d). The PFT abbreviations are explained in Table 1.
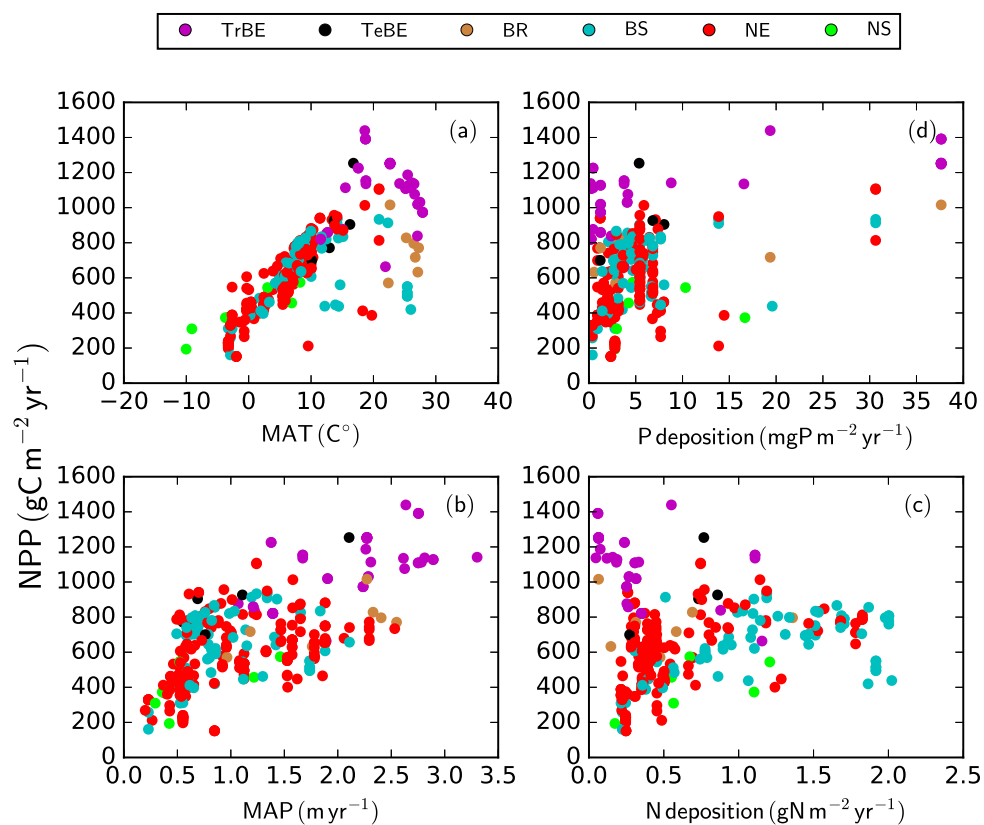
Figure S6. The NPP at the GFDB sites as a function of mean annual temperature (a), mean annual precipitation (b), nitrogen deposition (c) and phosphorus deposition (d). The PFT abbreviations are explained in Table 1.
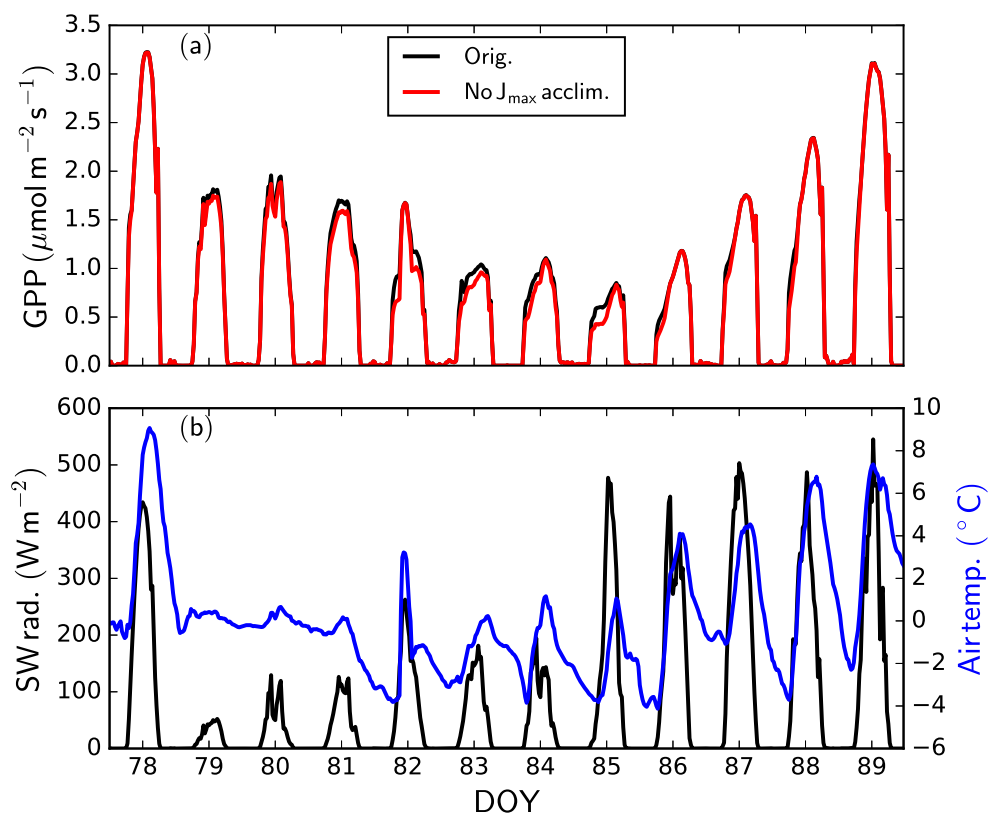
Figure S7. Effect of letting the temperature optimum of J_{max}, the maximum electron-transport rate for the calculation of photosynthesis, acclimate to growth temperature (black), or not (red). The simulated diurnal cycles of GPP (a) and shortwave radiation (in black) and air temperature (in blue) (b) at FI-Hyy in 2002 for twelve days.
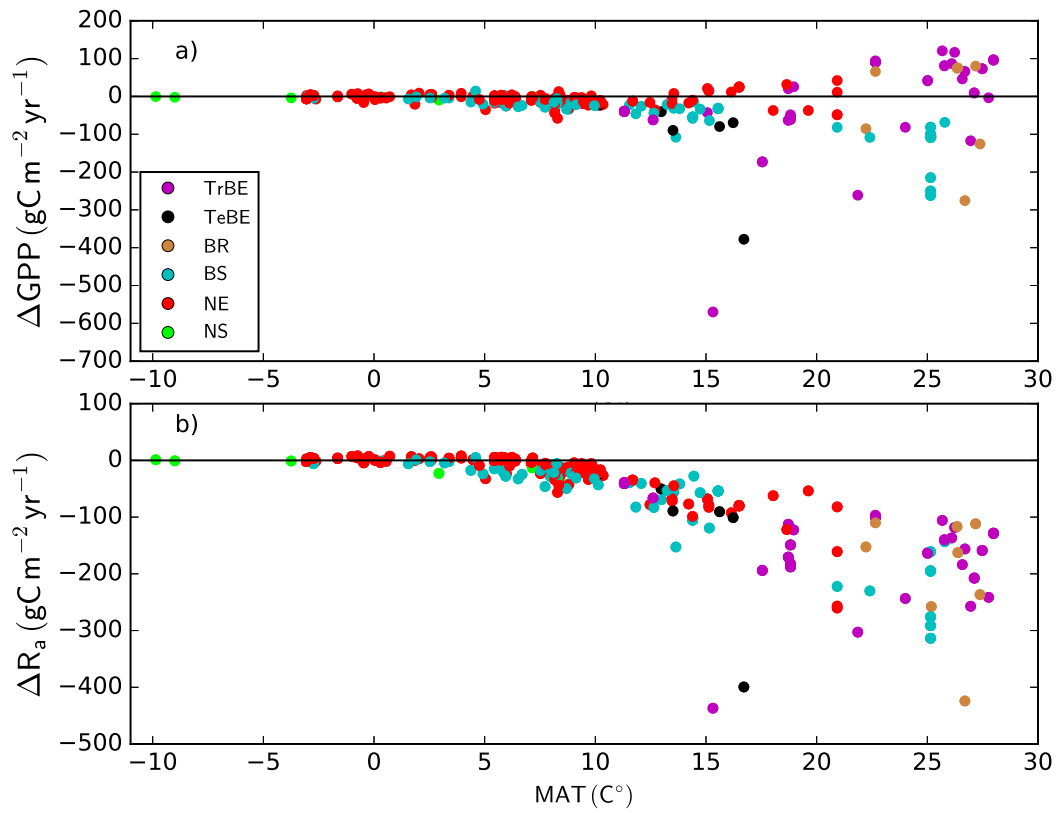
Figure S8. The residuals of averaged annual GPP (a) and autotrophic respiration (b), when the results without acclimation of maintenance respiration have been substracted from the original model simulations.
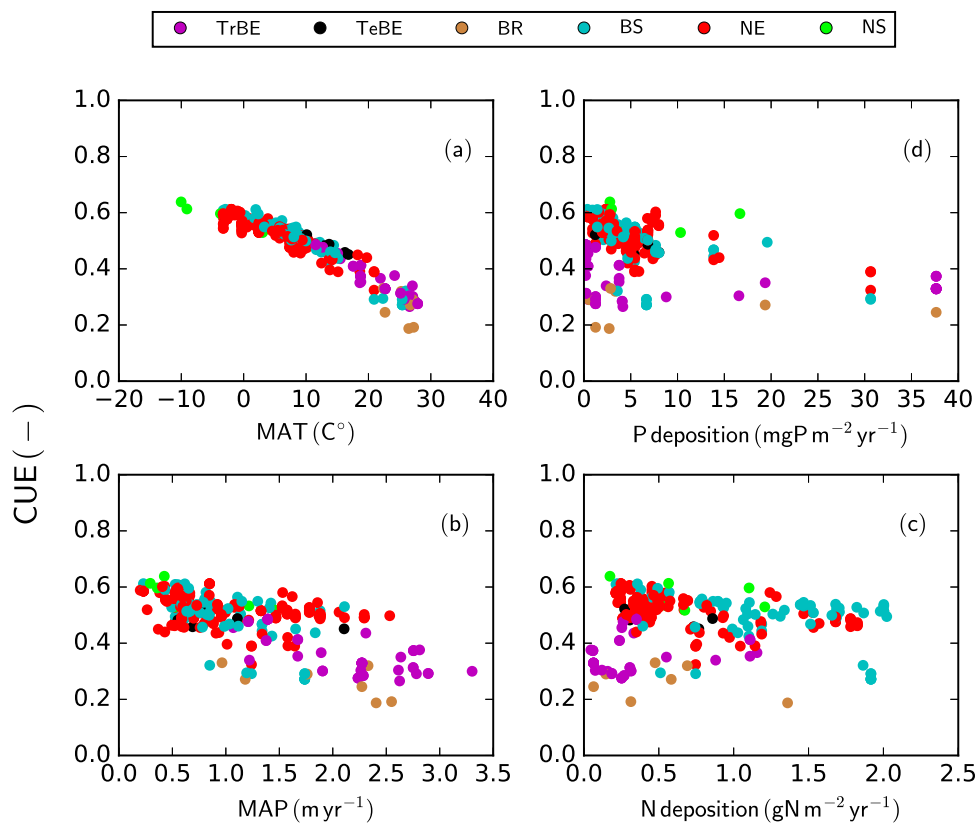
Figure S9. The CUE at the GFDB sites as a function of mean annual temperature (a), mean annual precipitation (b), nitrogen deposition (c) and phosphorus deposition (d). The PFT abbreviations are explained in Table 1.
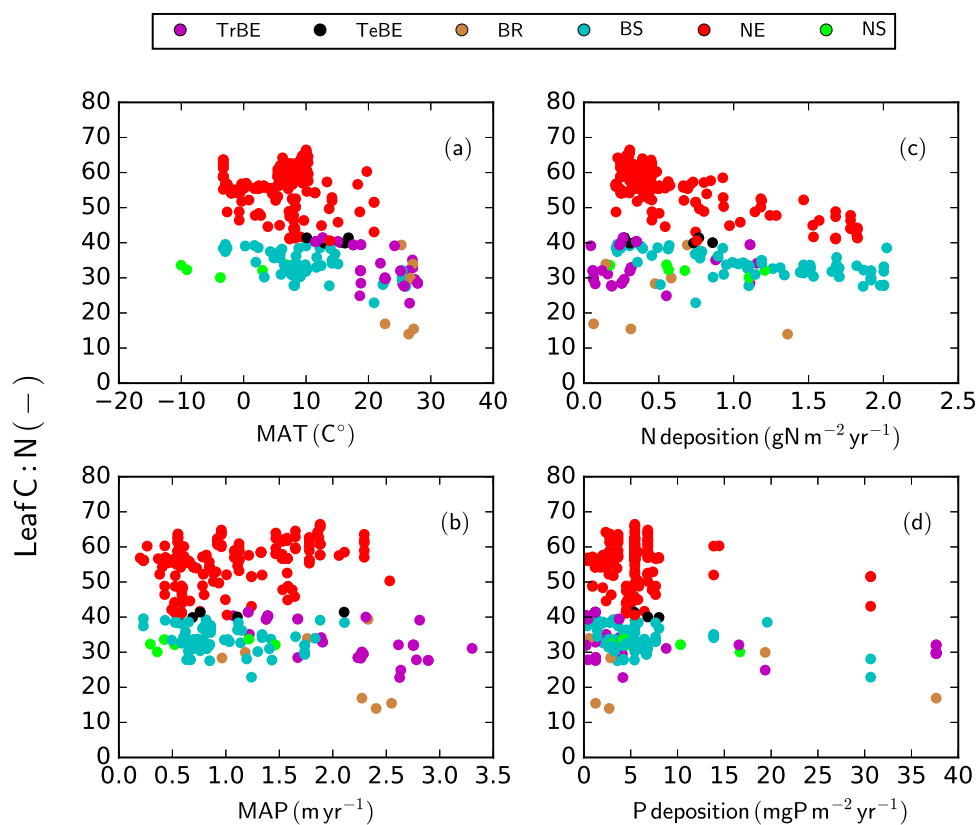
Figure S10. The leaf C:N at the GFDB sites as a function of mean annual temperature (a), mean annual precipitation (b), nitrogen deposition (c) and phosphorus deposition (d).
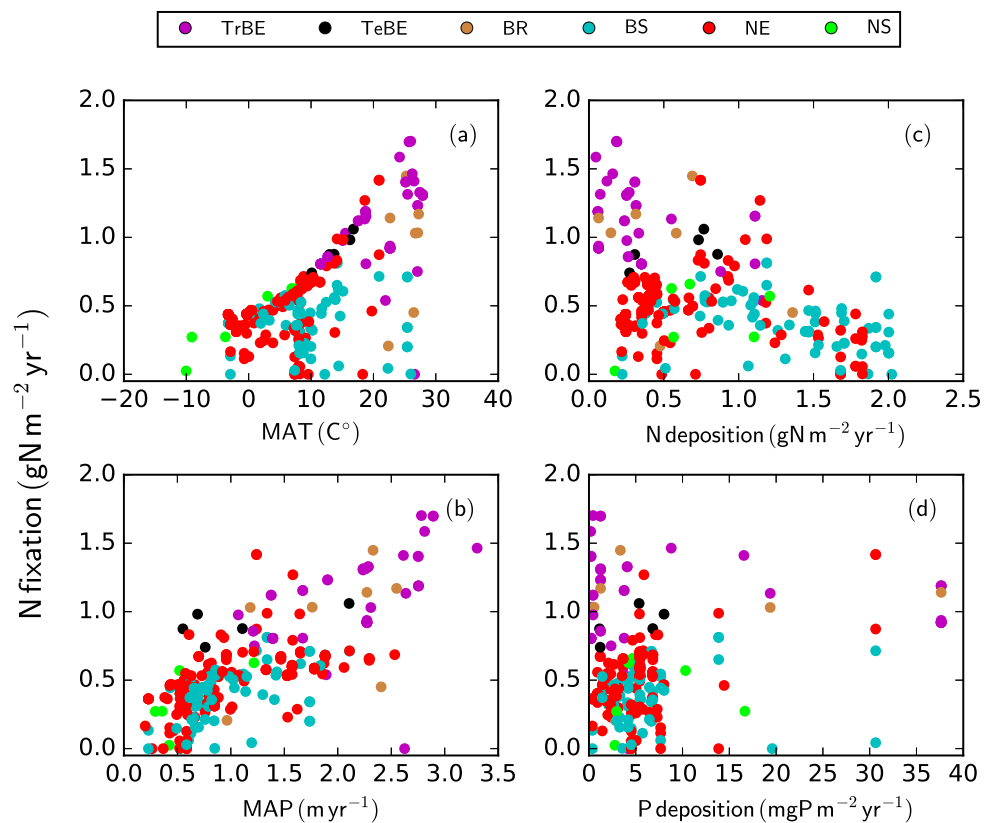
Figure S11. The nitrogen fixation at the GFDB sites as a function of mean annual temperature (a), mean annual precipitation (b), nitrogen deposition (c) and phosphorus deposition (d).
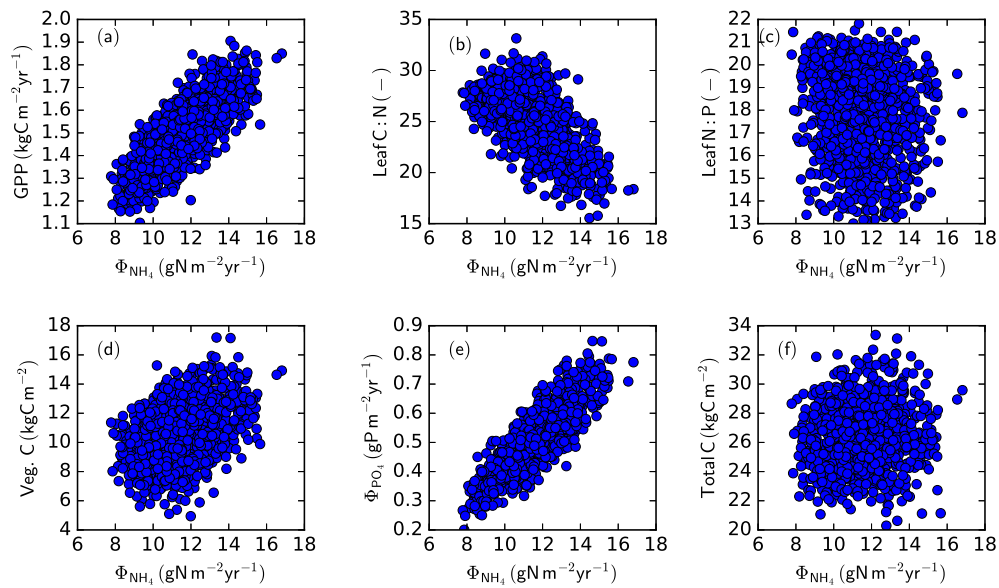
Figure S12. The GPP (a), leaf C:N (b), leaf P:N (c), vegetation carbon (d), phosphorus mineralization (e) and total ecosystem carbon (f) as function of nitrogen mineralization at FR-Hes for different parameter combinations from LHS.

References

Abekoe, M. K. and Sahrawat, K. L.: Phosphate retention and extractability in soils of the humid zone in West Africa, Geoderma, 102, 175–187, https://doi.org/10.1016/S0016-7061(00)00110-5, http://linkinghub.elsevier.com/retrieve/pii/S0016706100001105, 2001.

Ahmed, M. F., Kennedy, I. R., Choudhury, a. T. M. a., Kecskes, M. L., and Deaker, R.: Phosphorus adsorption in some Australian soils and influence of bacteria on the desorption of phosphorus, Communications in Soil Science and Plant Analysis, 39, 1269–1294, https://doi.org/10.1080/00103620802003963, http://www.tandfonline.com/doi/abs/10.1080/00103620802003963, 2008.

Ahrens, B., Hansson, K., Solly, E. F., and Schrumpf, M.: Reconcilable differences: a joint calibration of fine-root turnover times with radiocarbon and minirhizotrons, New Phytologist, 204, 932–942, 2014.

Ahrens, B., Braakhekke, M. C., Guggenberger, G., Schrumpf, M., and Reichstein, M.: Contribution of sorption, DOC transport and microbial interactions to the 14C age of a soil organic carbon profile: Insights from a calibrated process model, Soil Biology and Biochemistry, 88, 390–402, 2015.

Atkin, O. K., Meir, P., and Turnbull, M. H.: Improving representation of leaf respiration in large-scale predictive climate–vegetation models, New Phytologist, 202, 743–748, https://doi.org/10.1111/nph.12686, https://nph.onlinelibrary.wiley.com/doi/abs/10.1111/nph.12686, 2014.

Ball, J., Wooddrow, I., and Berry, J. A.: A model predicting stomatal conductance and its contribution to the control of photosynthesis under different environmental conditions, in: Progress in Photosynthesis Research, edited by Biggens, J., pp. 1–4, Dordrecht, The Netherlands, 1987.

Barrow, N. J.: The description of phosphate adsorption curves, Journal of Soil Science, 29, 447–462, 1978.

Bernacchi, C. J., Singsaas, E. L., Pimentel, C., Protis JR, A. R., and Long, S. P.: Improved temperature response functions for models of Rubisco-limited photosynthesis, Plant, Cell & Environment, 24, 253–259, 2001.

Bonan, G.: Ecological Climatology: Concepts and Applications, Cambridge University Press, 3 edn., https://doi.org/10.1017/CBO9781107339200, 2015.

Brüggemann, N., Gessler, A., Kayler, Z., Keel, S. G., Badeck, F., Barthel, M., Boeckx, P., Buchmann, N., Brugnoli, E., Esperschütz, J., Gavrichkova, O., Ghashghaie, J., Gomez-Casanovas, N., Keitel, C., Knohl, A., Kuptz, D., Palacio, S., Salmon, Y., Uchida, Y., and Bahn, M.: Carbon allocation and carbon isotope fluxes in the plant-soil-atmosphere continuum: a review, Biogeosciences, 8, 3457–3489, 2011.

Campbell, G. S. and Norman, J. M.: An Introduction to Environmental Biophysics, Springer, 1998.

Chakraborty, D., Nair, V. D., and Harris, W. G.: Compositional Differences Between Alaquods and Paleudults Affecting Phosphorus Sorption-Desorption Behavior, Soil Science, 177, 188–197, https://doi.org/10.1097/SS.0b013e31824329ca, http://content.wkhealth.com/linkback/openurl?sid=WKPTLP:landingpage&an=00010694-201203000-00006, 2012.

Chave, J., Coomes, D., Jansen, S., Lewis, S. L., Swenson, N. G., and Zanne, A. E.: Towards a worldwide wood economics spectrum, Ecology letters, 12, 351–366, https://doi.org/10.1111/j.1461-0248.2009.01285.x, http://dx.doi.org/10.1111/j.1461-0248.2009.01285.x, 2009.

Collatz, G. J., Ribas-Carbo, M., and Berry, J. A.: Coupled photosynthesis-stomatal conductance model for leaves of C4 plants, Australian Journal of Plant Physiology, 19, 519–538, 1992.

Davidson, E. A., Samanta, S., Caramori, S. S., and Savage, K.: The Dual Arrhenius and Michaelis-Menten kinetics model for decomposition of soil organic matter at hourly to seasonal time scales, Glob. Change Biol., 18, 371–384, 2012.

Debicka, M., Kocowicz, A., Weber, J., and Jamroz, E.: Organic matter effects on phosphorus sorption in sandy soils, Archives of Agronomy and Soil Science, 62, 840–855, https://doi.org/10.1080/03650340.2015.1083981, 2015.

Dossa, E. L., Baham, J., Khouma, M., Sene, M., Kizito, F., and Dick, R. P.: Phosphorus Sorption and Desorption in Semiarid Soils of Senegal Amended With Native Shrub Residues, Soil Science, 173, 669–682, https://doi.org/10.1097/SS.0b013e3181893999, http://content.wkhealth.com/linkback/openurl?sid=WKPTLP:landingpage&an=00010694-200810000-00001, 2008.

Drake, B. L.: Using Models of Carbon Isotope Fractionation during Photosynthesis to Understand the Natural Fractionation Ratio, Radiocarbon, 56, 29–38, 2014.

Evans, J. R.: Photosynthesis and nitrogen relationships in leaves of C3 plants, Oecologia, 78, 9–19, 1989.

Fan, H., Huang, D., Zhou, L., and Jia, Y.: Effects of freeze–thaw cycles on phosphorus adsorption and desorption in the black soil of northeastern China, Acta Agriculturae Scandinavica, Section B — Soil & Plant Science, 64, 24–32, https://doi.org/10.1080/09064710.2014.882401, 2014.

Farquhar, G. D., OLeary, M. H., and Berry, J. A.: On the Relationship Between Carbon Isotope Discrimination and the Intercellular Carbon Dioxide Concentration in Leaves, Functional Plant Biology, 9, 121–137, 1982.

Friend, A. D.: Modelling canopy CO2 fluxes: are 'big-leaf'simplifications justified?, Global ecology and biogeography: a journal of macroecology, 10, 603–619, https://nph.onlinelibrary.wiley.com/doi/abs/10.1046/j.1466-822x.2001.00268.x, 2001.

Friend, A. D.: Terrestrial plant production and climate change, Journal of Experimental Botany, 61, 1293–1309, 2010.

Friend, A. D., Stevens, A. K., Knox, R. G., and Cannell, M. G. R.: A process-based, terrestrial biosphere model of ecosystem dynamics (Hybrid v3.0), Ecological modelling, 95, 249–287, 1997.

Friend, A. D., Geider, R. J., Behrenfeld, M. J., and Still, C. J.: Photosynthesis in Global-Scale Models, in: Photosynthesis in silico: Understanding complexity from molecules to ecosystems, edited by Laisk, A., Nedbal, L., and Govindjee, pp. 465–497, Springer, 2009.

Guedes, R. S., Melo, L. C. A., Vergütz, L., Rodríguez-Vila, A., Covelo, E. F., and Fernandes, A. R.: Adsorption and desorption kinetics and phosphorus hysteresis in highly weathered soil by stirred flow chamber experiments, Soil and Tillage Research, 162, 46–54, https://doi.org/10.1016/j.still.2016.04.018, 2016.

Harrell, D. L. and Wang, J. J.: Fractionation and Sorption of Inorganic Phosphorus in Louisiana Calcareous Soils, Soil Science, 171, 39–51, https://doi.org/10.1097/01.ss.0000187347.37825.46, http://content.wkhealth.com/linkback/openurl?sid=WKPTLP:landingpage&an=00010694-200601000-00006, 2006.

Hartmann, H., Adams, H. D., Hammond, W. M., Hoch, G., Landhäusser, S. M., Wiley, E., and Zaehle, S.: Identifying differences in carbohydrate dynamics of seedlings and mature trees to improve carbon allocation in models for trees and forests, Environmental and Experimental Botany, 152, 7–18, 2018.

Hartono, A., Funakawa, S., and Kosaki, T.: Phosphorus sorption-desorption characteristics of selected acid upland soils in Indonesia, Soil Science and Plant Nutrition, 51, 787–799, https://doi.org/10.1111/j.1747-0765.2005.tb00113.x, http://www.tandfonline.com/doi/abs/10.1111/j.1747-0765.2005.tb00113.x, 2005.

Herlihy, M. and McCarthy, J.: Association of soil-test phosphorus with phosphorus fractions and adsorption characteristics, Nutrient Cycling in Agroecosystems, 75, 79–90, https://doi.org/10.1007/s10705-006-9013-2, http://link.springer.com/10.1007/s10705-006-9013-2, 2006.

Hickler, T., Prentice, I. C., Smith, B., SYKES, M. T., and Zaehle, S.: Implementing plant hydraulic architecture within the LPJ Dynamic Global Vegetation Model, Global Ecology and Biogeography, 15, 567–577, 2006.

Holford, i. C. R., Wedderburn, r. W. M., and Mattingly, g. E. G.: A langmuir two-surface equation as a model for phosphate adsorption by soils, Journal of Soil Science, 25, 242–255, https://doi.org/doi:10.1111/j.1365-2389.1974.tb01121.x, https://onlinelibrary.wiley.com/doi/abs/10.1111/j.1365-2389.1974.tb01121.x, 1974.

Horta, C., Monteiro, F., Madeira, M., and Torrent, J.: Phosphorus sorption and desorption properties of soils developed on basic rocks under a subhumid Mediterranean climate, Soil Use and Management, 29, 15–23, https://doi.org/10.1111/j.1475-2743.2012.00405.x, 2013.

Huang, Q., Liang, W., and Cai, P.: Adsorption, desorption and activities of acid phosphatase on various colloidal particles from an Ultisol, Colloids and surfaces B: Biointerfaces, 45, 209–214, https://doi.org/10.1016/j.colsurfb.2005.08.011, http://www.ncbi.nlm.nih.gov/pubmed/16198547, 2005.

Jackson, R. B., Canadell, J., Ehleringer, J. R., Mooney, H. A., Sala, O. E., and Schulze, E. D.: A global analysis of root distributions for terrestrial biomes, Oecologia, 108, 389–411, 1996.

Janardhanan, L. and Daroub, S. H.: Phosphorus Sorption in Organic Soils in South Florida, Soil Science Society of America Journal, 74, 1597–1597, https://doi.org/10.2136/sssaj2009.0137, https://www.soils.org/publications/sssaj/abstracts/74/5/1597, 2010.

June, T., Evans, J. R., and Farquhar, G. D.: A simple new equation for the reversible temperature dependence of photosynthetic electron transport: a study on soybean leaf, Functional Plant Biology, 31, 275, 2004.

Kattge, J., Díaz, S., Lavorel, S., Prentice, I. C., Leadley, P., Bönisch, G., Garnier, E., Westoby, M., Reich, P. B., Wright, I. J., Cornelissen, J. H. C., Violle, C., Harrison, S. P., Van Bodegom, P. M., Reichstein, M., Enquist, B. J., Soudzilovskaia, N. A., Ackerly, D. D., Anand, M., Atkin, O., Bahn, M., Baker, T. R., Baldocchi, D., Bekker, R., Blanco, C. C., Blonder, B., Bond, W. J., Bradstock, R., Bunker, D. E., Casanoves, F., Caverner-Bares, J., Chambers, J. Q., Chapin III, F. S., Chave, J., Coomes, D., Cornwell, W. K., Craine, J. M., Dobrin, B. H., Duarte, L., Durka, W., Elser, J., Esser, G., Estiarte, M., Fagan, W. F., Fand, J., Fernández-Méndez, F., Fidelis, A., Finegan, B., Flores, O., Ford, H., Frank, D., Freschet, G. T., Fyllas, N. M., Gallagher, R. V., Green, W. A., Gutierrez, A. G., Thomas, H., Higgins, S. I., Hodgson, J. G., Jalili, A., Jansen, S., Joly, C. A., Kerkhoff, A. J., Kirkup, D., Kitajima, K., Kleyer, M., Klotz, S., Knops, J. M. H., Kramer, K., Kühn, I., Kurokawa, H., Laughlin, D., Lee, T. D., Leishman, M., Lens, F., Lenz, T., Lewis, S. L., Lloyd, J., Llusià, J., Louault, F., Ma, S., Mahecha, M. D., Manning, P., Massad, T., Medlyn, B. E., Messier, J., Moles, A. T., Müller, S. C., Nadrowski, K., Naeem, S., Niinemets, Ü., Nöllert, S., Nüske, A., Ogaya, R., Oleksyn, J., Onipchenko, V. G., Onoda, Y., Ordoñez, J., Overbeck, G., Ozinga, W. A., Patino, S., Paula, S., Pausas, J. G., Peñuelas, J., Phillips, O. L., Pillar, V., Poorter, H., Poorter, L., Poschlod, P., Prinzing, A., Proulx, R., Rammig, A., Reinsch, S., Reu, B., Sack, L., Salgado-Negret, B., Sardans, J., Shiodera, S., Shipley, B., Siefert, A., Sosinski, E., Soussana, J. F., Swaine, E., Swenson, N., Thompson, K., Thornton, P., Waldram, M., Weiher, E., White, M., White, S., Wright, S. J., Yguel, B., Zaehle, S., Zanne, A. E., and Wirth, C.: TRY - a global database of plant traits, Global Change Biology, 17, 2905–2935, 2011.

Kavka, M. and Polle, A.: Phosphate uptake kinetics and tissue-specific transporter expression profiles in poplar (Populus × canescens) at different phosphorus availabilities, BMC Plant Biology, 16, 206, https://doi.org/10.1186/s12870-016-0892-3, https://doi.org/10.1186/s12870-016-0892-3, 2016.

Knauer, J., Werner, C., and Zaehle, S.: Evaluating stomatal models and their atmospheric drought response in a land surface scheme: A multibiome analysis, Journal of Geophysical Research: Biogeosciences, 120, 1894–1911, 2015.

Kolahchi, Z. and Jalali, M.: Phosphorus Movement and Retention by Two Calcareous Soils, Soil and Sediment Contamination: An International Journal, 22, 21–38, https://doi.org/10.1080/15320383.2012.697939, 2013.

Koven, C. D., Riley, W. J., Subin, Z. M., Tang, J. Y., Torn, M. S., Collins, W. D., Bonan, G. B., Lawrence, D. M., and Swenson, S. C.: The effect of vertically resolved soil biogeochemistry and alternate soil C and N models on C dynamics of CLM4, Biogeosciences, 10, 7109–7131, 2013.

Krinner, G., Viovy, N., de Noblet-Ducoudré, N., Ogée, J., Polcher, J., Friedlingstein, P., Ciais, P., Sitch, S. A., and Prentice, I. C.: A dynamic global vegetation model for studies of the coupled atmosphere-biosphere system, Global Biogeochemical Cycles, 19, GB1015, 2005.

Kronzucker, H. J., Siddiqi, M. Y., and Glass, A. D. M.: Kinetics Of NO3-Influx In Spruce, Plant Physiology, 109, 319–326, 1995.

Kronzucker, H. J., Siddiqi, M. Y., and Glass, A. D. M.: Kinetics of NH4+ influx in spruce, Plant Physiology, 110, 773–779, 1996.

Kull, O. and Kruijt, B.: Leaf photosynthetic light response: a mechanistic model for scaling photosynthesis to leaves and canopies, Functional Ecology, 12, 767–777, 1998.

Levin, I., Naegler, T., Kromer, B., Diehl, M., Francey, R., Gomez-Pelaez, A., Steele, P., Wagenbach, D., Weller, R., and Worthy, D.: Observations and modelling of the global distribution and long-term trend of atmospheric $^{14}CO_2$, Tellus Series B-Chemical and Physical Meteorology, 62, 26–46, 2010.

Lin, Y.-S., Medlyn, B. E., Duursma, R. A., Prentice, I. C., Wang, H., Baig, S., Eamus, D., de Dios, V. R., Mitchell, P., Ellsworth, D. S., de Beeck, M. O., Wallin, G., Uddling, J., Tarvainen, L., Linderson, M.-L., Cernusak, L. A., Nippert, J. B., Ocheltree, T. W., Tissue, D. T., Martin-StPaul, N. K., Rogers, A., Warren, J. M., De Angelis, P., Hikosaka, K., Han, Q., Onoda, Y., Gimeno, T. E., Barton, C. V. M., Bennie, J., Bonal, D., Bosc, A., Low, M., Macinins-Ng, C., Rey, A., Rowland, L., Setterfield, S. A., Tausz-Posch, S., Zaragoza-Castells, J., Broadmeadow, M. S. J., Drake, J. E., Freeman, M., Ghannoum, O., Hutley, L. B., Kelly, J. W., Kikuzawa, K., Kolari, P., Koyama, K., Limousin, J. M., Meir, P., Lola da Costa, A. C., Mikkelsen, T. N., Salinas, N., Sun, W., and Wingate, L.: Optimal stomatal behaviour around the world, Nature Climate Change, 5, 459–464, 2015.

Lloyd, J. and Taylor, J. A.: On the temperature dependence of soil respiration, Functional ecology, pp. 315–323, https://www.jstor.org/stable/2389824, 1994.

Makino, A., Sakuma, H., Sudo, E., and Mae, T.: Differences between maize and rice in N-use efficiency for photosynthesis and protein allocation, Plant & cell physiology, 44, 952–956, https://www.ncbi.nlm.nih.gov/pubmed/14519777, 2003.

Manzoni, S., Porporato, A., and Schimel, J. P.: Soil heterogeneity in lumped mineralization–immobilization models, Soil Biology and Biochemistry, 40, 1137–1148, 2008.

McGill, W. B. and Cole, C. V.: Comparative aspects of cycling of organic C, N, S and P through soil organic matter, Geoderma, 26, 267–286, 1981.

Meyerholt, J. and Zaehle, S.: The role of stoichiometric flexibility in modelling forest ecosystem responses to nitrogen fertilization, New Phytologist, pp. n/a–n/a, 2015.

Monteith, J. L. and Unsworth, M. H.: Principles of Environmental Physics (Fourth Edition), Academic Press, Boston, fourth edition edn., https://doi.org/https://doi.org/10.1016/B978-0-12-386910-4.00023-8, http://www.sciencedirect.com/science/article/pii/B9780123869104000238, 2013.

Mäkelä, A., Hari, P., Berninger, F., Hänninen, H., and Nikinmaa, E.: Acclimation of photosynthetic capacity in Scots pine to the annual cycle of temperature, Tree Physiology, 24, 369–376, https://doi.org/10.1093/treephys/24.4.369, http://dx.doi.org/10.1093/treephys/24.4.369, 2004.

Niinemets, Ü. and Tenhunen, J. D.: A model separating leaf structural and physiological effects on carbon gain along light gradients for the shade-tolerant species Acer saccharum, Plant, Cell and Environment, 20, 845–866, 1997.

Niinemets, Ü., Kull, O., and Tenhunen, J. D.: An analysis of light effects on foliar morphology, physiology, and light interception in temperate deciduous woody species of contrasting shade tolerance, Tree Physiology, 18, 681–696, https://doi.org/10.1093/treephys/18.10.681, http://dx.doi.org/10.1093/treephys/18.10.681, 1998.

Olander, L. P. and Vitousek, P. M.: Short-term controls over inorganic phosphorus during soil and ecosystem development, Soil Biology and Biochemistry, 37, 651–659, https://doi.org/10.1016/j.soilbio.2004.08.022, 2005.

Otto, J., Berveiller, D., Bréon, F.-M., Delpierre, N., Geppert, G., Granier, A., Jans, W., Knohl, A., Kuusk, A., Longdoz, B., and Others: Forest summer albedo is sensitive to species and thinning: how should we account for this in Earth system models?, Biogeosciences, 11, 2411–2427, https://goedoc.uni-goettingen.de/handle/1/10219, 2014.

Pal, S. K.: Phosphorus sorption-desorption characteristics of soils under different land use patterns of eastern India, Archives of Agronomy and Soil Science, 57, 365–376, https://doi.org/10.1080/03650341003605743, http://www.tandfonline.com/doi/abs/10.1080/03650341003605743, 2011.

Parton, W. J., Scurlock, J. M. O., Ojima, D. S., Gilmanov, T. G., Scholes, R. J., Schimmel, D. S., Kirchner, T., Menaut, J. C., Seastedt, T., Moya, E. G., Kamnalrut, A., and Kinyamario, J. I.: Observations and modelling of biomass and soil organic matter dynamics for the grassland biome worldwide, Global Biogeochemical Cycles, 7, 785–809, 1993.

Raddatz, T. J., Reick, C. H., Knorr, W., Kattge, J., Roeckner, E., Schnur, R., Schnitzler, K.-G., Wetzel, P., and Jungclaus, J.: Will the tropical land biosphere dominate the climate–carbon cycle feedback during the twenty-first century?, Climate Dynamics, 29, 565–574, https://doi.org/10.1007/s00382-007-0247-8, https://doi.org/10.1007/s00382-007-0247-8, 2007.

Robinson, D.: $\delta15N$ as an integrator of the nitrogen cycle, Trends in ecology & evolution, 16, 153–162, https://doi.org/10.1016/S0169-5347(00)02098-X, http://www.sciencedirect.com/science/article/pii/S016953470002098X, 2001.

Roeckner, E., Tompkins, A., Bäuml, G., Bonaventura, L., Brokopf, R., Esch, M., Giorgetta, M., Hagemann, S., Kirchner, I., Kornblueh, L., Manzini, E., Rhodin, E., Schlese, U., and Schulzweida, U.: The atmospheric general circulation model ECHAM5 - Part I: Model description, Tech. Rep. 349, Max Planck Institute for Meteorology, Hamburg, 2003.

Rogers, A., Medlyn, B. E., Dukes, J. S., Bonan, G. B., von Caemmerer, S., Dietze, M. C., Kattge, J., Leakey, A. D. B., Mercado, L. M., Niinemets, Ü., Prentice, I. C., Serbin, S. P., Sitch, S. A., Way, D. A., and Zaehle, S.: A roadmap for improving the representation of photosynthesis in Earth system models, New Phytologist, 213, 22–42, 2017.

Sakadevan, K. and Bavor, H. J.: Phosphate adsorption characteristics of soils, slags and zeolite to be used as substrates in constructed wetland systems, Water Research, 32, 393–399, https://doi.org/10.1016/S0043-1354(97)00271-6, 1998.

Sanyal, S. K., Chan, P. Y., and De Datta, S. K.: Phosphate Sorption-Desorption Behavior of Some Acidic Soils of South and Southeast Asia, Soil Science Society of America Journal, 57, 937–937, https://doi.org/10.2136/sssaj1993.03615995005700040011x, https://www.soils.org/publications/sssaj/abstracts/57/4/SS0570040937, 1993.

Sato, S. and Comerford, N. B.: Influence of soil pH on inorganic phosphorus sorption and desorption in a humid Brazilian Ultisol, Revista Brasileira de Ciencia do Solo, 29, 685–694, https://doi.org/10.1590/S0100-06832005000500004, 2005.

Saxton, K. E. and Rawls, W. J.: Soil Water Characteristic Estimates by Texture and Organic Matter for Hydrologic Solutions, Soil Science Society of America Journal, 70, 1569–10, 2006.

Shirvani, M., Khalili, B., Mohaghegh, P., Ghasemi, S., Arabzadegan, H., and Nourbakhsh, F.: Land-Use Conversion Effects on Phosphate Sorption Characteristics in Soils of Forest and Rangeland Sites from Zagros Area, Western Iran, Arid Land Research and Management, 24, 223–237, https://doi.org/10.1080/15324982.2010.487454, http://www.tandfonline.com/doi/abs/10.1080/15324982.2010.487454, 2010.

Singh, B. R., Krogstad, T., Shivay, Y. S., Shivakumar, B. G., and Bakkegard, M.: Phosphorus fractionation and sorption in P-enriched soils of Norway, Nutrient Cycling in Agroecosystems, 73, 245–256, https://doi.org/10.1007/s10705-005-2650-z, http://link.springer.com/10.1007/s10705-005-2650-z, 2005.

Singh, V., Dhillon, N. S., and Brar, B. S.: Influence of long-term use of fertilizers and farmyard manure on the adsorption-desorption behaviour and bioavailability of phosphorus in soils, Nutrient Cycling in Agroecosystems, 75, 67–78, https://doi.org/10.1007/s10705-006-9012-3, http://link.springer.com/10.1007/s10705-006-9012-3, 2006.

Sitch, S. A., Smith, B., Prentice, I. C., Arneth, A., Bondeau, A., Cramer, W., Kaplan, J. O., Levis, S., Lucht, W., Sykes, M. T., and Venevsky, S.: Evaluation of ecosystem dynamics, plant geography and terrestrial carbon cycling in the LPJ Dynamic Global Vegetation Model, Global Change Biology, 9, 161–185, 2003.

Spitters, C. J. T.: Separating the Diffuse and Direct Component of Global Radiation and Its Implications for Modeling Canopy Photosynthesis .2. Calculation of Canopy Photosynthesis, Agricultural and Forest Meteorology, 38, 231–242, 1986.

Sprugel, D. G., Ryan, M. G., Brooks, J. R., Vogt, K. A., and Martin, T. A.: Respiration from the Organ Level to the Stand, in: Resource Physiology of Conifers, edited by Smith, W. K. and Hinckley, T. M., pp. 255–299, Academic Press, San Diego, https://doi.org/10.1016/B978-0-08-092591-2.50013-3, http://www.sciencedirect.com/science/article/pii/B9780080925912500133, 1995.

Tazoe, Y., Noguchi, K. O., and Terachima, I.: Effects of growth light and nitrogen nutrition on the organization of the photosynthetic apparatus in leaves of a C4 plant, Amaranthus cruentus, Plant, Cell and Environment, 29, 691–700, 2006.

Villapando, R. R. and Graetz, D. a.: Phosphorus Sorption and Desorption Properties of the Spodic Horizon from Selected Florida Spodosols, Soil Science Society of America Journal, 65, 331–331, https://doi.org/10.2136/sssaj2001.652331x, 2001.

Wang, Y. P., Law, R. M., and Pak, B.: A global model of carbon, nitrogen and phosphorus cycles for the terrestrial biosphere, Biogeosciences, 7, 2261–2282, 2010.

White, M. A., Thornton, P. E., Running, S., and Nemani, R.: Parameterization and Sensitivity Analysis of the BIOME-BGC Terrestrial Ecosystem Model: Net Primary Production Controls, Earth Interactions, 4, 1–55, 2000.

Wisawapipat, W., Kheoruenromne, I., Suddhiprakarn, A., and Gilkes, R. J.: Phosphate sorption and desorption by Thai upland soils, Geoderma, 153, 408–415, https://doi.org/10.1016/j.geoderma.2009.09.005, http://linkinghub.elsevier.com/retrieve/pii/S0016706109002821, 2009.

Wullschleger, S. D.: Biochemical Limitations to Carbon Assimilation in C3 Plants—A Retrospective Analysis of the A/Ci Curves from 109 Species, Journal of experimental botany, 44, 907–920, https://doi.org/10.1093/jxb/44.5.907, https://academic.oup.com/jxb/article-abstract/44/5/907/503778, 1993.

Xu, D., Xu, J., Wu, J., and Muhammad, A.: Studies on the phosphorus sorption capacity of substrates used in constructed wetland systems, Chemosphere, 63, 344–352, https://doi.org/10.1016/j.chemosphere.2005.08.036, http://www.ncbi.nlm.nih.gov/pubmed/16242173, 2006.

Xu-Ri and Prentice, I. C.: Terrestrial nitrogen cycle simulation with a dynamic global vegetation model, Global Change Biology, 14, 1745–1764, 2008.

Yang, X., Thornton, P. E., Ricciuto, D. M., and Post, W. M.: The role of phosphorus dynamics in tropical forests – a modeling study using CLM-CNP, Biogeosciences, 11, 1667–1681, https://doi.org/10.5194/bg-11-1667-2014, https://www.biogeosciences.net/11/1667/2014/, 2014.

Zaehle, S. and Friend, A. D.: Carbon and nitrogen cycle dynamics in the O-CN land surface model: 1. Model description, site-scale evaluation, and sensitivity to parameter estimates, Global Biogeochemical Cycles, 24, GB 1005, 2010.

Zaehle, S., Friedlingstein, P., and Friend, A. D.: Terrestrial nitrogen feedbacks may accelerate future climate change, Geophysical Research Letters, 37, https://doi.org/10.1029/2009GL041345, https://agupubs.onlinelibrary.wiley.com/doi/abs/10.1029/2009GL041345, 2010.

Zaehle, S., Ciais, P., Friend, A. D., and Prieur, V.: Carbon benefits of anthropogenic reactive nitrogen offset by nitrous oxide emissions, Nature Geoscience, 4, 601–605, 2011.

Zafar, M., Tiecher, T., de Castro Lima, J. A., Schaefer, G. L., Santanna, M. A., and Dos Santos, D. R.: Phosphorus seasonal sorption-desorption kinetics in suspended sediment in response to land use and management in the Guapore catchment, Southern Brazil, Environ Monit Assess, 188, 643, https://doi.org/10.1007/s10661-016-5650-3, https://www.ncbi.nlm.nih.gov/pubmed/27796828, 2016.

Zanne, A., Lopez-Gonzalez, G., Coomes, D., Ilic, J., Jansen, S., Lewis, S., Miller, R., Swenson, N., Wiemann, M., and Chave, J.: Data from: Towards a worldwide wood economics spectrum, https://doi.org/doi:10.5061/dryad.234, https://doi.org/10.5061/dryad.234, 2009.

Zerihun, A., McKenzie, B. A., and Morton, J. D.: Photosynthate costs associated with the utilization of different nitrogen–forms: influence on the carbon balance of plants and shoot–root biomass partitioning, The New Phytologist, 138, 1–11, 1998.

5 Zhou, M. and Li, Y.: Phosphorus-Sorption Characteristics of Calcareous Soils and Limestone from the Southern Everglades and Adjacent Farmlands, Soil Science Society of America Journal, 65, 1404–1404, https://doi.org/10.2136/sssaj2001.6551404x, 2001.

Zou, P., Fu, J., and Cao, Z.: Chronosequence of paddy soils and phosphorus sorption-desorption properties, Journal of Soils and Sediments, 11, 249–259, https://doi.org/10.1007/s11368-010-0301-8, http://link.springer.com/10.1007/s11368-010-0301-8, 2011.